PREPARATION, CHARACTERIZATION AND APPLICATIONS OF GRAPHENE AND ITS COMPOSITES

Thesis

Submitted in partial fulfillment of the requirements for the degree of

DOCTOR OF PHILOSOPHY

by

SREEJESH M
(Reg. No: 110680PH11F05)

DEPARTMENT OF PHYSICS
NATIONAL INSTITUTE OF TECHNOLOGY KARNATAKA,
SURATHKAL, MANGALORE – 575 025

June, 2017

DECLARATION

I hereby *declare* that the Research Thesis entitled **"Preparation, characterization and applications of graphene and its composites"** which is being submitted to the National Institute of Technology Karnataka, Surathkal in partial fulfillment of the requirements for the award of the **Degree of Doctor of Philosophy** in **Physics** is *a bonafide report of the research work carried out by me*. The material contained in this Research Thesis has not been submitted to any University or Institution for the award of any degree.

Mr. Sreejesh M
(Reg. No. 110680PH11F05)
Department of Physics

Place: NITK, Surathkal
Date: June 15, 2017

CERTIFICATE

This is to *certify* that the Research Thesis entitled **"Preparation, characterization and applications of graphene and its composites"** submitted by Sreejesh M (Register Number110680PH11F05) as the record of the research work carried out by him, is accepted as the *Research Thesis* submission in partial fulfillment of the requirements for the award of degree of Doctor of Philosophy.

Dr. H. S. NAGARAJA

(Research Guide)

Chairman-DRPC

Acknowledgments

On this happy occasion I wish to express my deep sense of gratitude to my research supervisor, Dr. H. S. Nagaraja, Department of Physics, NITK Surathkal for his guidance, valuable suggestions, constant support and encouragement throughout the research period.

I wish to thank Dr. N. K. Udayashankar, Department of Physics, NITK Surathakal and Dr. S. M. Kulkarni, Department of Mechanical Engineering, NITK Surathkal for their timely suggestions, help, and guidance as members of the research program assessment committee.

I wish to thank Dr. M.N. Sathyanarayan, Head of the Department of Physics, NITK Surathkal as well as Dr. H. D. Shahikala former H.O.D for providing all the facilities and support they have provided during the course of the research work. I also express my gratitude to Dr. Ajith K M, Department of Physics NITK for his constant support and throughout the research period. I also acknowledge the support provided by Dr. Kishore Sridharan, DST faculty, Department of Physics. The helps and support provided by all the faculty members of the department is also acknowledged.

I thank my labmates the Materials Research Lab NITK Surathkal for their cooperation they have provided in the past. I thank Dr. K.K. Nagaraja, Dr. Santhosh Kumar A, Bindu K, Amudha A and Brijesh K my Ph.D colleagues at NITK. I also thank the post graduate students Sulakshana, Dhanush, Aarathy, Sona and Veena who were always helpful in setting up the experiment and timely discussions.

I thank to my Ph.D collegues at NITK Surathkal, notably Siby Thomas, Nimith K.M, Sterin N.S, Khasim K, Dr. Arun P Parameshwaran, Dr. Manoj K Narayaran, Dr. Gautam Sarang, Dr. Gibin Gerorge, Rizwan, Safir T.K and Manju M.S for their love and help. I also acknowledge the support provided by all teaching and non-teaching staff members of the Department of Physics, NITK Surathkal at different stages of my research project.

Above all I am indebted to my father C. Damodaran, who has inspired me from my childhood to chase my dreams. I dedicate this thesis in front of the loving memories of him. My mother, Yesodha M, who is always my strength, without whom I couldn't have done anything in life. This thesis is also dedicated to her. Sreena M, my loving sister who is always with me to support in life, I thank her for all her support and love. Last but not least, my friends, you guys are always awesome, keep supporting .

(Sreejesh M)

Abstract

The preparation, characterization and applications of graphene and its composites are investigated in this thesis. Solar exfoliation, a relatively simple and viable method, is used for the production of the reduced graphene oxide. The prepared graphene oxide is tested for applications in supercapacitors and electrochemical sensor for hydrogen peroxide, which is an important chemical species in the biological systems. Later on, vanadium oxide –graphene composite has been prepared and characterized. The prepared composite has been used as sensor for dopamine detection at nanomolar range, a neurotransmitter which can be vital in finding the irregularities related to Alzheimer's detection. A better performance in terms of lower detection limit (0.07 µM) and sensitivity (25.02 µA mM^{-1} cm^{-2}) is reported. Also, Lithium ion batteries are fabricated using the prepared composites and the composite offers a good capacitance of around 200 Fg^{-1}. The fifth chapter describes the preparation of zinc oxide - graphene composites. The electrochemical sensor fabricated using zinc oxide - graphene oxide composite was found to be sensitive towards glucose, which is important in the control of diabetes mellitus. Also, supercapacitors electrodes were fabricated and tested using above composites reveals promising performance with hghest specific capacitance of 635 Fg^{-1}.

Keywords: *Graphene, Solar Exfoliated Graphene, Vanadium pentoxide (V_2O_5), Zinc Oxide, Electrochemistry, Cyclic Voltammetry, Charge-discharge Chronoamperomtry, Impedance Spectroscopy, Biosensors, Supercapacitors, Lithium-ion Batteries*

Contents

List of figures

List of tables

Nomenclature

λ	Wavelength
θ	Bragg angle
ALCVD	Atomic Layer Chemical Vapour Deposition
C	Carbon
CV	Cyclic Voltammetry
CVD	Chemical Vapour Deposition
d	Interplanar spacing
DMF	Dimethyl Formamide
EDAX	Energy Dispersive X-ray Spectroscopy
EDLC	Electrochemical Double Layer Capacitance
EIS	Electrochemical Impedance Spectroscopy
FLG	Few Layered Graphene
FTIR	Fourier Transform Infrared Spectroscopy
GCE	Glassy Carbon Electrode
GO	Graphene Oxide
I	Current
IUPAC	International Union of Pure and Applied Chemistry
LIB's	Li-ion Batteries
$LiCoO_2$	Lithium Cobalt Oxide
$LiMn_2O_4$	Lithium Manganese Oxide
MWCNT	Multi-Walled Carbon Nanotubes

$NaBH_4$	Sodium Borohydride
NMP	N-Methyl-2-Pyrrolidone
PBS	Phosphate Buffer Saline
PECVD	Plasma Enhanced Chemical Vapour Deposition
PVDF	Polyvinylidene Fluoride
rGO	Reduced Graphene Oxide
SCE	Saturated Calomel Electrode
SEM	Scanning Electron Microscopy
TEM	Transmission Electron Microscopy
TGA	Thermo Gravimetric Analysis
V	Voltage

Chapter 1

1. Introduction

Chapter 1 contains a brief overview of the graphene and its properties. Also the applications of graphene are discussed. This chapter also contains a brief discussion on the important composites of graphene. The electrochemical applications of these composites in the energy storage devices and biosensors are also discussed.

1.1 Review of graphene and its applications

Abundant and naturally occurring graphite, which is considered as the multi layered form of graphene, is known to the humans for many thousands of years. The history of the graphene started with the discovery by Geim and co-workers (Geim et. al. 2004). The very existence of a two-dimensional crystal was a new knowledge to the physicists across the world, since it contradicted some of the existing theories stating the unstable nature of two dimensional crystals (Landau, L. D. 1937).

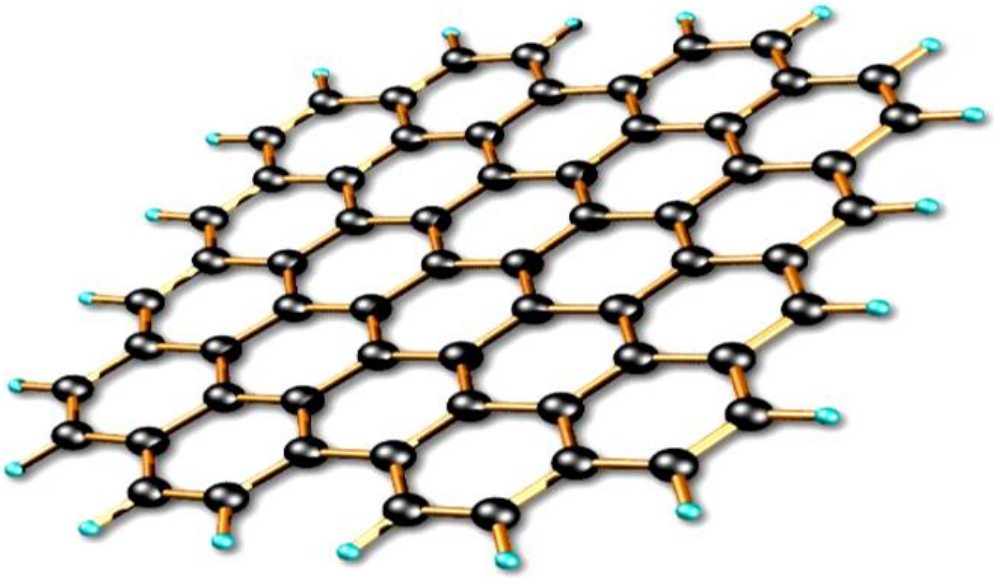

Figure. 1. 1: Representative image of a graphene monolayer showing the honeycomb structure with hexagonally arranged carbon atoms

The term ‘‘graphene’’ was recommended by the relevant IUPAC (International Union of Pure and Applied Chemistry) commission to replace the older term ‘‘graphite layers’’. The term “graphite layers” was unsuitable in the research of single carbon layer structure, since the term referred to a three-dimensional (3D) stacking structure. The IUPAC definition can be stated as *“the term graphene should be used only when the relations, structural relations or other properties of individual layers are discussed”* (Dreyer et al. 2010). The graphene can be described as a two-dimensional monolayer of carbon atoms, which is the basic building block of graphitic materials (i.e. fullerene, nanotube, graphite). All these forms can be built, starting from the basic graphene sheets.

Properties of graphene (Singh et al. 2011)

- Large theoretical specific area (2360 m^2/g).
- High intrinsic mobility (200,000 $cm^2\ V^{-1}\ s^{-1}$).
- Extremely high Young’s modulus (~1.0 TPa).
- Thermal conductivity (~5000 $Wm^{-1}\ K^{-1}$).
- Optical transmittance (~97.7%)

Graphene was first prepared by Geim et al. using the scotch tape based mechanical exfoliation. Later, methods like chemical vapour deposition (CVD), chemical methods etc. were also suggested to prepare high quality graphene sheets. Even though, the bulk synthesis of graphene was largely affected because of the low efficiency of these methods. The suggested alternative was the chemical synthesis of graphene by oxidizing and reducing graphite (Marcano et al. 2010). Graphene oxide, the oxidized form of graphene needs a special mention because of this reason.

1.1.1 Graphene Synthesis Methods

First ever preparation of graphene sheet employed the mechanical exfoliation of pyrolytic graphite. Thereafter numerous methods were proposed and experimentally proved by the scientists around the world. The methods for the preparation of the graphene can be briefly categorized into (Choi et al. 2010),

- Exfoliation and cleavage
- Thermal and chemical vapour deposition techniques
- Plasma enhanced chemical vapour deposition techniques
- Chemical and other methods

1.1.1.1 Exfoliation and cleavage

Graphite is a continuum of graphene layers, each attached together by van der Waals force. If one can give enough energy either mechanically or chemically it could be possible to peel off some of the layers. Exfoliation techniques use the same for the synthesis of graphene layers. In the Nobel Prize winning work, the researchers demonstrated first ever production of the graphene single layers (Novoselov et al. 2004). The technique used by them for peeling off the layers of the pyrolytic graphite is known as scotch tape method. The method yielded good quality graphene sheets with a considerably lower number of defects and utilized in demonstrating many properties of the graphene (Gass et al. 2008). However, the method was seriously lacking a large-scale production capacity, which could hinder any commercialization of the possible applications. A better method with a better production rate is achieved through liquid phase exfoliation of the graphite. In this method, ultrasonic assisted exfoliation was tried in N-methyl-pyrrolidone (NMP) (Hernandez et al. 2008). It was also observed that the exfoliation depends upon the interaction of the graphite and the solvent used.

1.1.1.2 Thermal and chemical vapour deposition techniques

Thermal and Chemical Vapour Deposition (CVD) of graphene has emerged as a versatile technique to grow large area graphene on substrates for various applications. The graphene growth on these substrates also depends on the surface segregation of carbon and in some cases, it was observed to be a CVD/ surface segregation process

(Avouris et al. 2012). In the earliest report, few layered graphene (FLG) was prepared through the pyrolysis of camphor on nickel substrate. The authors described the method as a simple and cost effective thermal method (Somani et al. 2006). The reported graphene sheet was made up of more than 30 layers, but paved the way to the new synthetic route for the production of graphene. The effect of the substrate was critical in most of the CVD methods, 1-2 nm thick graphene sheets were grown over Ni substrate, whereas the experiment was unsuccessful in the case of Si wafer (Obraztsov et al. 2007). Apart from the substrate properties, the reacting gas ratios, pressure and cooling rate acted as deciding factors. Different cooling rates results in the segregation of the C atoms, which is to be controlled to achieve different thickness and crystallinities in the graphene layers. Further substrate free strategies were tested for preparing graphene sheets using CVD. MgO supported Co catalysts were employed to grow graphene in a ceramic boat using CH_4 and Ar gases. The obtained graphene sheets were separated and cleaned by repeated washing with HCl and deionized water. The characterizations revealed the presence of rippled graphene sheets. This method has the advantage that it can be scaled up for the industrial production of graphene (Wang et al. 2009).

1.1.1.3 Plasma Enhanced Chemical Vapour Deposition (PECVD)

Plasma enhanced chemical vapour deposition (PECVD) is a modified chemical vapour deposition, which allows more flexibility in choosing the substrates and comparatively avoiding the use of catalysts. The first report on this method utilized a dc discharge PECVD which resulted in nano graphite like structure with graphene like sheets at the edges (Obraztsov et al. 2003). The free standing graphene sheets were reported later using radio frequency plasma enhanced CVD. The researchers reported this without the use of any catalyst or special substrate treatment (Wang et al 2004). The PECVD methods brought control over the method, bringing less importance to the catalyst and substrate parameters.

1.1.1.4 Chemical Methods

The large-scale synthesis of graphene was the major issue in the development of devices and technologies using graphene. The chemical method was suggested for catering the

need of the industries. Even though, many methods reported earlier can be called as a chemical method, for the purpose of understanding the discussion here it is restricted to the production of graphene by the reduction/exfoliation of graphene oxide. The process involved in the graphene synthesis can be summarized as a two-step process via,

1) Oxidation of the graphite using strong oxidizing agent.
2) Reduction/exfoliation of the obtained graphene oxide in the solution/solid state using reducing agents such as hydrazine hydrate or by thermal annealing.

The earliest report on the oxidation of graphite to graphite oxide is dated back to 1859. The most famous among the reported method was put forward by Hummer et al. in 1958. The method describes the production of graphite oxide from graphite. Graphite flakes were treated in sulphuric acid and sodium nitrate, which is further treated with potassium permanganate. This mixture was treated with water and hydrogen peroxide to obtain graphite oxide (Hummer et al. 1958). This method is considered as one of the easiest and productive method to obtain graphite oxide, which is the starting material for other reduction/exfoliation processes. Recently, there have been many attempts to develop better methods to oxidize graphite. The efforts in improving the Hummer's method have to be highlighted because of the wide acceptance among the scientific communities. The method suggested using a mixture of (9:1 concentration), H_2SO_4/H_3PO_4 which is fed with 1 equivalent of graphite flake and 6 weight equivalents of potassium permanganate. The reaction was continued at elevated (50 ºC) for 12 hours, which is then poured into ice containing 30% H_2O_2 resulting in the formation of graphene oxide. The slight change in the process and the ratios of the oxidants used to improve the efficiency of the oxidation process. The method also had the added advantages that, it does not produce toxic gases and greater controllability over the temperature (Macrano et al. 2010). Although, other methods have been suggested and reported to produce graphene oxide (Jainfreg et al. 2009) an altered Hummer's method has been used in this work.

Graphene oxide (GO) obtained after the oxidation of graphite flakes shows insulating or high resistance. In order to restore the properties of the graphene, exfoliation or

reduction is required in the sample. The methods can be broadly divided as chemical reduction and physical reduction.

Chemical reduction of GO is a much discussed method to restore the properties of graphene. During the oxidation of graphite, functional groups get attached to the graphitic planes. This will also allow the water molecules to occupy space in between the graphitic planes, resulting in the increased interplanar distance. Once the bonding between these planes broken by the reducing agent that results in the formation of free standing sheets of graphene. Hydrazine is one of the most discussed reducing agent for the reduction of GO. Prior to the reaction, a well dispersed solution of GO was prepared by the ultrasonic agitation. The solution was then mixed with hydrazine hydrate in the required ratio. This was kept under constant stirring in a Teflon lined glass beaker which is maintained at 80 ºC. The resultimg black precipitate is filtered and cleaned to obtain the reduced GO [rGO]. The prepared rGO shows higher surface area and electrical conductivity (Park et al. 2011). In general, hydrazine reduction results in high quality of graphene, but the inherent toxic nature of this chemical makes its important to avoid the use of Hydrazine as much as possible. Another redox agent, which is reported as an alternative to the hydrazine is vitamin C. Dispersion of GO was reacted with vitamin C at temperature around 95 ºC. The reaction resulted in highly reduced graphene oxide, which can be easily dispersed in water or other common organic solvents. This method also has the advantage that, vitamin C is environmentally friendly in nature (Fernandez et al. 2010). Sodium borohydride is another reducing agent, which shows promising performance. The spray coating technique was used for the preparation of the graphene oxide films. It was noticed that the electrical resistance of these films was higher [6.8×10^{-8} S m^{-1}]. These films were dipped in $NaBH_4$ solution to reduce it. The reduced films were found to be showing lesser resistance than the initial film [4.5 S m^{-1}](Shin et al. 2009). Another alternate method for producing chemically reduced graphene oxide, is to treat them under alkaline conditions. A mixture of GO and NaOH was kept in a Teflon beaker and allowed to react at 120 ºC in a hydrothermal chamber. This resulted in the reduction of the graphene oxide to a black reduced GO (Perera et al. 2012). The chemical reduction of GO is already well established and there are numerous ways put forward to achieve reduction. But, the toxic nature of reacting

species, time consuming processes and problems involved in mass production hinder the further growth in the field.

The reduction involving the treatments with high temperature or high energy radiation is an alternate way of achieving reduced graphene oxide. Dip coating technique was used for the preparation of GO films over the pre-treated quartz substrate. The thickness was adjusted by varying the number of layers and dipping time. This resulted in GO films, which is less conducting in nature. In order to restore the conductivity, the film was kept under high temperature (1000 ºC) in Ar/H_2 environment. This resulted in the improvement in conductivity around 500 S/cm. The films also exhibited good optical transmittance (> 70%) (Wang et al. 2008). In a similar report, solution processed graphene oxide films are reduced to obtain a film, which can be used as transparent conductor. The authors tried to graphitize the GO films at 1100 ºC in vacuum. The result was promising, that the films showed less sheet resistance with more than 80% transparency (Becerril et al. 2008). Another approach to achieve reduced graphene oxide is, exfoliating with the help of microwave irradiation. GO powder obtained was irradiated in a domestic microwave oven for 1 minute at 700 W. This resulted in the exfoliation of graphene oxide with violent fuming. The results were so interesting that within a short time reduced graphene oxide with worm like morphology was obtained. This process also restored the electronic conductivity of the graphene sheets (Zhu et al. 2010). In another paper, the authors described the exfoliation of graphene oxide by the concentrated solar radiation. A convex lens with diameter 90 mm was used for concentrating solar energy to the graphene oxide. The energy produced by this was sufficient for the exfoliation of graphene oxide. There are many methods which are described well in the literatures. But most of the literatures focussed on the reduction of graphene oxide, the applications of these graphene sheets are not studied. So using the reported procedures for the material production and using them in innovative applications could be a promising step the studies of graphene.

1.1.2 Applications of Graphene

Graphene finds applications in a variety of fields such as energy generation and storage, electronics, biomedical applications etc. (Chabot et al. 2014).

Graphene-silicon (Gr-Si) Schottky junction solar cells have been prepared and well-studied in the past. In a recent report, Gr-Si solar cell was prepared by the CVD method, after construction of the solar cell, internal electric field doping was used for the performance enhancement (Yu et. al. 2015). Single layer graphene/ n-silicon solar cells have been reported earlier. The doped versions of the device reach 8.6% efficiency, demonstrating the applications of graphene in solar cells. These junctions formed works like a Schottky junction solar cell (Miao et al. 2012). Graphene also finds application as a transparent conductive electrode in the solar cells. Many research groups explored the possibility of replacing the usual transparent conducting oxides with graphene films, which is prepared by different methods (Grane et al. 2012).

Energy storage is one of the fields where graphene has made a major impact. With the recent advance graphene has found applications in Li-ion Batteries (LIB's), supercapacitors, Lithium-sulphur batteries and Lithium air/oxygen batteries(Zhu et al. 2014).

1.1.2.1 Li-ion Batteries (LIB's)

Lithium ion batteries possess longer life and better safety compared to the other traditional batteries, but the lower power density compared to the electrochemical capacitors, which is a major problem affecting its wide utilization. The charging time is another important parameter, the current charging time for LIB's stands in hours. It is important to have a fast charging. The charge and discharge in LIB's achieved through the insertion and deintercalation of Li ions at the anode and cathode. The speed of the intercalation/de-intercalation reaction depends on the speed of the Li ions transported through the electrolyte and electrode. Developing materials with high electrical conductivity, faster electron transport with large surface area and shortened diffusion length for the Li ions is a key point in having better batteries (Zhu et al. 2014). The existing studies show that graphene itself cannot act as a good electrode material due to its low coulombic efficiency, high charge-discharge platform and poor cyclic stability. But when used as a matrix material/ nano composites, graphene can play a significant role (Atabaki et al. 2013).

1.1.2.2Supercapacitors

The very high electrical conductivity and the large surface area makes graphene a suitable candidate for the supercapacitor applications. Graphene, in its own and as a composite exhibits excellent energy storage capabilities, as an electrode in supercapacitors. Graphene shows EDLC (Electrochemical Double Layer Capacitance) type performance while used as an electrode. Over the last decade, there have been many reports regarding the use of graphene in supercapacitors. The applications in supercapacitors can be categorized based on the method of reduction of the graphene/reduced graphene.

1.1.2.2.1 Review of graphene electrodes through the chemical reduction of graphene oxide.

Chemical reduction of graphene oxide is a simple and effective tool to obtain reduced graphene oxide. Because of the simplicity many methods are employed to obtain the reduced graphene oxide with desired quality for a supercapacitor electrode.

Table 1.1 : Chemical reduction of graphene oxide for supercapacitor electrodes

No	Reducing agent	Results	Reference
1	Hydrazine hydrate	The graphitic properties are restored through the hydrazine reduction. Improved electrical conductivities are also observed. Electrochemical properties are evaluated using two electrode configurations in differet solvents, and improved capacitance values are observed. 1) KOH – 135 Fg^{-1} 2) $TEABF_4$/PC – 94 Fg^{-1} 3) $TEABF_4$/AC – 99 Fg^{-1}	(Stoller et al. 2008)

		The restacking of the graphene sheets after the reduction is, one of the main challenges in chemical reduction mehod..	
2	Hydrazine hydrate	The reduced graphene oxide was prepared by the deoxydation using hydrazine hydrate. The reduction time was varied. Also, the effect of the annealing in argon atmosphere was studied. A very high specific capacitance of 205 Fg^{-1} was reported.	(Wang et al. 2009)
3	Hydrobromic acid	Reduced graphene has been obtained by the reduction using hydrobromic acid. The rGO obtained can be re-dispersed in water, making it easy to process. Because of the partial reduction, due to the nature of the reducing agent, some of the functional groups remain in the sample. This facilitated better performance with the aqueous electrolyte and offered some pesuodocapacitive part in the total capacitance. The observed capacitance in 1-butyl-3-methylimidazolium, hexafluorophosphate ($BMIPF_6$) and H_2SO_4 are 148, 348 and 205 Fg^{-1} respectively.	(Chen et al. 2010)

1.1.2.2.2 Review of graphene electrodes through the thermal reduction of graphene oxide

Thermal reduction is one of the ways to obtain reduced graphene oxide. The thermal reduction has the advantage, that it takes relatively less time compared to the other methods. Some of the earlier attempts to prepare electrodes from the graphene oxide through thermal and related methods are listed below. `

Table 1.2: Thermal reduction of graphene oxide for supercapacitor electrodes

No	Process	Results	Reference
1	Reduction of graphene oxide at 1050^0C	Graphite oxide reduced at 1050^0C and was tested for its capabilities as an electrode material under ionic and aqueous electrolytes. A capacitance of 75 and 117 Fg^{-1} was reported for the ionic and aqueous electrolytes respectively.	(Vivekchand et al. 2008)
2	Exfoliation at 200^0C in vacuum	Higher temperature required for the exfoliation makes it inconvenient in some cases. The authors took effort to decrease the temperature and could achieve the reduced graphene oxide around 200^0C, at low vacuum conditions. The sample shows a capacitance of 264 and 122 Fg^{-1} in aqueous and organic electrolytes respectively.	(Wei Lv et al. 2009)
3	Exfoliation at 200^0C in air	Thermal exfoliation of graphite oxide was used, to obtain the low temperature treatment in air at 200^0C, the sample was further treated in N_2 atmosphere at elevated temperature, to obtain nitrogen doped graphene. The electrochemical properties are studied. The material shows a capacitance of 230 Fg^{-1} in KOH solution.	(Du et al. 2010)
4	Solvothermal process without any reducing agent at 150^0C	The authors exfoliated graphene oxide in the dispersed form, in propylene carbonate. The reduction was carried out without the aid of any reducing agent.	(Zhu et al. 2010)

		The method was found to be scalable. Also the prepared samples show a very high capacitance of 120 Fg^{-1} in two electrode configuration.	
5	GO dispersed and heated at 150^0C in dimethylformamide (DMF)	Heating at 150^0C in DMF controlls the functionalities of the graphene oxide. The surface functional groups lead to extra pseudocapacitance, which was due to the interaction between the electrolyte and functional groups. A very high capacitance of 276 Fg^{-1} in 1M H_2SO_4 was reported.	(Lin et al. 2011)
6	Microwave reduction	Graphene oxide has the tendency to absorb the microwaves. This result in the sudden heating leading to the expansion and exfoliation. The obtained product is worm like in structure. The electrochemical studies show, that the material has good energy storage properties and a high capacitance of 196 Fg^{-1} in 1M KOH solution.	(Zhu et al. 2010)
7	Photothermal reduction	Graphene oxide was coated on the substrate using drop casting. The GO has been reduced by using the photothermal energy, using a camera flash. The reduction parameters were be tuned by varying the flash energy.	(Jhung et al. 2014)

From the literature, it can be seen that graphene oxide can be reduced to graphene using thermal energy. Usual furnace heating is not energy efficient in nature. The low temperature methods need longer exposure of the material at certain temperatures to

achieve the same. Microwave and photothermal are other methods to achieve the required reduction in less time. It can be concluded that a good thermal reduction method for supercapacitor should be fast, energy efficient and viable.

1.1.2.2.3 Review of graphene hydrogels as supercapacitor electrodes

Hydrogels have the advantage that, its porosity helps in better wetting, when used as an electrode material. Also, this enhances the charging and discharging properties. Graphene hydrogels has been reported to show good electrochemical properties.

Table. 1.3: Graphene hydrogels as supercapacitor electrodes

No	Process	Results	Reference
1	Hydrogel via one step hydrothermal process.	The preparation method is simple. Graphene oxide solution in a Teflon lined autoclave is heated at 180 ^{0}C for 12 hours. The reduced graphene hydrogel was be formed because of the temperature and pressure. The slices from the hydrogel are directly used as an electrode, without any additional binder. The material reported to have a good capacitance of 175 Fg^{-1} .	(Xu et al. 2010)
2	2-aminoantrouinone grafted graphene	2-aminoantrouinone grafted graphene was prepared by a chemical route, followed by heat treatment. This resulted in hydrogel formation. The electrochemical properties were evaluated in 1 M H_2SO_4. The material showed a high capacity of 258 $Fg^{-1.}$ It was also observed that the larger part of the capacitance arises from the pseudocapacitance obtained through the bridging of graphene.	(Wu et al. 2011)
3	Hydrothermal followed by	The method includes the formation of hydrogels via hydrothermal reaction. The	(Zhang et al. 2011)

	chemical reduction	hydrogel was further reduced, using hydrazine hydrate to achieve better electrical properties. The electrochemical property studies reveal a capacitance of 220 $Fg^{-1.}$ Also good stability was observed for the samples.	
4	Hydroquinone as the reducing and functionalizing agent	The method involves a single step hydrothermal process, in which hydroquinone acts as the reducing and functionalizing agent. The material can be directly used as a supercapacitor electrode. Also the electrode shows a very high capacitance of 441 Fg^{-1}. The electrode also shows excellent electrochemical stability up to 1000 cycles.	(Xu et al. 2013)
5	Nitrogen doped hydrogel	Nitrogen doped graphene was prepared in a Teflon lined autoclave at 200 ^{0}C. The material was tested for its energy storage properties in an organic electrolyte at a potential window of 3.2 V. It shows a capacitance of 48.6 Fg^{-1}.	(Liu et al. 2016)
6	Flourinated graphene hydrogel	Flourinated graphene hydrogel was synthesized through a one step process using HF, as the fluorine source. The prepared electrode material from this experiment shows a capacitance of 227 Fg^{-1}.	(Au et al. 2016)

1.1.2.2.4 Review of graphene synthesized through other methods for applications in supercapacitor electrodes

Apart from the widely used methods, there are unconventional and modified methods used for the preparation of graphene for superpcapacitor applications. This section deals with some of the methods reported for the preparation of graphene.

Table. 1.4: Graphene prepared through various methods for supercapacitor electrodes

No	Process	Results	Reference
1	Electrochemical activation	Partially reduced graphene oxide was electrohcemiacally cycled in 1M Et_4NBF_4 in acetonitrile electrolyte. The cycling helped in the reduction of the GO and increased the interplanar spacing. The increased spacing also exposed more active area. During initial cycles the capacitance was negligible. After few cycles the capacitance reached high values of 220 Fg^{-1}. The practical limitation of the method is the volume expansion of the cells during the cell cycling.	(Hantel et al. 2011)
2	Chemical activation using (KOH)	Graphene was dispersed in KOH solution and treated under elevated temperature, which helped in the activation of graphene. The electrochemical analysis reveals that the performance increased by 35%. A capacitance of 136 Fg^{-1} was reported.	(Li et al. 2011)
3	Microwave exfoliated graphene activated by KOH.	The authors exfoliated graphene oxide using the microwave assisted method. The exfoliated graphene was then treated using KOH to activate the layers. The activation helped in reaching the capacitance up to 166 Fg^{-1}.	(Zhu et al. 2011)
4	Template activated calcined graphene	The authors prepared the reduced graphene oxide, through a template assisted method. Polyurethane (PU) sponge was immersed in the GO solution and allowed to absorb it. Once the PU sponge absorbed the solution, it was subjected to calcination leading to the formation of the reduced graphene oxide.	(Xu et al. 2016)

		Electrochemical studies show that the material possesses a high capacitance of 207 Fg^{-1}.	
5	Multilayer graphene coating via capillary driven, self-assembly	Capillary driven self-assembly of monolayers technique was used for the coating of the graphene on substrates. These electrodes show good electrochemical properties and specific capacitance of 80 Fg^{-1}.	(Biswas et al. 2010)
6	Silk cocoon derived graphene	The authors observed that carbonization at 400 ^0C helps in the formation of heavily nitrogen doped graphene. The graphene formed was studied extensively for electrochemical applications. The material shows a capacitance of 220 Fg^{-1}.	(Sahu et al. 2015)

1.2 Review of graphene based composites and its applications

Graphene based composites can be broadly classified into graphene-polymer composites and graphene nanoparticle composites.

1.2.1 Graphene based polymer composites

Graphene and graphene oxide gained attention as filler, to improve the properties of polymers. In the past, carbon nanotubes have been used as a filler to improve the properties. The better mechanical properties and large surface area of the graphene makes it a better choice over CNT's for the composite applications.

Incorporating graphene on to the polymer matrix is a challenging task. There are various challenges like, effective functionalization of graphene sheets, homogenous and effective mixing, controlling the stacking and folding of the graphene sheets inside the matrix etc. This thesis, however, focus on the review of graphene-metal oxide nanoparticle composites and their applications.

1.2.2 Graphene nanoparticle composites and its applications

The addition of graphene or graphene oxide to nanomaterial expected to improve the overall properties of the material by the synergistic interaction between graphene and the nanoparticles. Also, graphene with a very high surface area acts as a substrate over which, the nanoparticle could adhere, and at the same time, it can increase electronic properties because of the excellent electronic conductivity of the individual graphene sheets. Also, the nanoparticles could avoid the restacking of the graphene sheets. In this section a brief discussion about the graphene nanoparticle composites is included.

1.2.2.1 Graphene – zinc oxide composites and its applications in supercapacitors and biosensors

Zinc oxide is a wide band gap semiconductor with wurtzite structure. The band gap of ZnO is 3.2 eV, which can be tuned by the suitable band gap engineering. Low production cost and the non-toxic nature of the ZnO attracts the researchers to exploit the properties of ZnO, for low cost devices and other applications. ZnO finds applications in the fields of rubber manufacture industry, glass industry, medicine, food industry, as a pigment, UV coatings etc. (Pearton et al. 2005). The conductivity and stability of the ZnO vary with the experimental conditions and the doping level. The properties of ZnO are often tuned by varying the shapes, size, doping level and making composites with other materials. In this section, the properties and applications of ZnO nanocrystals and composites with graphene for the electrochemical applications are discussed. The various preparation methods and applications of the graphene – zinc oxide composites are reported by the researchers in the literature. The method of preparation, size, shape, graphene and zinc oxide ratios and the oxidation levels of the graphene determines the properties of the composites. The composites of ZnO and graphene oxide finds applications in the fields of photocatalysis, bio-sensing, electronics, photovoltaics, energy storage etc.

The electrochemical properties of ZnO are well described in the earlier literatures. ZnO and its composites are interesting candidates for the supercapacitor applications. Cobalt doped ZnO nanocrystals shows very high capacitance. The nanocrystals were around 4 nm in size and high surface area (> 200 m^2g^{-1}). The capacitance values of this doped

nanostrucutures reached up to 700 Fg^{-1} (Davis et al. 2012). This also shows that ZnO in its doped or composite form could be a good material for supercapacitor applications. ZnO nanocrystals, which are electrochemically deposited over the titania nanostructures shows good capacitive properties. The interaction between the porous structure of the titania template and the ZnO nanocrystals resulted in the enhancement of capacitance and the values reached up to 304 Fg^{-1} (Ray et al. 2015). Carbon nanotube is another material, which made considerable enhancement through the composite with ZnO. CNT, was coated on the carbon paper, which was further coated with ZnO with the help of sputtering. The composites thus made, are tested for its energy storage properties. The composite was found to be showing a capacitance of 48 Fg^{-1} in two electrode configuration. Also, the stability of the electrode was studied with the electrochemical cycling up to 300 cycles (Aravinda et al. 2013). In another attempt, ZnO and CNT composites were grown over Cu-Ni alloy. The morphological analysis revealed that the ZnO nanoparticles grown over the CNT surface. The prepared composites show high capacitance of 323 Fg^{-1}. The observed capacitance is better than that of the bare CNT and ZnO, indicating the enhancement in properties. Also, the good capacitance retention was observed up to 100 cycles (Zhang et al. 2009). In a similar work, the same group deposited ZnO by spray pyrolysis on to the CNT and electrochemical properties are studied. The capacitance reached up to 126 Fg^{-1}. In a recent work, carbon sphere core shell @ ZnO nanoparticles are tested for supercapacitor applications. The authors employed low temperature methods and avoided annealing, to avoid the structural changes. Electrochemical testing shows that the material reached capacities up to 630 Fg^{-1}. Also, the composites exhibited good cycling stability, keeping up to 70 % of its initial capacities even after 5000 cycles (Xiao et al. 2017). In general, composites of ZnO with carbon allotropes found to increase the properties of the material in a significant way and can be a good material for supercapacitors.

Graphene being an important allotrope of carbon, has got fantastic properties and established itself as a supercapacitor electrode material (Xiao et al. 2017). So it's interesting to study the effect of ZnO on the performance of the graphene oxide. One approach is, the green synthesis of the ZnO nanocrystals, on reduced graphene oxide through the use of supercritical carbon dioxide. The capacitance of this composite could

reach up to 314 Fg^{-1} (Haldorai et al. 2014). The electrodeposition method avoids the usage of binders, which acts as poorly conducting part of the supercapacitor electrode. The authors used one-pot synthesis of reduced graphene oxide and ZnO through electrodeposition. The performance of this electrode was promising and reached very high capacitance value up to 291 Fg^{-1}. The origin of the improved capacitance was attributed to lower internal resistance and the good contact properties of the electrode (Zhang et al. 2015). One pot synthesis of the composite was tried with the help of microwave. A mixture of zinc nitrate along with hydrazine hydrate and graphene oxide allowed to interact under microwave irradiation, which resulted in the formation of ZnO nanoparticles over the graphene sheets. The electrochemical measurements revealed that the composite shows high capacitance (201 Fg^{-1}) in sodium sulphate solutions. The cycle life of the electrodes also found be promising, retaining high capacitance values up to 3000 cycles (Guo et al. 2016). In another report, the synthesis of graphene-ZnO composites through solvothermal methods. This method produced graphene sheets which are embedded with ZnO nanoparticles having size distributions between 30 and 70 nm. The electrochemical performance was evaluated in 6M KOH solution and yielded capacitance values up to 122 Fg^{-1}. The authors also noticed that, the capacitance values obtained are greater than the capacitance values of the individual components in the composites, suggesting the synergistic improvement in the electrochemical properties (Saranya et al. 2016). The available literatures on the supercapacitor performance of the graphene-ZnO composite clearly shows that, there is synergistic improvement in the capacitance values through the introduction of ZnO. Developing better methods for the production and achieving good capacitance along with stability will be the key issue in the development of the graphene-ZnO composites for supercapacitor applications.

Graphene oxide and ZnO are reported to be good materials for the electrochemical sensing of glucose. Enzymatic sensing of the glucose was tested in most of the available literatures and non-enzymatic sensing was not much studied. Zinc oxide nanorods coated on ITO glass, reported to show sensing of glucose. The sensing mechanism was mediated by the glucose oxidaze enzyme. The challenge in enzymatic sensing is the denaturing of the enzyme at elevated temperatures. A temperature above 5 ^{0}C could

destroy the enzyme causing detection problems. Non-enzymatic sensing could be a good alternative to this, where the room temperature is not going to affect any of the components in the sensing system (Marie et al. 2015). Zinc oxide nanoparticles composite with multi-walled carbon nanotubes shows non-enzymatic glucose sensing properties in 1M NaOH solution. The authors observed that the alkaline condition mediates the sensing reaction. The size and shape of the ZnO nanoparticles, carbon nanotube content also affects the sensing mechanism (Baby et al. 2011). There are no reports in the literature, regarding the non-enzymatic sensing using graphene-ZnO nanoparticle composites. In this thesis, efforts are taken to explore the properties of these materials to achieve improved performance in trace detection and sensitivity.

Hydrazine hydrate is a chemical used in many chemical industries. Because of the widespread use in industries, the chances of leakage of hydrazine to the environment are quite high. Hydrazine is a highly poisonous substance and causes a number of problems in humans on prolonged exposure and believed to be carcinogenic. The accepted level of the hydrazine hydrate is restricted to ppm levels in foods and water. In order to control the hydrazine levels in the permitted levels, it is necessary to continuously monitor the presence of this chemical (Meneghelli et al. 2004). Electrochemical sensing is one of the easiest and reliable methods to achieve this. Different materials were tried to achieve good sensing properties in the past. Graphene and zinc oxide are known to be electrochemically active for hydrazine, hence allowing it as a hydrazine sensing electrode material.

Zinc oxide is reported to have good electrochemical activity towards hydrazine, nano nail structures of ZnO was tested for its hydrazine sensing properties in the past. These special structures effectively allowed the interaction of the molecule with the surface of the electrocatalyst. ZnO shows high sensitivity of 8.56 $\mu A cm^{-2}$ μM^{-1} and reproducibility over many cycles (Umar et al. 2008). The response time of the sensor was also under 5 s indicating a good sensor behaviour. The same group in another report discussed high aspect ratio ZnO nanowires, which show sensitivity of 12.76 $\mu A cm^{-2}$ μM^{-1} and quick response against the analyte. The electron mediation on the ZnO surface is the prominent factor affecting the sensing, varying the morphology of the nanoparticle can be a good method to tune the sensing (Umar et al. 2009). The inherent

conductivity of ZnO was one of the problems in utilizing the material to its full potential. The idea of making composites with materials having a higher conductivity is a suggested method. Multi-walled carbon nanotubes (MWCNT), having good electronic conductivity and excellent mechanical properties was incorporated with the ZnO nanoparticles to achieve this. The resulting composite shows a lower detection limit on 0.18 µM and a quick response time under 3 seconds (Fang et al. 2009). Another approach was, loading the carbon on top of ZnO nanoparticles through a calcination route, which resulted in sensing capabilities up to 9.4 μAcm^{-2} $\mu M^{-1.}$ The lower detection limit of the same composite was found to be 0.1 µM, which is lower than that of the MWCNT composites. In another report, graphene-ZnO composites were prepared by hydrothermal method. The composite shows larger linear range and lower detection limit. But the paper did not mention anything about the sensitivity values. The improved properties are attributed to the synergistic enhancement due to the graphene and ZnO interaction. From the literature, it can concluded that there is enough scope for hydrazine sensing using ZnO and its composites with graphene. In this thesis, emphasis is given to this part to find out the suitable composite concentration and other parameters of the electrochemical sensor.

1.2.2.2 Graphene – vanadium oxide composites and its application

Vanadium pentoxide (V_2O_5) is an easily synthesizable transition metal oxide, occurring abundantly in nature, with a unique layered structure, having mixed oxidation states (V^{2+}, V^{3+}, $V^{4+}$and V^{5+}) and possessing high energy density (Yang et al. 2011). V_2O_5 is a promising cathode material in lithium-ion batteries and supercapacitors (Tang et al. 2013). V_2O_5 hinder enhanced device performance, owing to its poor electrical conductivity and bulk material properties (Van et al. 2006). The usual strategy adopted was to make nanosized particles which shortens the electronic path, which is combined with doping or making composite with materials, like CNT, graphene etc. to overcome the limitations.

Amorphous hydrated vanadium pentoxide was reported in the past, (Lee et al. 1999) which shows excellent electrochemical properties. The authors described a simple preparation method, where V_2O_5 powder was heated in a crucible using a muffle furnace up to 950^0C and quenched into distilled water. The quenching resulted in the

formation of crystalline phase in the vanadium oxide, also water was absorbed on the amorphous surface leading to the formation of amorphous hydrated vanadium pentoxide (Lee et al. 1999). In a recent report, amorphous vanadium oxide was found to be a good material for sodium ion batteries (Uchekar et al. 2014). The better properties of the amorphous V_2O_5 were attributed to the fast Faradic reaction, that in the material stemming from a percolated diffusion network. In another attempt, to utilize the properties of amorphous V2O5, crystalline and amorphous V_2O_5 were mixed in different weight ratios and tested as Lithium-ion battery electrode. This improvement arises from the better reversibility in the amorphous regions and the mending of defect structures (Chang et al. 2013). Amorphous vanadium oxide/carbon electrode was reported by another group for rechargeable aluminium battery applications. The addition of carbon, resulted in improvement of the properties of amorphous vanadium oxide, which may be due to the better electronic conductivity and diffusion process (Chiku et al. 2015). Atomic layer chemical vapour deposition [ALCVD] is another method reported in the literature to produce amorphous vanadium oxide. This method produced homogeneous amorphous and intact thin films on the substrate. The lithium insertion capacity was found to be better than the crystalline vanadium pentoxide (Van et al. 2006). In general, the electrochemical properties of the amorphous vanadium oxide were always found to be better than the crystalline counterpart, suggesting amorphous hydrated vanadium oxide as a potential candidate for the lithium ion battery and other applications.

The properties of vanadium pentoxide were reported to be modified with the addition of graphene. Mostly the improvement in the properties came from the better surface area and electrical properties offered by graphene in the composite, which compensate the inherent problems in the vanadium oxide. Graphene modified nanostructures of vanadium pentoxide hybrids are reported by the researchers (Liu et al. 2015). A 2% addition of graphene in vanadium pentoxide results in capacitance of 438 mAh g^{-1}, which is almost equal to its theoretical capacitance (443 mAh g^{-1}). This hybrid also exhibits, the increased rate capability and longer cyclic stability. The authors attributed the improved performance to the combined effect of graphene on the structural stability, electronic conduction, vanadium redox reaction and lithium-ion diffusion supported by

various experimental studies (Liu et al. 2015). The free standing composite films of graphene and vanadium oxide was prepared by the simple filtration of the aqueous solutions of vanadium oxide and graphene sheets. This allowed the control over the graphene concentration, by simply varying the concentration in the filtrate solution. Graphene concentrations of 25% delivered highest capacitance value. This also shows that the addition of graphene will have some synergistic effects on the vanadium pentoxide, which will increase the lithium storage properties of the material (Qian et al. 2012). Ultralong single crystalline vanadium pentoxide/graphene composite was prepared through a green synthesis using an autoclave. This material shows a very high capacitance nearing the theoretical capacity of the vanadium pentoxide. Also, the material shows good rate capacities, which are attributed to the good kinetic properties of the composite material (Liu et al. 2011).

The literature review clearly shows that amorphous hydrated vanadium pentoxide is a good candidate for electrochemical applications. Also, it can be seen that the properties of vanadium pentoxide in lithium ion storage are greatly enhanced by the addition of graphene or graphene oxide owing to the synergistic enhancement in the kinetic properties. In this thesis, efforts are taken to incorporate the properties of these two materials to produce a better composite and studied its properties as an electrode material for lithium ion battery applications.

Dopamine is well known important catecholamine neurotransmitter in the mammalian central nervous system, whose detection is critically important, as it is effective in the determination of diseases related to human nervous system, such as Parkinson's disease (Qian et al. 2012) and schizophrenia (Adams et al. 2012). Vanadium pentoxide was reported to have shown the properties of electrochemical sensing (Suresh et al. 2014). Lithium doped vanadium oxide nanoribbons were prepared using a hydrothermal method (Zhuo et al. 2011). The prepared nanoribbons were, few micrometres in length and 200 nm in width. Glassy carbon electrode (GCE) surface was coated with this material along with the nafion® as a binder. The modified electrodes were used in phosphate buffer solutions for dopamine sensing applications. These modified electrodes show a detection limit of 1×10^{-7} M and a wide linear range. In another report, composites of vanadium oxide and polyaniline was used for the detection of

dopamine. The preparation method involved the oxidative polymerization of the aniline monomers in the presence of a vanadium oxide colloidal solution leading to a composite containing polyaniline over the vanadium oxide. GCE was modified with this composite and used as dopamine sensor. The composite shows a wide linear range between 6.6 μ M and 1.1×10^{-4} M concentrations. Also, the detection limit of the electrode was found to be 3.9×10^{-5} M (Suresh et al. 2014). Nickel doped vanadium oxide was investigated for the dopamine sensing by the same group. Ni doped materials were used for modifying GCE and used as an electrode, for the dopamine oxidation. This electrode shows a sensitivity of 132 nA μM^{-1}. Also, the wide linear range [6.6 – 96.4 μM] and better lower detection limit [28 nM] makes this electrode a better candidate as a sensor.

The studies on the dopamine sensing properties of vanadium pentoxide is limited in the literature. The reported results show that vanadium pentoxide is a good candidate for dopamine sensing. Amorphous hydrated vanadium pentoxide is not reported for its electrochemical sensing properties towards dopamine. In this thesis, efforts are taken to study the dopamine sensing properties of the amorphous hydrated vanadium pentoxide. Also, the effect of graphene loading on the sensing properties is also studied.

1.3 Objectives

- To prepare and characterize graphene oxide and reduced graphene oxide.

- To test reduced graphene for the applications in sensor for non-enzymatic hydrogen peroxide and as an electrode for supercapacitor.

- To prepare and characterize graphene – zinc oxide composites. Testing and application of graphene – zinc oxide composite as an electrochemical sensor of glucose. Investigation of above composite for the supercapacitor applications.

- To prepare and characterize graphene – vanadium oxide composites. To test application of these composites towards non-enzymatic dopamine sensor and cathode of Lithium ion battery.

Chapter 2

Experimental methods

2.1 Characterization techniques

2.1.1 X-Ray Diffraction (XRD)

X-ray diffraction is a non-destructive testing method, utilizing X-rays for understanding the crystal structure of the materials. X-rays have a wavelength (0.5 – 2.5 Aº) comparable to the magnitude of interatomic distances. The X-ray photons interact with the electrons, some of them will be deflected. This results in the interference of the deflected rays. Fig. 2.1 represents the interaction of X-rays inside the crystal.

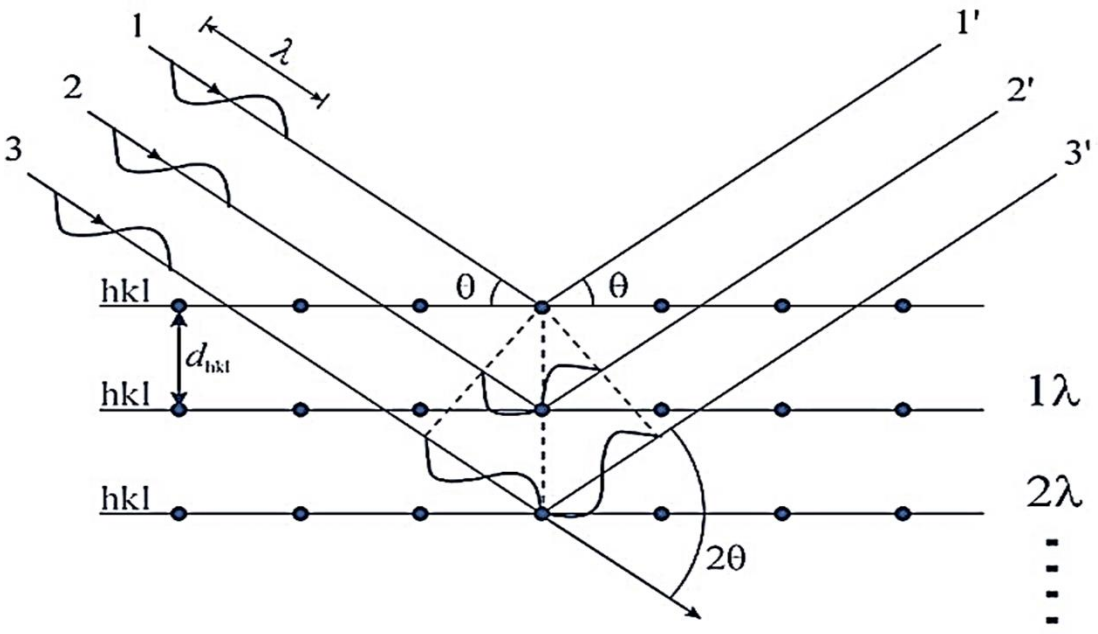

Figure 2.1: Schematic representation of the reflection of X-rays from the atomic planes.

Bragg's law can be written as,

$$n\,\lambda = 2d\sin\theta$$

Where, d is the distance between two planes, λ is the X-ray wavelength, θ is the angle which incident photon makes with the surface of the crystal. Different d-spaces satisfies the Bragg's condition at different angles, resulting in the XRD spectrum of the sample, which is like a fingerprint of the sample. XRD is a major technique to differentiate between the materials and to understand the material quality. For a polycrystalline material, powder diffractometer is the ideal instrument to study the properties. Once the pattern is recorded by the instrument, the spectrum can be compared and matched with the available standard libraries and a conclusion about the material can be attained. The Figure 2.2 schematically represents the elements of a powder diffraction pattern (Cullity, 1956). Rigaku MiniFlex600 is used for the XRD analysis of the samples in this work. All the samples are powdered and mounted on glass grove with the help of special adhesive and tested to obtain the crystallographic data.

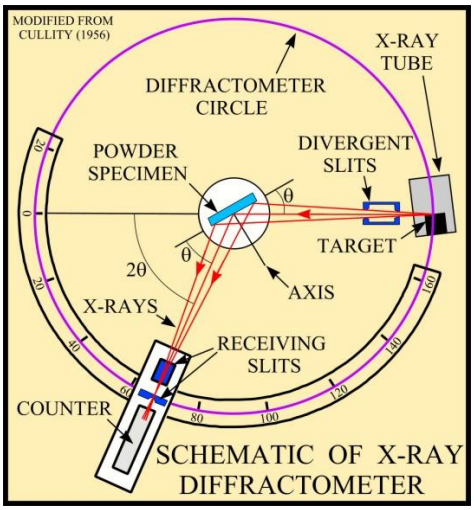

Figure 2.2: Schematic representation of a powder XRD system.

The crystallite size of the material can be approximated from the XRD data using Debye-Scherrer formulae,

$$\text{Particle Size} = (0.9 \times \lambda)/ (d \cos\theta)$$

where, $\lambda = 1.54060$ Å (in the case of CuKα1) so, $\Theta = 2\theta/2$ (in the example = 20/2) and d = the full width at half maximum intensity of the peak (in Rad). The dominating peak is used for the calculation of the crystallite size.

2.1.2 Raman Spectroscopy

Raman spectra is an important tool to differentiate and measure the quality of different carbon species such as graphene, carbon nanotubes (CNT's), fullerenes and graphite. The investigations of carbon species using Raman spectroscopy were started long back (Wang et al. 1990). In graphene the occurrence of G and D bands can distinguish the number of layers and the quality of the graphene produced. The G band is usually observed around 1580 cm^{-1}.

The underlying principles of Raman spectroscopy were first reported by C.V. Raman. Raman spectroscopy works on the principles of Raman Effect. The majority of the radiation is scattered elastically and known as Rayleigh scattering. When an inelastic scattering occurs for an incident radiation at the vibrating molecules, the frequency of a small part of the scattered radiation is different from the incident monochromatic radiation. The wavelength shifted (Raman scattered) radiations can be either in the shorter side or longer side. The longer wavelength shift is known as Stokes shift and the shorter wavelength shift is known as anti-Stokes shift. The Fig. 2.3 schematically represents the Rayleigh scattering, Stokes Raman scattering and anti-Stokes Raman scattering. In this case, the photons excite electron to a virtual energy level and on deexcitation, they emit a scattered photon. The Stokes scattering is commonly observed compared to the anti-Stokes Raman scattering. Mostly the Raman spectroscopy relies on Stokes scattering for deducing information about the sample.

The measurement of the inelastically scattered radiation is the key part in a Raman measurement. The current Raman spectrometers use laser as the monochromatic light source. With the help of laser it is possible to get sufficient intensity of the Raman scattered light out of the material which was not possible earlier.

The Raman spectroscopy has a major advantage over other spectroscopic techniques, owing to the fact that, it can be used for qualitative and quantitative analysis of the samples. The measurement of frequency of the sample can be used for the qualitative analysis, whereas the measurement of intensity can be used for the quantitative analysis of the sample.

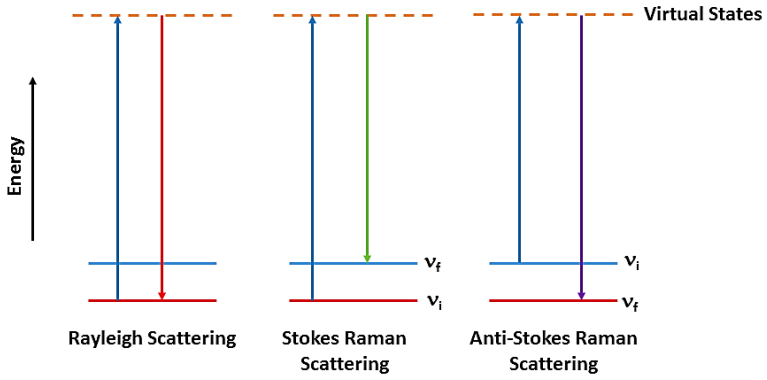

Figure 2.3: Schematic representation of the Raman scattering.

2.1.3 Scanning Electron Microscopy (SEM)

In SEM, electrons are produced, either using thermionic or field emission. The field emission produces electron beams with higher current density and can be operated without high temperature and results in better imaging. Field emission SEM's are preferred over the normal SEM's because of the higher resolution. The electron beams are focussed using an array of electromagnets. Compared to the optical microscopes, where the lenses with fixed focus is employed, the electromagnetic lenses offer a lot more control over the focussing of the beam used. The focus can be controlled by controlling the current passing through the electromagnet, which enables us to fine tune the imaging technique. SEM finds applications in a vast variety of the fields including life sciences, materials science, semiconductors and microelectronics and earth sciences.

2.1.4 Energy Dispersive X-ray Analysis (EDAX)

Energy Dispersive X-ray Analysis is a technique used to analyze the elemental composition of the material. During the interaction of electrons with the sample, X-rays are produced, which consist of vital informations regarding the elemental composition. An associated detector could find out the intensity of these X-rays, which can be used for the determination of the composition. EDAX can give the atomic percentage and weight percentage of the atoms present.

2.1.5 Transmission Electron Microscopy (TEM)

Transmission Electron Microscope (TEM) finds application in many fields, such as nanotechnology, life sciences, gemmology etc. TEM analysis could reveal the size, shape, morphology and crystalline size of the material. TEM utilizes a beam of electron for the analysis of the material. Compared to an ordinary microscope, TEM has a higher resolution, since it uses electrons. A relation between the wavelength and the voltage can be established ($\lambda \approx (15/V)^{1/2}$ nm). Also, the wavelength of the electron can be controlled by the accelerating field. Because of the high energy of the electron, high depth of field, high resolution and high magnification are possible inside a TEM.

An electron gun generates electrons, either by field emission or thermionic emission. Electromagnetic lenses bend the electron beam for focusing. A projector lens, vacuum system and electronic system are designed to act as the electromagnetic lens. The electron beam from an electron gun is focused on the specimen with an electromagnetic condenser lens by varying the current to the lens. Air is removed from the system containing the lenses and specimen by using a high efficiency vacuum system to obtain a clear image since electrons are deflected by collisions with air molecules. The specimen scatters electrons passing through it, and the beam is focused by magnetic lenses to form an enlarged, visible image of the specimen on a phosphorescent screen. Depending on the nature of the specimen, a diffraction pattern usually consists of a series of rings (for specimens consisting of many randomly oriented microcrystals) or a discrete lattice of sharp spots (for specimens with a single crystalline domain). Each sharp spot in the diffraction

pattern is an image of the electron source. Selected area diffraction mode is similar to XRD, but with a higher resolution so it is possible to index nano structures (CaO and Wang 2011, Quinten et al. 2010).

2.1.6 UV-Visible Spectroscopy

Ultra Violet and visible (UV-Vis) absorption spectroscopy is the measurement of the attenuation of a beam of light with a wavelength in the range, after it passes through a sample or after reflection from a sample surface. When light passes through a sample,

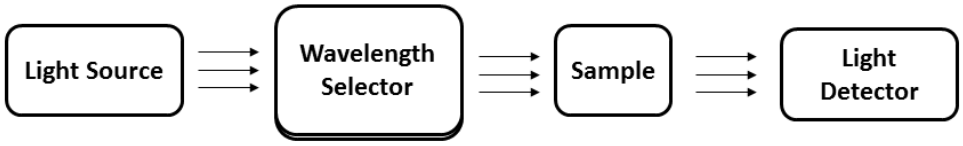

Figure 2.4: schematic representation of the UV-Visible spectrometer

some amount of light will be transmitted and some amount will be absorbed. The amount of light absorbed can be calculated by finding out the difference between the intensities of the incident and absorbed radiations. This value of absorption intensities can be plotted against the wavelength of the light to obtain the absorption spectra of the sample of interest. The absorption coefficient, α can be written in terms of the initial intensity (I_0), the final intensity (I) and the thickness of the medium (t) as,

$$I(\lambda) = I_0(\lambda)e^{-\alpha(\lambda)t}$$

The absorption coefficient depends upon on the wavelength of the incident light. If the energy of the incident beam is less than the energy bandgap, almost all the energy is transmitted, since there are no transitions occurring. If the energy of the incident photon is equal to the energy band gap, it will be absorbed by the material and can be seen as an absorption maximum in the spectra. In this work, UV-Visible studies were carried out using Ocean Optics UV2000 UV-Vis spectrophotometer. Fig. 2.4 Represents the schematic of the UV-Visible spectrometer used.

2.1.7 Fourier Transform Infrared Spectroscopy (FTIR)

FTIR is a powerful technique to characterize materials to understand the chemical bonding and molecular structure of the material, which can be considered as a fingerprint of the material. The proper analysis of these bonding can lead to the

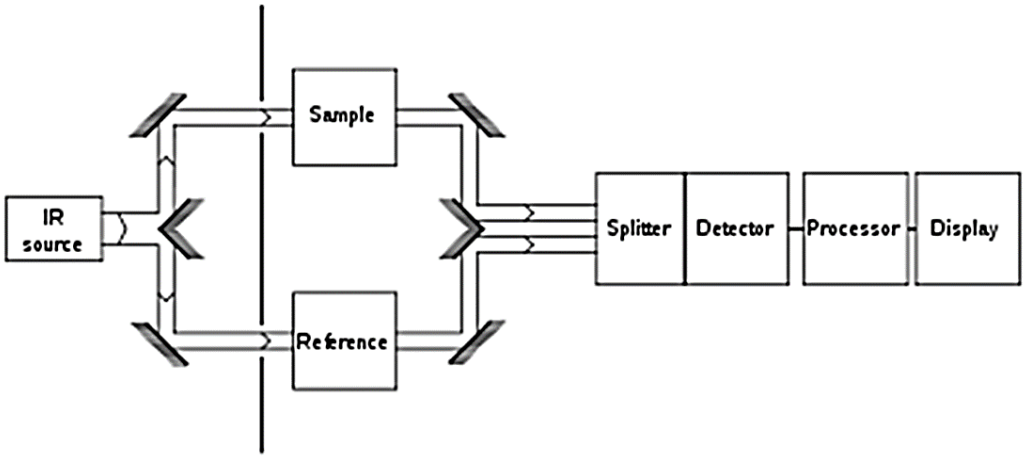

Fig. 2.5: Schematic representation of the parts of an FTIR spectrometer

identification of the material. Fig. 2.5 schematically represents an FTIR spectrometer. An IR radiator source, monochromator and the IR detector are the main components of an FTIR spectrometer. IR radiators are heated to emit radiations in the IR region. Two IR beams from the same source will be passing through the sample and reference cavities. An optical chopper focusses these beams alternatively on the detector. Using a series of prism or grating arrangement the beam from the sample will be focussed on the detector. The detector generates corresponding electrical signals, to take the data out of the instrument.

2.2 Electrochemical characterizations

Electrochemistry can be considered as the response of a chemical system towards an electrical signal. There are two processes happening at the electrodes, namely

- Oxidation: Loss of electron during a reaction causes oxidation
- Reduction: Gain of electron during the reaction

Commonly these reactions are called as redox reactions. The study of these reactions throw light on the electrochemistry of the system.

2.2.1 Cyclic Voltammetry (CV)

The advancement in the field of voltammetry can be related to the early progress in the field of polarography (electrochemical process at the mercury electrode). These initial studies in this field brought Nobel Prize for Heyrovský in the field of chemistry (Heyrovský et al. 1966). Cyclic voltammetry is a widely used technique in the electrochemistry. CV is equally powerful in giving details about the thermodynamics and kinetics of the system at the same time. CV was used as a method to study the thermodynamics of the reaction in the initial stages of the development of the field. Thereafter, with the arrival of new studies on the time dependent properties, power to deal with the kinetics of the reaction is explored. Even in complex systems like a modified electrode, where the electrode interaction is complex, CV will be able to show the underlying trends.

Further developments in the field give rise to the scanning of potential and cyclic voltammetry (Nicholson et al. 1964). Today CV has grown to a stage, that it can be applied to a variety of fields from pure electrochemistry to the biological sciences and a properly interpreted data, along with other characterization techniques to throw light on the underlying principles. Also to understand the mechanism behind an electrochemical reaction, cyclic voltammetry can be combined with other techniques such as diffraction techniques, quartz crystal microbalance, UV-Visible spectroscopy etc.

2.2.2 Chronoamperometric (CA) measurements

Chronoamperometry is a controlled potentiometric technique. It involves applying a step potential from a point where no faradic reaction occurs, to a potential at which, surface concentration of reactive species is zero. In a reaction, the rate can be considered as diffusion controlled ie, the diffusion of the analyte from the electrolyte to the electrode. Hence, the current depends upon the concentration of the analyte. If current is plotted against time, one could observe that it is maintained constant, as long as the analyte concentration remains the same. Once, the analyte is starting to deplete the current also decreases. Such a mechanism can be used for finding out the concentration of the analyte in a solution, which is the basis of chronoamperometric sensor.

2.2.3 Constant Current Charge-Discharge Measurement

The constant current charge-discharge is used to check the performance and the cyclic life of the electrochemical energy storage systems. Even though, the current can be varied within, a constant current charging and discharging cycle is preferred over the other. Once the set voltage is reached, the device is allowed to discharge. The capacity of the device can be calculated from the charge-discharge behaviour of the material. At the discharge cycle it can often be noticed that, there will be an ohmic drop in the voltage. The ohmic drop can be related to the equivalent series resistance of the circuit. Further, the resistance value can be deducted from the ohmic drop using Ohm's law.

2.2.4 Electrochemical Impedance Spectroscopy (EIS)

Electrode kinetics of a complex electrochemical system can be studied using non-steady state measuring techniques. Reaction rate constants, diffusion coefficients, charge transfer resistance and double layer capacity affect the proceeding of the reaction to a new steady state. In this regard impedance spectroscopy represents a powerful method for investigation of electrical properties of materials and interfaces of conducting electrodes. By definition, if a monochromatic alternating voltage $U(t) = U_m \sin(\omega t)$ is applied to an electrode then the resulting current is $I(t) = I_m \sin(\omega t - \vartheta)$, where ϑ is the phase difference between the voltage and the current and U_m and I_m are the amplitudes of the sinusoidal voltage and current, respectively. Then the impedance is defined as

$$Z = U(t)/I(t) = |Z|\, e^{j\vartheta} = Z^1 + jZ^{11}$$

with $$J = (-1)^{1/2}$$

where Z^1 and Z^{11} are the real and imaginary part of impedance Z, respectively.

The measurement of the impedance spectroscopy consists of the application of a small signal, which can be a time dependent potential or current. Keeping the amplitude of the signal as low as possible, helps in avoiding frequency mix products. The equivalent circuits can be drawn from the obtained impedance plot, by considering it, as a combination of linear solution resistance and capacitive interfaces. This equivalent circuit will be much helpful in understanding the mechanism involved in the reaction.

Equivalent circuits: Any electrochemical cell can be represented in terms of an equivalent electrical circuit that comprises the combination of resistances, capacitances or inductances, as well as mathematical components. Representing the electrochemical cell in such a way, will be helpful in understanding the underlying mechanisam and tweaking the material properties, to obtain better electrochemical cells. An ideal electrode consists of double layer capacitance element and solution resistance in series. Different models have been proposed for the fitting and analysis of the equivalent circuits. In this thesis, EC-Lab® software is used for the fitting and analysis of the circuit.

Some of the basic elements used in the impedance analysis is given in Table 2.1

Table. 2.1: Common electrical elements

Component	Current Vs Voltage	Impedance
Resistor	E = IR	Z = R
Inductor	E = L (di/dt)	Z = jwL
Capacitor	I = C (dE/dt)	Z = 1/ jwC

Serial and parallel combinations of circuit elements: For an effective modelling of the electrochemical cell, more than one elements may be required. In this case, the elements can be arranged serially or parallaly to obtain better fit models.

Some of the physical parameters, which are part of any electrochemical cells are like, solution resistance, double layer capacitance, polarization resistance etc. The solution resistance is an integral part of most of the electrochemical cells, which arises from the resistance offered by the electrolyte and the electrode-electrolyte interfaces. The double layer capacitance is another parameter, when an electrode is immersed on the electrolyte, the charged ions will be adsorbed on the electrode surface. This layer and the charged electrolyte will be separated, by an insulating layer leading to capacitive nature. While modelling such an electrode, this double layer has to be replaced with a capacitive element. Similarly, other processes happening on the electrodes also have to be incorporated, with the fitted equivalent circuit to obtain better results.

The coatings on electrodes have to be analysed carefully using impedance spectroscopy, in order to have a better idea about the electrochemistry. As a starting step, a purely capacitive cell model consisting of resistance and capacitor can be considered. But the real electrodes usually does not follow such a simple model, in these case more complex models have to be utilized. Randles cell is one of the widely used cell models. It includes, solution resistance, double layer capacitor and a charge transfer resistance. Usually, this model is used as a stepping stone for building other complex models.

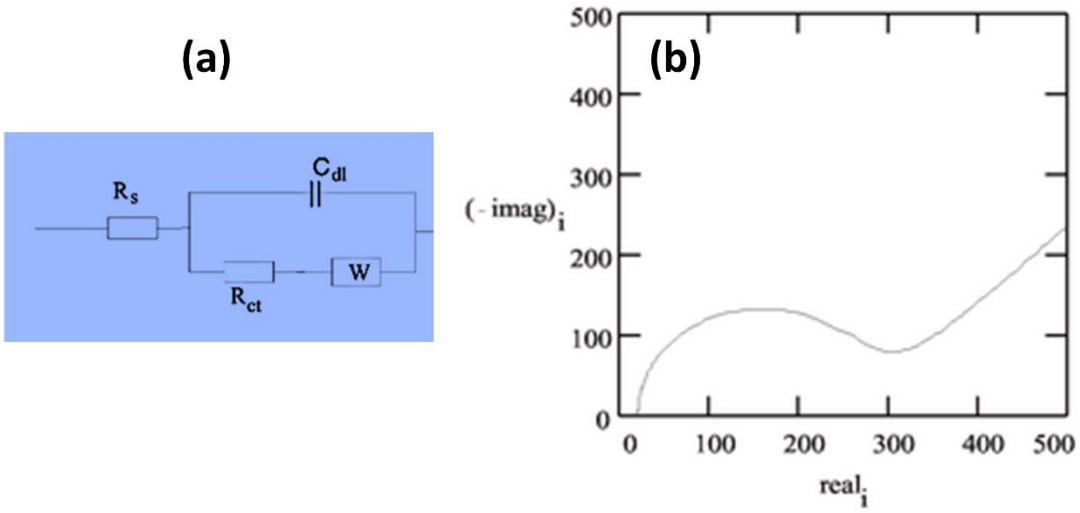

Fig. 2.6: (a) Randles cell: equivalent circuit with mixed kinetic and charge-transfer control (b) Nyquist diagram of mixed circuit.

The kinetics of the electrochemical reaction in Randels cell is determined by the diffusion process at the electrode. The Fig. 3.6(a) shows, the equivalent circuit of such a cell with mixed kinetic and charge-transfer control. The Nyquist plot for such a circuit is given in Fig. 2.6(b). Here, the plot is characterized by a semicircular region and the straight line region, which refers to the capacitive part of the circuit.

2.3. Electrochemical applications

2.3.1 Supercapacitors

Supercapacitors, also called as electrochemical capacitors or ultracapacitors, are high power energy storage devices, that can be charged to the maximum and discharged in seconds. Supercapacitors can be considered as a device between the conventional

capacitors and batteries. Fig. 2.7 shows the Ragone's plot for various energy storage devices. It can be seen that they have high energy density compared to the normal capacitors and high power density compared to the batteries and fuel cells. This makes it important in some of the hybrid vehicles and power supplies. Supercapacitors can be deployed to deliver high power density whenever it is required along with a battery/supercapacitor to run a battery powered vehicle. This makes it is important to have better supercapacitors for cleaner and greener energy systems. Supercapacitors have high power densities [> 10kW/kg], long cycle life and long shelf life and there are efforts going around the globe to increase its capacities.

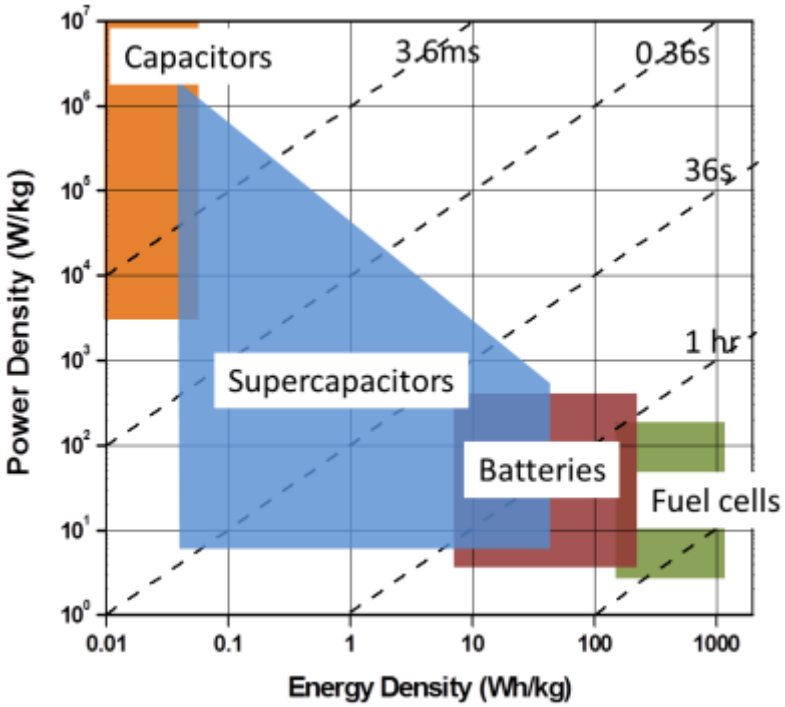

Figure 2.7: Ragone plot for various energy storage device (Ko et al. 2000)

Based on the energy storage mechanism supercapacitors can be divided into two categories, namely non faradic and Faradic supercapacitors. Non faradic capacitor stores charge in an electric double layer, that is set up by the charge separation, at the interface between the high surface area electrode and an electrolyte. Fig. 2.8 schematically represent the charge storage mechanism in a non - faradic capacitor. Graphene, CNT etc. are examples for materials exhibiting non faradic charge storage mechanism. Faradic exhibit an electrode reaction along with the electrochemical double

layer capacitance. Usually faradic capacitors possess high capacity compared to the non-faradic capacitors, but lacks long cyclic life. Usually materials exhibiting faradic and non-faradic properties are used for making composites in search for synergistic effect and improving the properties (Conway 1999).

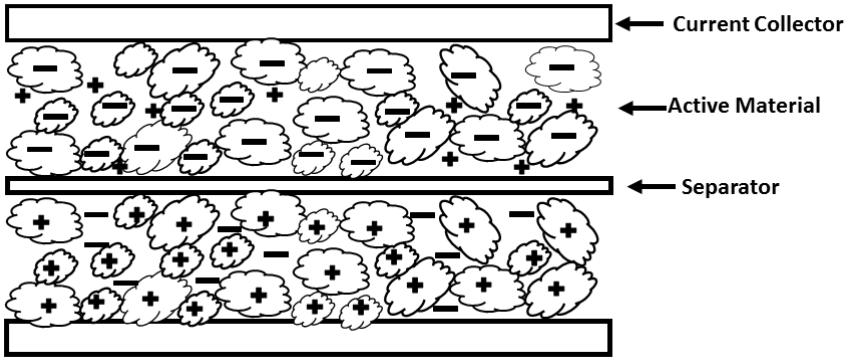

Figure 2.8 Schematic of an electrochemical double layer capacitor.

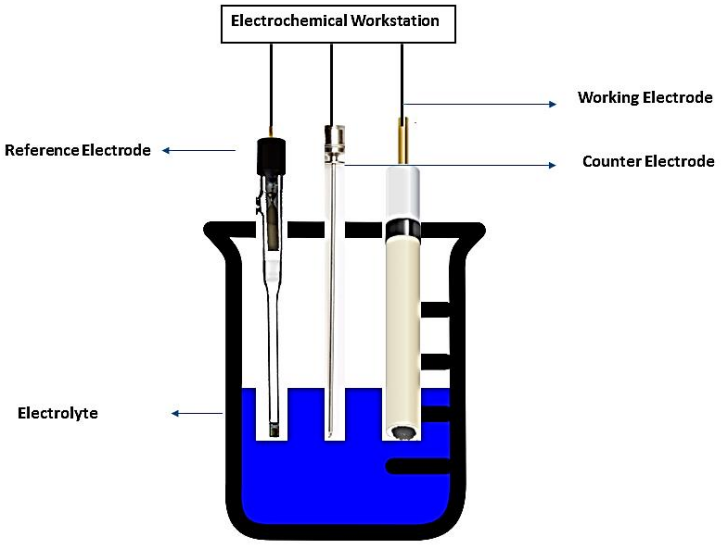

Figure 2.9 Schematic representation of three electrode configuration

The capacitance of a material can be tested using two different methods viz. three electrode configuration and two electrode configuration. Three electrode configuration is usually seen in electrochemical research and consist of a working electrode, reference electrode and counter electrode dipped in an electrolyte and connected to a workstation.

Fig. 2.9 schematically represent the three electrode configuration used for the measurement of capacitance of a sample. This method could clearly reveal the material property and its usability as an electrode material in supercapacitors. The drawback of the method is that the method overestimates the capacitance to twice or more. So, the method can be used for estimating the capacitance at a laboratory scale and proposing its applications. Whereas, the two electrode configuration, exactly mimic a normal capacitor (Stoller et al. 2010).

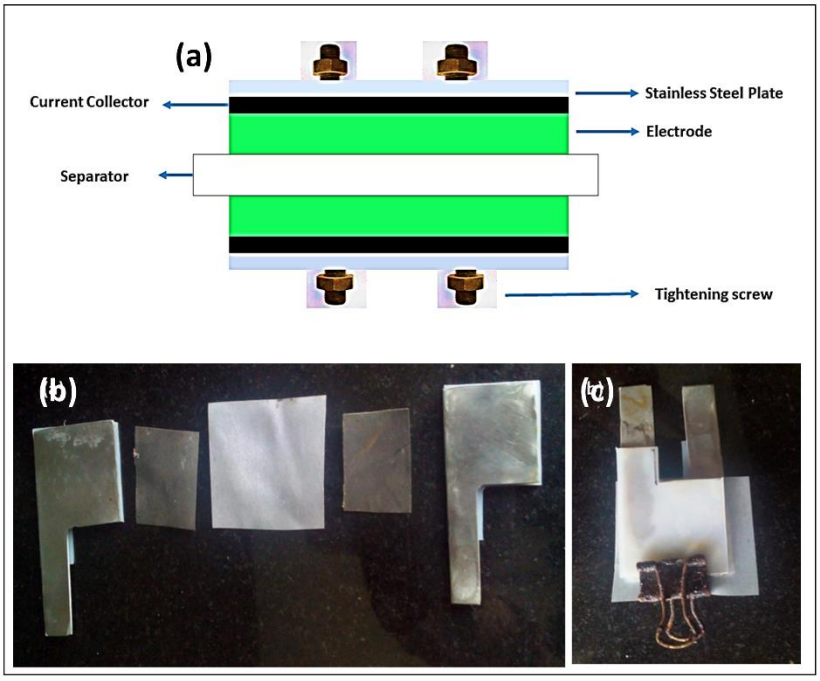

Figure 2.10 (a)Schematic of a supercapacitor using two electrode assembly (b) parts of a two electrode assembly and (c) assembled supercapacitor for testing

The schematic representation of a two electrode supercapacitor configuration is given in Fig. 2.10 (a). The main components of this configuration are, the current collector, electrodes, separator and the electrolyte. All these components will be tightened inside two stainless steel plates using Teflon screws. Fig. 2.10 (a) and (b) represents the parts of a real supercapacitor and assembled prototytpe for testing.

- Current collector: The current collector acts as the substrate for pasting the active material as well as connecting the material to the outside circuit. Normally, materials like carbon paper or carbon fabric is used as the current

collector. The capacitance offered by the current collector will be negligible compared to the active material present.

- Separator: Separator is an ionic conducting membrane that separates the positive and negative electrode. The separator will be impregnated with the electrolyte and it avoids any electronic short circuit between the two electrodes.
- Electrolyte: Electrolyte is one of the key parts of the supercapacitors. They act as the ionic conducting medium and supply the ions. They can be either aqueous based electrolytes or organic liquid based electrolytes. Acids, alkaline solutions are part of aqueous electrolytes. The operation voltage for this aqueous based electrolytes are limited, but possess a higher charge storage capacity. The organic and ionic electrolytes offer a wider range of operating potential, compared to aqueous based electrolytes but possess a lower capacity. There are are still research interests in the field, to replace the electrolyte solutions by solid or gel polymer based electrolytes, to overcome the complexity arising in handling the solution inside the capacitors.
- Electrode material: This is one of the most important parts of the supercapacitor. The capacity, cycle life, power density and energy density of the capacitor can be tuned to some extend by varying the electrode material properties. The electrode material can be faradic, non-faradic or hybrid in nature. The electrode material, usually consists of conducting agent, binder and the active material. The capacitance of an electrode may be greatly affected by higher internal resistance. In such case, so as to reduce the internal resistance of the system, a conducting agent will be added to the electrode material. Carbon black is usually used as a conducting agent. Binder makes sure that, there is proper adhesion between the active material and the surface of the current collector. It also stabilizes the electrode from peeling off during the operation. The peeling off of the electrode material can cause a major drop in capacity or the failure of the supercapacitor. Polymers like PVDF in N-methyl pyroledene is a commonly used binding agent. Together, the binding agent and the conducting agent constitute 10-30% of the total weight of the working electrode. Active material constitutes the largest portion (70-90%) of the working electrode. The active material can be of faradic or non-faradic in nature depending upon the charge

storage mechanism. The electrode is prepared by mixing binder, active material and conducting agent in the respective ratios and making a fine slurry and coating it over the current collector.

2.3.2 Electrochemical Sensors

The commercial miniaturized electrochemical sensors were available in the mid-80s showing an increasing research in the field and owing to the demand from the biological and environmental sciences. Today they have grown in such a way that, electrochemical sensors are part of wearable electronics like watches and pedometers. The field is still demanding for accurate and reliable sensors to cope up with the advancement in the other fileds like artificial intelligence.

The important components in an electrochemical sensor are, the electrolyte and electrode material. By varying these two in different ways, selectivity and sensitivity can be tuned.

A typical electrochemical sensor consist of

- Working electrode

  Working electrode is the one, in which the sensing reaction occurs. The reaction can be either oxidation or reduction, and depending on that, the current flow will be in the respective direction. Usually, a modified electrode act as the working electrode. Modified electrode is the one, in which there is one unreactive conducting material (such as platinum, gold, or glassy carbon electrode) and one active material along with a binder. The electrode reaction depends on the properties of all these materials and how they are interacting with each other.
- Reference electrode

  Reference electrode has a fixed potential and does not vary with the analyte or other fluctuations in the system. The commonly used reference electrodes include, standard hydrogen electrode (SHE), saturated calomel electrode (SCE) and silver-silver chloride electrode.

- Counter electrode (Auxiliary electrode)

  In the electrochemical system the current is not allowed to pass through the third electrode, known as the counter electrode. This is to ensure that, there is no fluctuation in the potential of the reference electrode. The counter electrode should be selected in such a way that, the electrode should not react with the electrolyte or analyte or dissolve in the electrolyte. Usually, platinum is used as the counter electrode, because of its less reactivity towards electrolytes.

- Electrolyte

  The electrolyte is the solution in which, all the three electrodes are dipped and the reaction taking place. The analyte is added directly to this electrolyte and mass transport and diffusion take place from the electrolyte to the working electrode. Usually, the electrolyte is chosen is such a way that, the electrode or analyte does not react with the solution and does not make any changes in the signal output. The ions present in the electrolyte does not contribute to any electrode interaction. Most of the electrochemical reactions are pH sensitive in nature. In that case buffer solutions are used to prevent any fluctuations in the electrolyte pH. Ammonia buffer, Phosphate buffer, etc. are the examples of the buffer solutions. The buffer solution is also selected depending on the analyte to be sensed.

- Electrochemical workstation/ measurement setup.

  The workstation is basically the controlling unit, which applies the potential and measures the current. The studies, described here are carried out on the Bio-Logic SP-150 instrument.

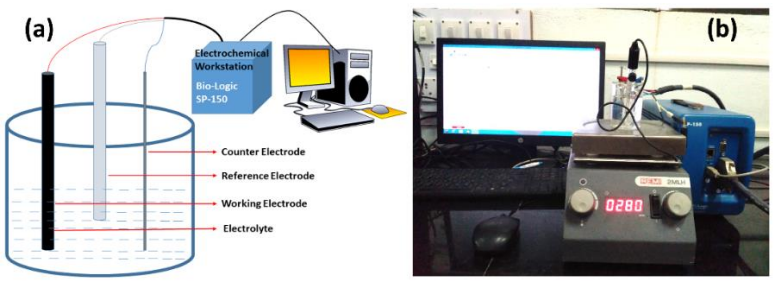

.2.11 (a) Schematically represent the setup used for the sensor measurement with the respective parts marked (b) image of the Bio-Logic system used for the measurements.

The schematic representation of an electrochemical sensor is shown in the Fig. 2.11. The sensing mechanism is usually based on the oxidation or reduction of the analyte during the reaction. The amperometric response (the change in current with respect to the change in concentration of analyte), and potentiometric response (change in the potential with respect to the change in concentration of the analyte) are the commonly used techniques for the determination of the analyte. Throughout the study, amperometric sensing is used for the sensing in this thesis. The analyte used can be, hazardous molecules to biomolecules provided there should be an electrochemical reaction or electron transfer at the working electrode, which can be recorded as a signal.

2.3.3 Lithium-ion Batteries

A battery is a device that converts the chemical energy into electric energy by means of an electrochemical oxidation-reduction (redox) reaction. During charging and discharging, opposite reactions take place at the electrodes, during which conversion of electrical energy to chemical energy and vice versa occurs. A battery can be considered as consisting of one or more cells, which is a basic electrochemical unit. The development of batteries in the initial stages started with dischargeable batteries and later rechargeable batteries, where the redox reaction is used to charge and discharge the batteries. Even though, the anode and cathode interchanges in a redox reaction, conventionally the anode and cathode is fixed according to the discharge pattern in batteries. Recently, there have been discussions regarding this use of terms anode and cathode in batteries. In this thesis, the conventional anode and cathode terms are used and they are defined as,

- The anode or negative electrode-the reducing or fuel electrode-which gives up electrons to the external circuit and is oxidized during the electrochemical reaction.
- The cathode or positive electrode-the oxidizing electrode-which accepts electrons from the external circuit and is reduced during the electrochemical reaction.

The batteries can be broadly classified into four and they are,

- Primary batteries

  Primary batteries cannot be recharged by common methods. Once the battery is fully discharged, they are discarded. Depending on the electrolyte they can be dry or wet cell. Dry cell is used in many portable electronics devices, toys, etc. because of its low cost and ease of use.

- Secondary or rechargeable cells or batteries

  These are cells which can be recharged to its initial state by passing a current in the opposite direction of the discharge. The main advantage of these kind of batteries is that, they can be reused again. These kind of batteries are mainly used in applications like hybrid vehicles, UPS power supply, mobile devices etc.

- Reserve batteries

  This battery is intended to store for a long time without any discharge. A molten salt battery used in missiles is an example for reserve battery. To activate the battery, the solid salt should be melted to conduct and discharge the battery. These batteries are very important in the defence related applications.

Lithium ion batteries [LIB's] belongs to the secondary batteries. It consist of electrodes made up of compounds, which can take part in the lithium ion intercalation reaction. These batteries are also called rocking batteries, since the lithium ions rock back between the anode and cathode during charging and discharging. Usually, the positive electrode will be a metal oxide such as lithium cobalt oxide ($LiCoO_2$), lithium manganese oxide ($LiMn_2O_4$) etc. The commonly used negative electrode is graphitic carbon. These materials are also layered in structure, making it possible to insert or extract the lithium ions from the material effectively.

The main advantages and disadvantages of the LIB's are listed below,

Advantages

- Sealed cells; no maintenance required
- Long cycle life
- Broad temperature range of operation
- Long shelf life
- Low self-discharge rate
- Rapid charge capability
- High rate and high power discharge capability
- High coulombic and energy efficiency
- High specific energy and energy density
- No memory effect

Disadvantages

- Moderate initial cost
- Degrades at high temperature
- Need for protective circuitry
- Capacity loss or thermal runaway when overcharged
- Venting and possible thermal runaway when crushed
- Cylindrical designs typically offer lower power density than NiCd or NiMH

2.3.3.1 Lithium intercalation and working of a Lithium-ion battery

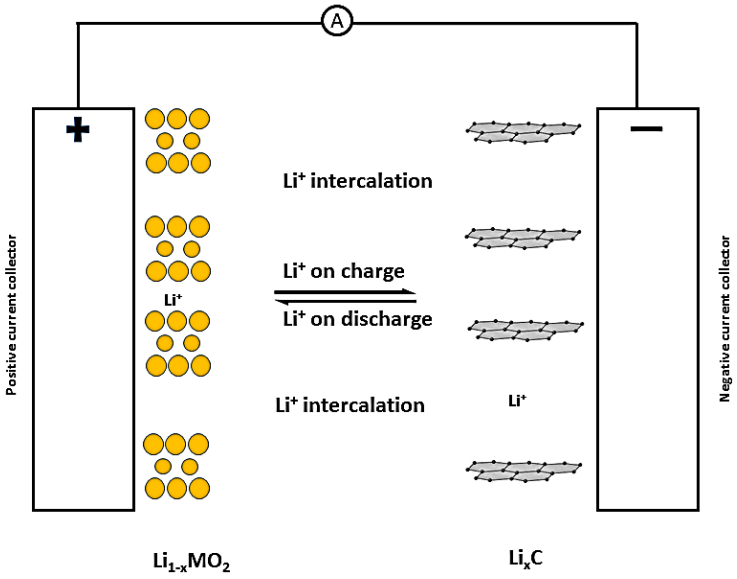

Figure 2.12: Schematic of the lithium intercalation process in a cell.

LIB's operate by reversible reactions incorporating and removing the lithium ions from the electrode through a reversible electrode reaction, without significant structural changes in the host materials. Usually, materials with layered structures are preferred as an electrode material, to improve the lithiation and de-lithiation process. Metal oxides are the prefered candidates for the positive electrodes and the graphitic carbon species are used as the negative electrode. During oxidation of the positive electrode (charging), lithium ions from the positive electrode intercalate to the negative electrode. Fig. 2.12 schematically represents the lithium the reaction mechanism. Here, $LiMO_x$ represents the positive electrode material and the other electrode is the carbonaceous negative electrode. As far as lithium ion batteries are concerned, the use of crude Li metal is discarded and this helps in lesser risk, because of the lesser reactivity and better cyclic life. Even though, a half cell arrangement where, the capacity of the electrode is measured against the lithium metal is employed in the estimation of the capacity of the material.

Positive electrode material

Commercially, lithiated metal oxides are used as the positive electrode material. The capacity of the material to insert lithium ions can change the charge storage capacity of the material. Along with that, the reversible nature of the reaction also important. The inability to reverse the reaction, can badly affect the longer cyclic life of the reaction. The cell voltage and energy density of the cell depend upon the potential, at which the lithium exchange reaction occurs with respect to the lithium metal. Also, there should be adequate electronic conductivity and Li^+ ion mobility inside the material to ensure the proper charge-discharge process. The requirements for a good positive electrode material is listed out below,

- High free energy of reaction with lithium
- Can incorporate large quantities of lithium
- Reversibly incorporates lithium without structural change
- High lithium ion diffusivity
- Good electronic conductivity
- Insoluble in the electrolyte
- Prepared from inexpensive reagents
- Low cost synthesis

2.3.3.2 Coin cell fabrication

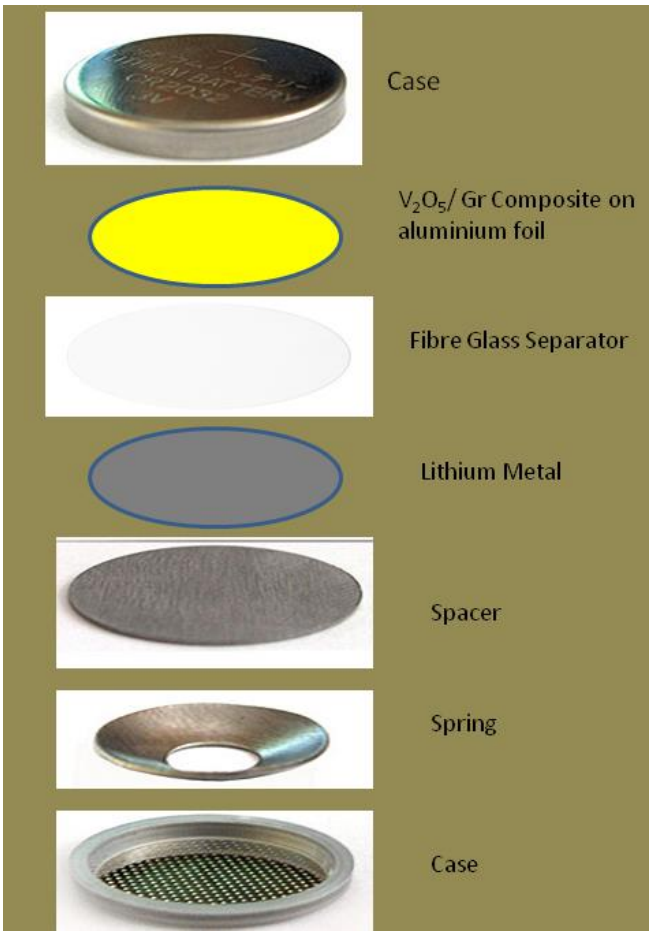

Figure 2.13: represents the parts of the coin cell.

The parts of a coin cell are schematically represented in the Fig. 2.13. The coin cell described in this work was prepared in the following way. Initially, the required amount of the composite was measured and taken. A slurry was prepared by mixing and grinding active material, carbon black and polyvinylidene fluoride (PVDF) in 90:10:10 ratios in an agate mortar. N – Methyl – 2 - pyrrolidone (NMP) was used as the solvent for the preparation. The prepared slurry was cast onto an aluminium foil, by doctor blade technique. The foil was then left to dry in vacuum at 120 ºC. The test cells were constructed using coin cell assembly (CR2032). All the cell fabrication process was done in the argon inert atmosphere within a glove box [Fig 2.14]. Li anode/ Separator / Composite cathode, configuration was employed throughout the study. The glass fibre membrane was used as the separator and commercially available electrolyte [1 M LiPF6

with EC/DMC (1:1 volume ratio)] was used for the entire measurement. The prepared coin cells were cycled between 1.5 V to 4.3 V to test the performance.

Figure 2.14: Glovebox used for the battery preparation.

Chapter 3

Preparation, Characterization and Applications of Graphene Oxide and Solar Exfoliated Graphene

This chapter contains the preparation of graphene oxide using chemical methods and exfoliation of graphene oxide, using solar light and its structural characterization using XRD, Raman and TEM. The electrochemical energy storage using supercapacitor electrode and sensing of hydrogen peroxide is also discussed in the chapter.

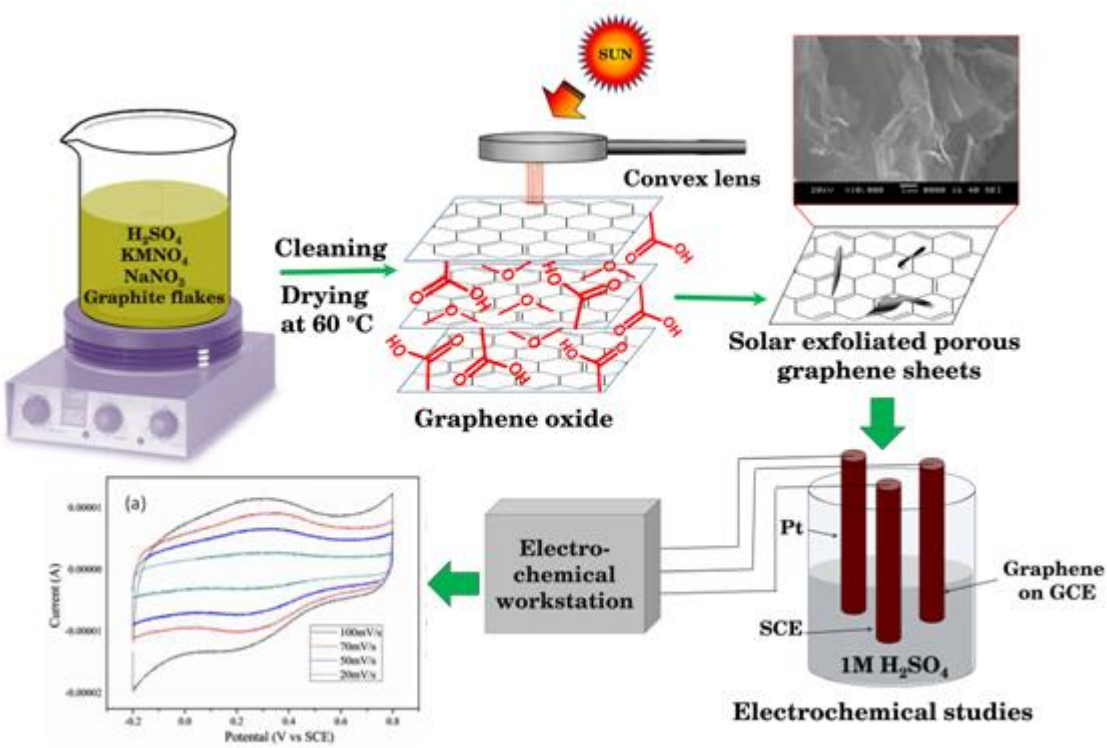

3.1 Preparation of Graphene Oxide and Solar Exfoliated Graphene

3.1.1 Introduction

Preparation of Graphene oxide and its conversion to reduced graphene oxide is a viable method for making graphene for applications where it is required in bulk quantities. Graphene was first obtained by the Geim and Novoslev using the famous scotch tape method which one of the mechanical exfoliation methods. There are different graphene preparation methods such as chemical vapour deposition, chemical methods, epitaxial method and creation of colloidal suspension. The graphene prepared by all these methods finds application in energy storage, electronic sensors etc.

Among the methods employed, chemical methods need a special mention because of its ease of execution, high efficiency and cost effectiveness. Chemical methods include, the oxidation of the graphite to graphite oxide and the successive reduction to graphene, using physical or chemical reduction methods. The physical reduction methods include, the reduction using high temperature, microwave, laser light, solar light irradiation, etc. These methods are environmental friendly, since it does not use any hazardous chemical, where as in the chemical reduction methods, the commonly used chemicals like hydrazine hydrate, sodium borohydride etc. are hazardous. The chemical methods followed by physical reduction could be the best alternative for the bulk production of graphene within short time. In this work, graphene oxide is synthesised using a chemical method called modified Hummer's method. The hazardous chemicals were avoided for the reduction of the graphene oxide to graphene; instead a low temperature energetically favourable method is used for the simultaneous reduction. This method leads to a rapid formation of reduced graphene oxide.

3.1.2 Experimental details

3.1.2.1 Preparation of graphene oxide

The graphite oxide samples are prepared using the modified Hummer's method (Hummers et al. 1958). In brief, weight equivalents of graphite flakes and $NaNO_3$ are mixed with 46 mL of concentrated H_2SO_4 in an ice bath for about 30 min. Thereafter, 3 weight equivalents of $KMnO_4$ is added with the solution for a certain time to avoid excess heating. The solution is then stirred at room temperature till it becomes a thick

paste. Later, 46 ml of water is slowly added to the solution. After 30 minutes, 140 ml of de-ionized water and 10 ml of H_2O_2 (30%) are poured into the mixture in sequence. This solution is filtered and washed with 3% HCl and distilled water several times till the sample pH is neutral. The sample is then collected and dried at 60ºC for 12 hours to obtain dried graphene oxide.

3.1.2.2 Preparation of Solar Exfoliated Graphene

The simultaneous reduction and exfoliation of graphene oxide to graphene is achieved using focussed solar irradiation (Eswaraiah et al. 2011). In brief, 100 mg of the sample is taken in a small container and solar energy is focussed on it using a convex lens. The exfoliation begins due to a sudden rise in temperature by focusing solar radiation, which imparts the high energy required for exfoliation. The rapid exfoliation is accompanied by changes in colour and volume expansion. The exfoliated product is separated and then collected for further studies.

3.2. Characterization of the solar exfoliated graphene

3.2.1 SEM and TEM analysis

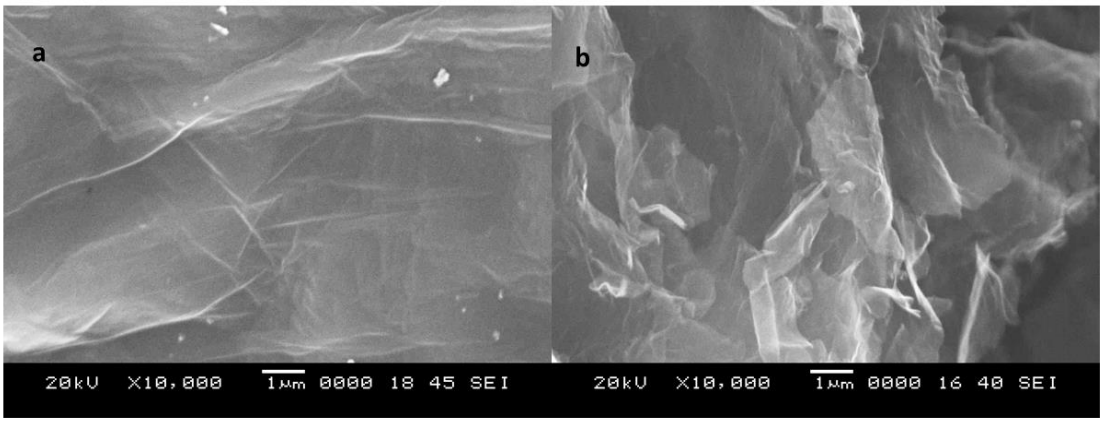

Figure 3.1: SEM images of the (a) graphene oxide and (b) solar exfoliated graphene.

Fig. 3.1 (a) represents the SEM image of obtained graphene oxide. It can be seen that the layers are aggregated in GO. This may result in the lesser surface area of the sample. Fig. 3.1 (b) shows the SEM image of the obtained solar graphene. After the exfoliation, individual layers are seen to be separated from each other's clearly indicating a better

surface area. The wrinkled morphology of the solar graphene is clearly visible in the image. Fig. 3.2 (a) and (b) shows the TEM image of the obtained graphene, layered structure can be easily observed. It is clear that there are nanosized pores in the obtained graphene sheets. These pores are formed during the solar exfoliation process due to the rapid reaction. The pores play an important role in the proper wetting of the surfaces while in contact with the electrolytes and can avail all the stacked surfaces for the adsorption of the materials (Wang et al. 2013).

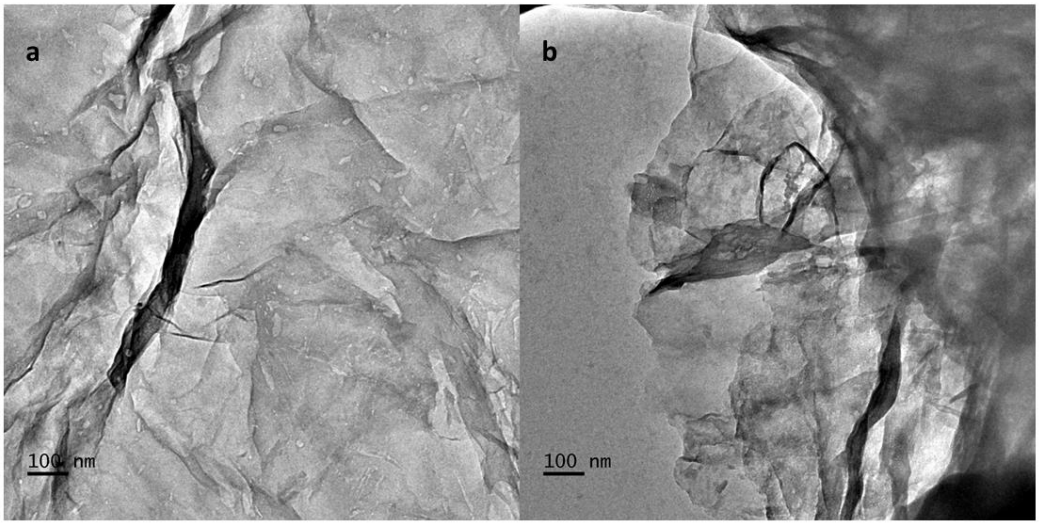

Figure. 3.2: (a) and (b) TEM images of the solar exfoliated graphene showing the porous and layered structure.

3.2.2 EDAX analysis

Energy Dispersive X-ray Spectra (EDAX) was used for the determination of oxygen content in the prepared sample. The marked area in the SEM images shows the region in which the EDAX analysis has been done (Fig. 3.3). Table. 3.1 shows the carbon and oxygen ratios in the sample. It was found that the solar exfoliation reduced the oxygen

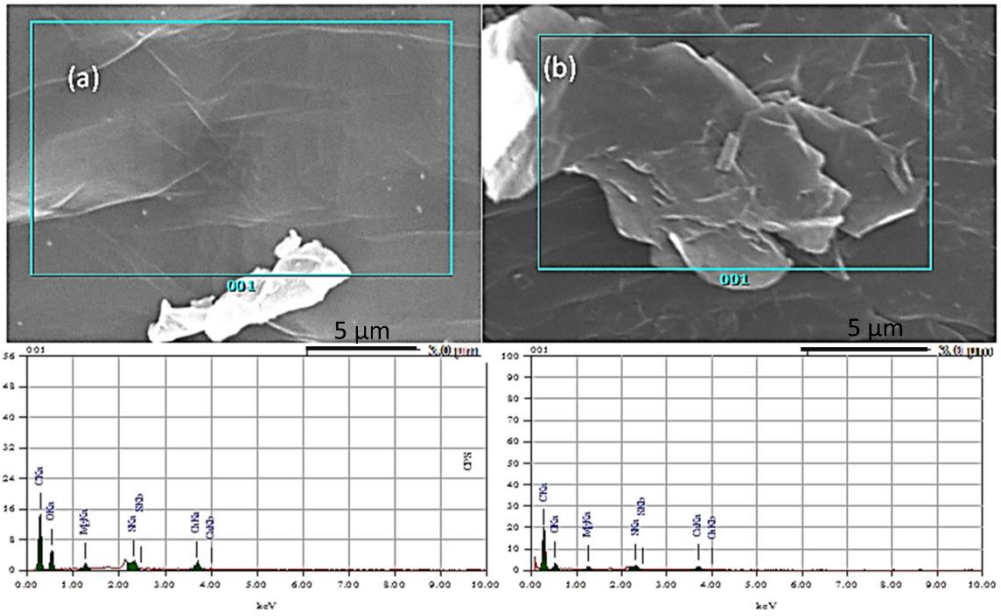

Figure. 3.3: SEM and corresponding EDAX patterns of (a) graphene oxide and (b) solar exfoliated graphene

content by around 11.37 atomic percentages. Upon exfoliation, the carbon to oxygen ratio has been increased to 3.74 from 2.05. Similar observations were noticed by Ganguly et al. in the thermal deoxygenation of Graphene oxide (Bose et al. 2011). This helped in concluding the fact that, the solar exfoliation of the Graphene oxide is successful in reducing the oxygen content. FTIR analysis also throws light into the successful reduction of Graphite oxide. The existing oxygen content may exist as other functional groups attached to the Graphene structure. These observations were also supported by the FTIR data.

Table 3.1: Carbon and oxygen ratios in the graphene oxide and solar exfoliated graphene oxide.

	Carbon %	Oxygen %	C/O ratio
Graphene Oxide	65.55	31.96	2.05
Solar Graphene	77.14	20.59	3.74

3.2.3 XRD analysis

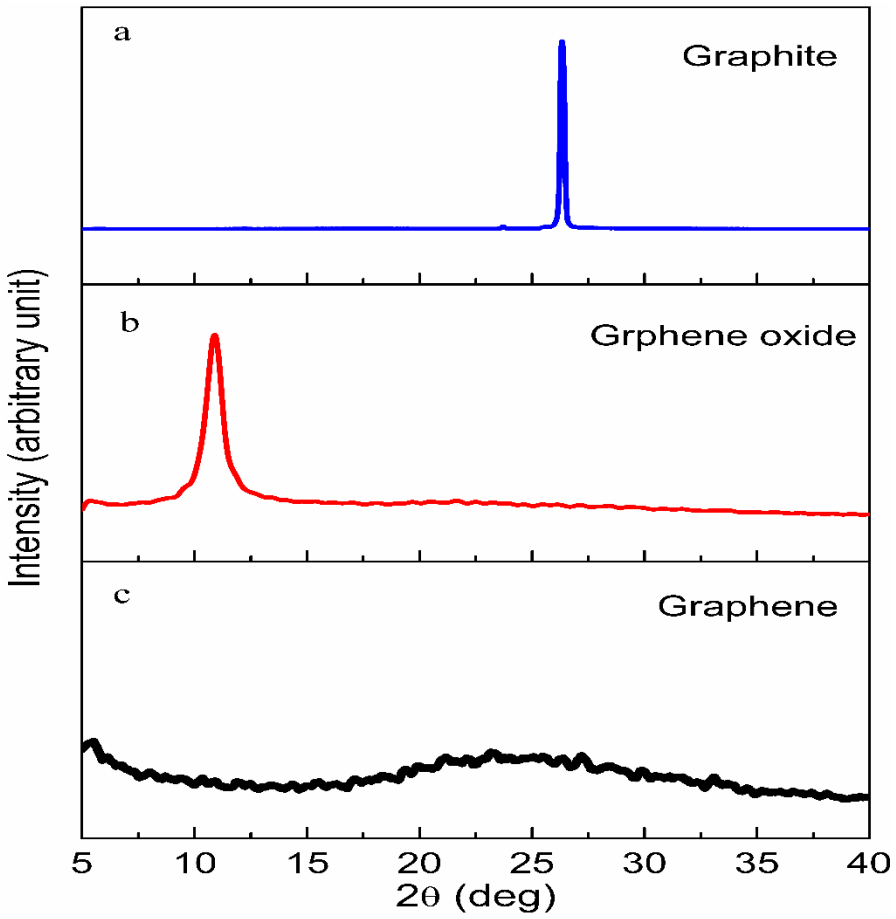

Figure. 3.4: XRD patterns of the (a) Graphite, (b) Graphite oxide and solar graphene samples.

Figure 3.4 (a) shows the XRD pattern of graphite. The crystalline peak at 26.4º in graphite corresponds to the reflections from (002) plane. This corresponds to an interplanar spacing of 0.327 nm. The XRD spectrum of graphene oxide shows a peak at 10.9º which corresponds to an interplanar spacing of 0.805 nm. The increase in interplanar distance is due to the increase in spacing between the layers to incorporate water molecules and oxygen containing functional groups (Kaniyoor et al. 2012). This increase in spacing allows to exfoliate the graphene oxide by giving lower energy whereas, in the case of graphite, it is not practical because of the smaller spacing and stronger bonding. The absence of the sharp peak at 26º in graphene oxide is the clear indication of absence of graphite. The XRD of solar graphene (Fig. 3.4 (c)) shows a broad peak around 25º indicates the absence of three dimensional crystal structure and

is due to the small size of the layers or a relatively short domain order of the stacked sheet (Eswaraiah et al. 2011). Hence, XRD gives a clear indication of formation of graphene.

3.2.4 Raman analysis

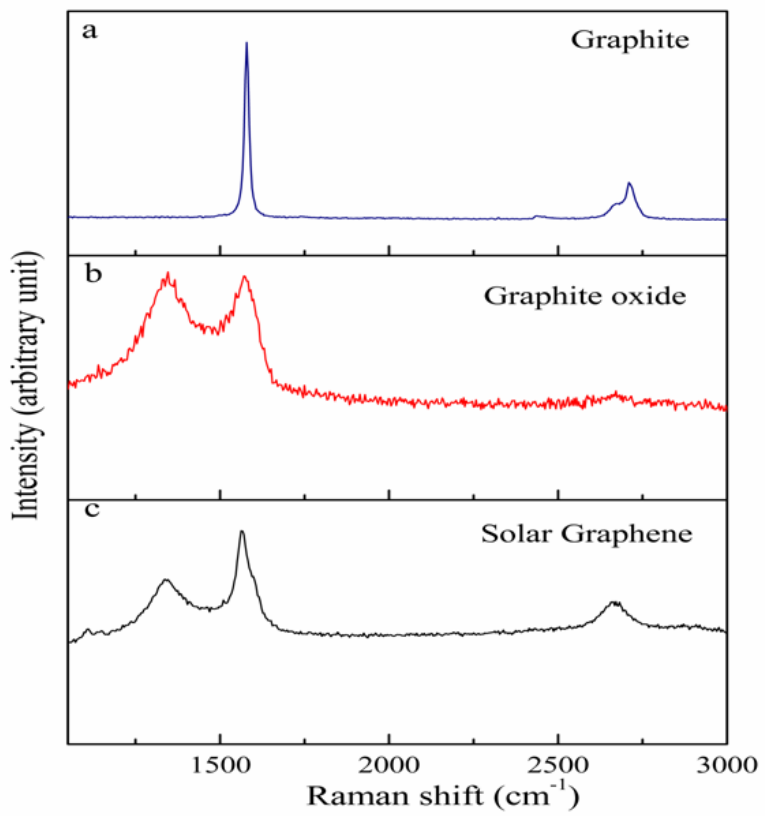

Figure 3.5: Raman spectra of the (a) Graphite, (b) Graphene oxide and (c) solar graphene samples.

Fig. 3.5 shows the Raman spectra of the graphite, GO and graphene samples. Raman spectrum gives clear insight into the formation of graphene layers. Graphite, graphene oxide and solar graphene are analyzed using Raman spectra and compared using the intensity ratios of D to G bands (I_D/I_G). Graphite shows the characteristic sharp peaks at 1575 cm^{-1} and 2707 cm^{-1}. The Raman spectrum of solar graphene is characterized by G band at 1565 cm^{-1} arising due to first order Raman scattering of the E_{2g} phonon at the Brillouin zone centre of sp^2 carbon atoms. The D band at 1348 cm^{-1} is due to the defects, vacancies, grain boundaries and amorphous carbon species, which indicats the quality

of graphene produced. The intensity ratio of D band to G band (I_D/I_G) is found to be 1.002 and 0.8847 for graphite oxide and solar graphene, respectively. The decrease in the I_D/I_G ratio of solar graphene is due to the restoration of sp^2 network. It is noticed that the intensity ratio of D band to G band is reduced in graphene compared to graphene oxide due to less number of defects (Kaniyoor et al. 2012).

3.3 Applications of solar exfoliated graphene

3.3.1 Supercapacitor applications

The performance of the solar graphene for supercapacitor applications is evaluated by cyclic voltammetry (CV) and galvanostatic charge-discharge tests using a three electrode configuration. Platinum electrode is used as the counter electrode and saturated calomel electrode (SCE) as the reference electrode. 0.5 M H_2SO_4 is used as the electrolyte throughout the study.

Fig. 3.6 shows the CV curves for solar graphene at different scan rates. The redox curves show almost rectangular shape with a broad peak around 0.3 V. This peak is due to the presence of additional functional groups which can interact with the protons from the acidic medium and, resulted in an increase in the capacitance value (Mai et al. 2012). The specific capacitance of the electrode is calculated using the following equation,

$$C = \left(\int IdV\right) / vmV \qquad (3.1)$$

Where, C is the specific capacitance in Fg^{-1}, I is the current (A), V is the potential (V), v is the scan rate and m is the mass of the material on the electrode (g). In each measurements, the weights of the samples are accurately measured and used for the calculation throughout the thesis.

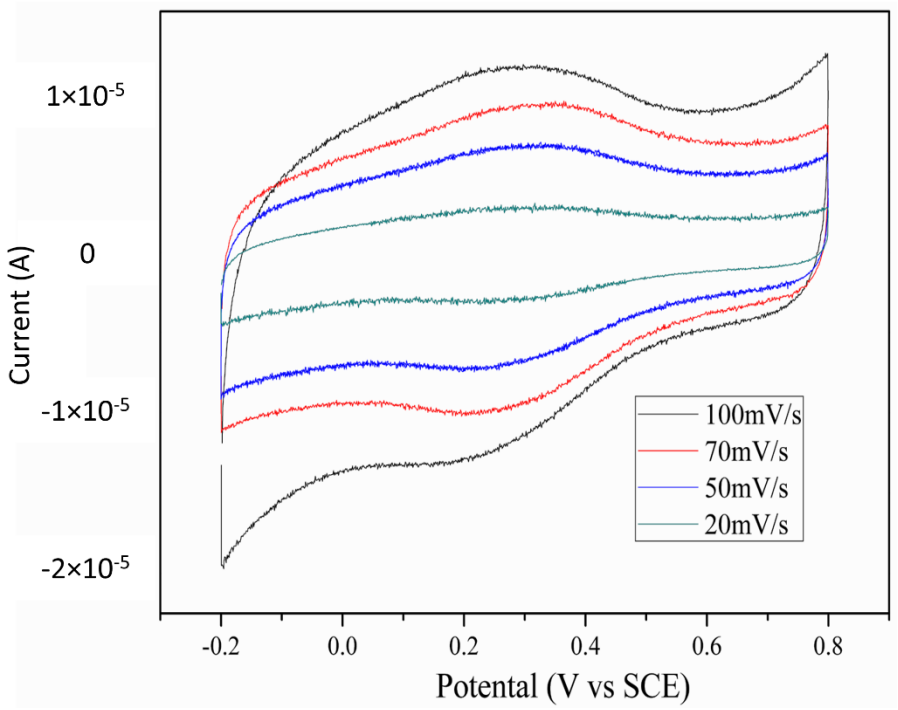

Figure. 3.6: CV curve for solar exfoliated graphene at different scan rates

The specific capacitance of solar graphene is found to be 223 Fg^{-1} at a scan rate of 20 mVs^{-1}. An increasing trend is observed in the specific capacitance with the decrease in the scanning rate due to the insufficient time available for the ions to occupy the adsorption sites. With time, more sites will be available for the electrolyte to wet the surface properly and diffuse into the stacked layers of graphene. The relatively high specific capacity of the sample is due to the structure of solar reduced graphene. The TEM images reveal the presence of nanopores in the graphene sample. The nanopores give additional sites for the ions and help in proper wetting of the surface and stacked layers, in turn solving the problem of material restacking and reduction of capacitance. The higher mass transfer rate offered due to the porous structure clearly contributes to the electrochemical properties of the samples (Wang et al. 2013, Yuan et al.2013, Wen et al. 2012). The Faradic interaction at 0.3 V due to the available functional groups also played an important role in the increased capacitance. Table 3.2 shows the comparison of the capacitance of the solar graphene with other reports. Fig. 3.7 shows the variation of specific capacitance with the scan rates. It is found that the specific capacitance

decreases with increase in scan rate, which is due to the insufficient time for the ion diffusion and adsorption at the sites (Zhao et al. 2012).

Table 3.2 The comparison of the capacitance of the solar graphene with other reports

Description about the graphene preparation	Specific Capacitance (Fg^{-1})	Reference
Hydrazine hydrated graphene	99	(Stroller et al. 2008)
Reduction at 1050^0C	117	(Vivekchand et al. 2008)
Solvothermmal deoxydation	230	(Du et al. 2010)
Microwave reduction	196	(Zhu et al. 2010)
Electrochemical activation	220	(Hantel et al. 2011)
Solar exfoliation	223	This work

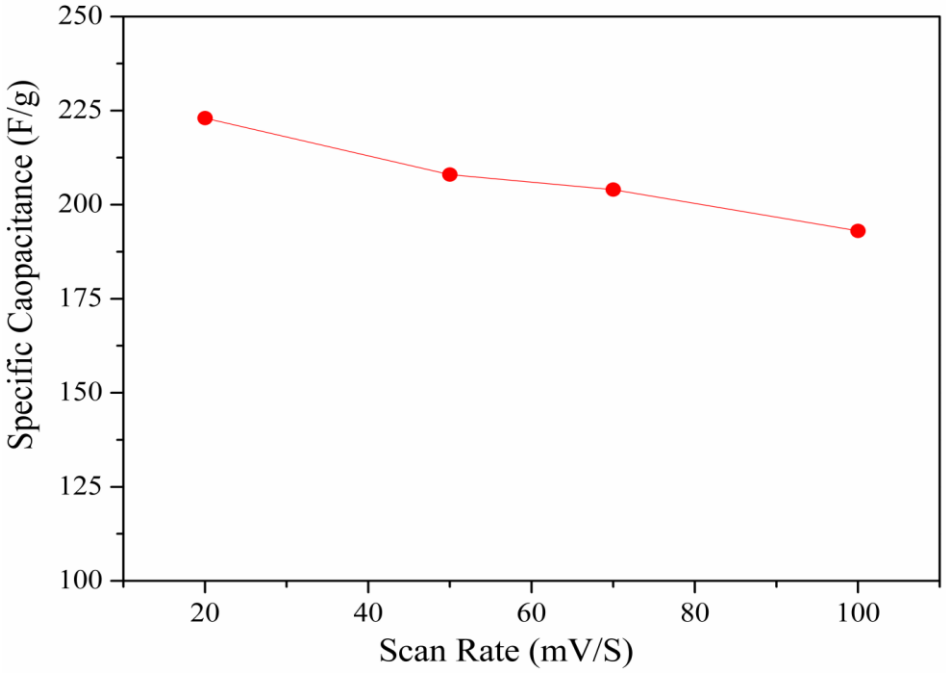

Figure. 3.7: Variation of specific capacitance of solar graphene with the change in scan rate

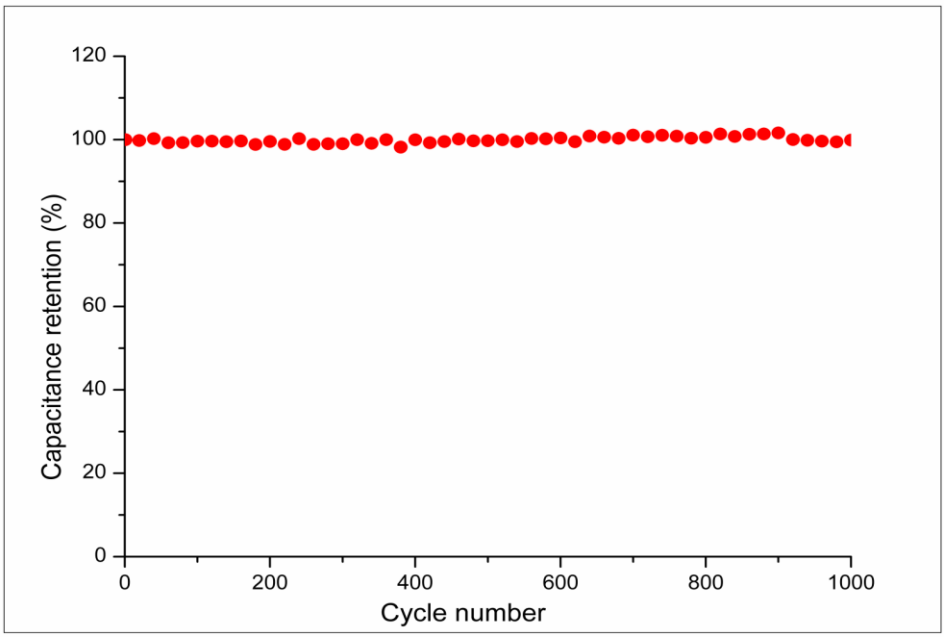

Figure. 3.8: Capacitance retention of the electrode with cycles

Fig. 3.8 shows the capacitance retention of the material. The retention ability is calculated by taking the ratio of capacitance at a particular cycle to the initial capacitance. The performance is checked by collecting data for 1000 cycles, it is observed that the specific capacitance increases by about 8 %. The increase in capacitance is due to the activation of nanopores during the initial cycles (Perera et al. 2012 and Yan et al. 2012). This shows that the prepared graphene samples possess long cycle life.

The galvanostatic charge-discharge tests are conducted for the prepared solar graphene samples at constant current to study the capacitance behaviour. Fig. 3.9 shows the galvanostatic charge-discharge characteristic of the solar graphene. The symmetric charge-discharge curves have been observed for the sample and the near linear variation of charge and discharge cycles suggests, the good capacitive behaviour with the electrochemical stability and reversibility (Wu et al. 2010, El-Kady et al. 2012 and Bose et al. 2012). The specific capacitance values are found to be in agreement with the one obtained from the CV measurement.

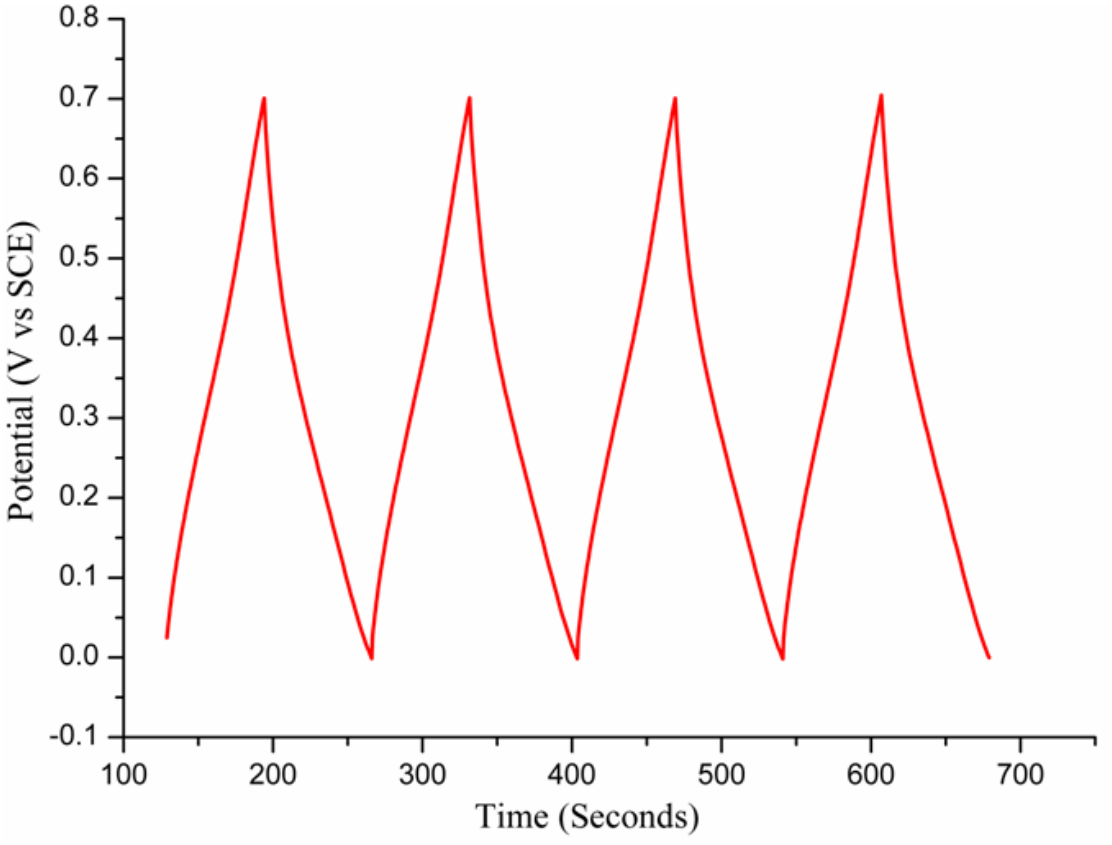

Figure. 3.9: Galvanostatic charge-discharge curve of the solar graphene at a potential window of 0.7 V and charge-discharge ratio of 1 A/g showing the supercapacitor nature.

The Electrochemical Impedance Analysis (EIS) analysis is done at a frequency range of 1 Hz to 100 kHz to study the impedance behaviour of the prepared solar graphene. Fig. 3.10 shows Nyquist plot for the solar graphene sample. The plot shows a loop in the higher frequency region and a straight line in the lower frequencies. This loop refers to the low electronic resistance offered by the material. The relatively smaller region at the high-medium frequency region suggests that the electrode possesses much lower contact resistance and charge-transfer resistance (Yang et al. 2012). The more vertical the curve is, the more it goes to ideal capacitor behaviour. Therefore, the results are promising and show lower charge transfer resistance and better capacitive behaviour.

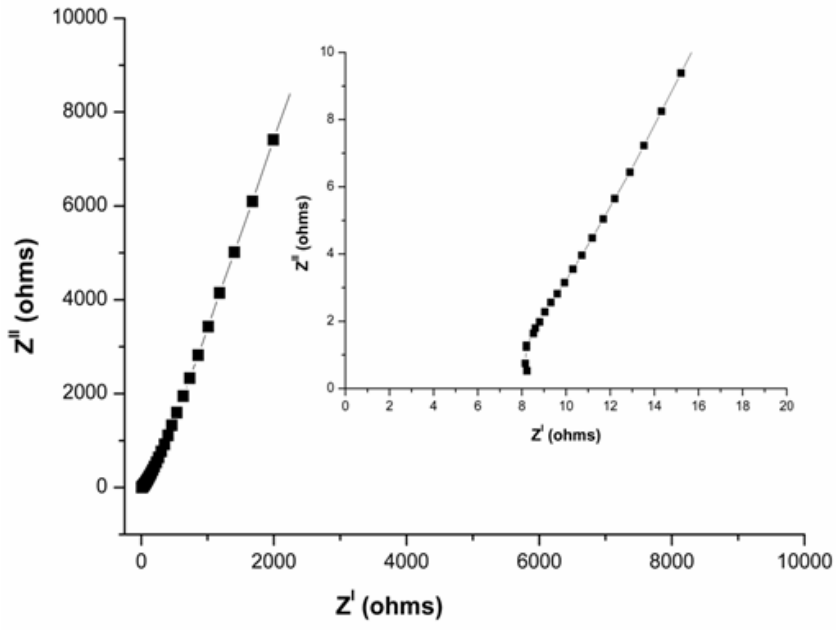

Figure. 3.10: Impedance plot for the solar reduced graphene. Inset shows the behaviour at higher frequency.

3.3.2 Hydrogen peroxide sensing application

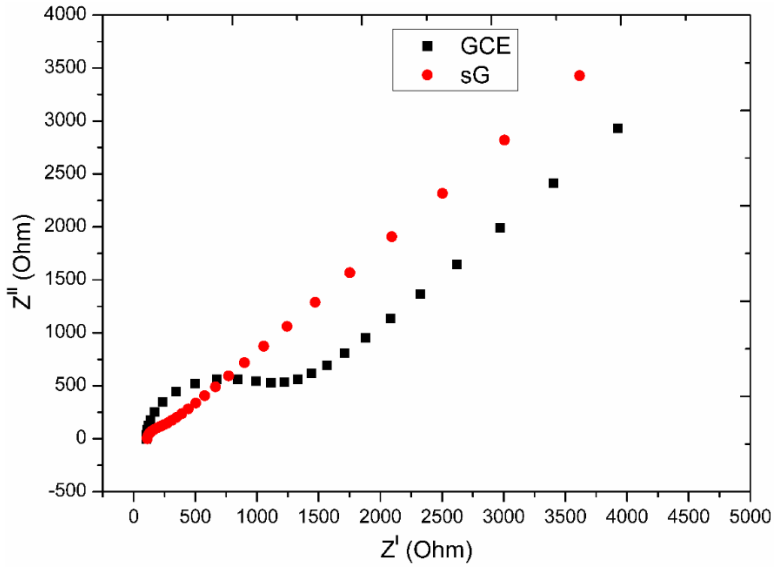

Figure. 3.11: Impedance spectra of the graphene and bare GCE in 5 mM $Fe(CN)_6^{3-/-4}$ in 0.1M PBS solution.

Fig. 3.11 represents the impedance spectra of the graphene and bare GCE in 5 mM $Fe(CN)_6^{3-/-4}$ in 0.1 M Phosphate buffer solution (PBS) solution. Impedance spectra reveal the electron transfer properties of the material. The semi-circular portion observed in the spectrum corresponds to the high frequency response and corresponds to the electron transfer limited process, whereas the linear portion corresponds to the low frequency response which depends on the diffusion process. It is observed that the solar graphene offered less resistance compared to the GCE. This clearly indicates that the solar graphene has a higher electron transfer rate which helps in the electrocatalytic detection of the materials (Woo et al. 2012).

Fig. 3.12 shows the CV for the solar graphene coated GCE sample and bare GCE in pH7 PBS buffer solution with 0.5 mM H_2O_2 concentration. The data is acquired between -0.4 V and 1 V. Higher electrocatalytic behaviour is observed for the graphene samples compared to the bare GCE electrode. Both the oxidation and reduction showed an earlier onset of the potential indicating a very high electrocatalytic activity of the solar graphene samples. Fig. 3.12 compares the performance of the solar graphene in PBS solution with and without H_2O_2, which shows an increase in current, suggesting the electrocatalytic activity of the electrode (Woo et al. 2012). This may be due to the very high surface area and high concentration of defects which may increase the heterogeneous electron transfer and the sensing (Alwarappan et al. 2009).

Fig. 3.13 shows the amperometric response of the electrode towards the solar graphene towards change in concentration. The measurement is recorded at a voltage of -0.4 V. The response is recorded for concentrations starting from 2×10^{-5} to 3×10^{-3} M. Solar graphene shows a very good response to the hydrogen peroxide concentration in this region. The sensing mechanism (Zhao et al. 2009) can be described using adsorption of H_2O_2 on the graphene surface and the reduction to water molecules. Once H_2O_2 is added to the sensor chamber, graphene provides surface for the adsorption of the material on the surface and edges. Further, the H_2O_2 will be reduced on this surface. This electron transfer is converted into the electronic signals and recorded in the potetiostat.

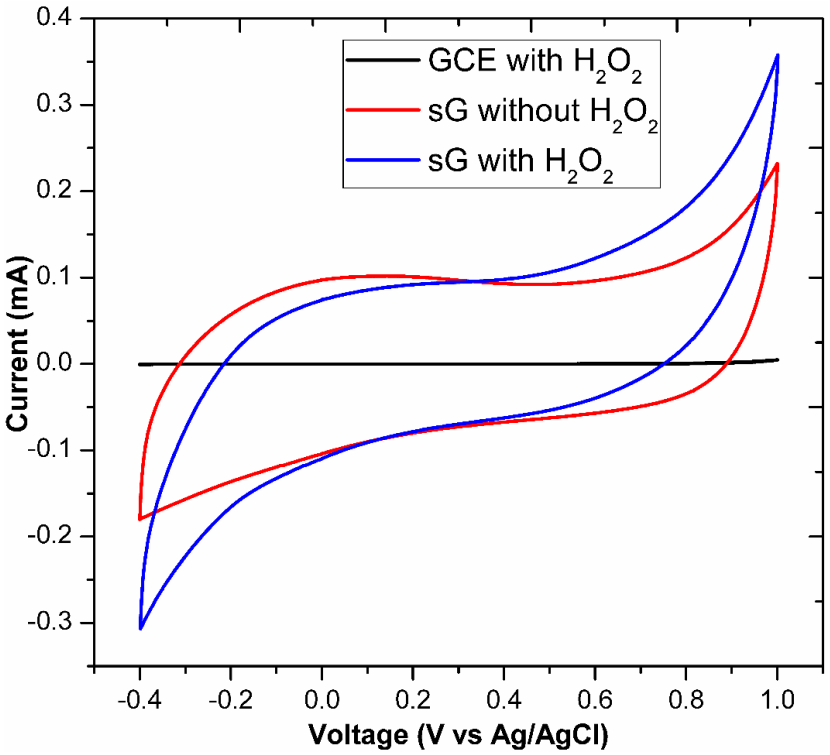

Figure. 3.12: Comparison of CV in PBS (PH7) buffer solution with/without H_2O_2 for SG coated on GCE

The mechanism can be written as,

$$H_2O_{2+} e^- \leftrightarrow OH_{(adsorbed)} + OH^-$$

$$OH_{(adsorbed)} + e^- \leftrightarrow OH^-$$

$$2\ OH^- + 2\ H^+ \leftrightarrow 2H_2O$$

Figure 3.14 shows the calibration curve for the H_2O_2 sensor. The regression equation, $I_{pa}\ (\mu A) = 2.457 + 18.31c\ (mM)$ with R = 0.98592 is obtained. The observed sensitivity is around 64.79 µA mM^{-1} cm^{-2} for the solar graphene which is very high compared to the earlier report (15.16 µA mM^{-1} cm^{-2}) by Woo et al. (2012).

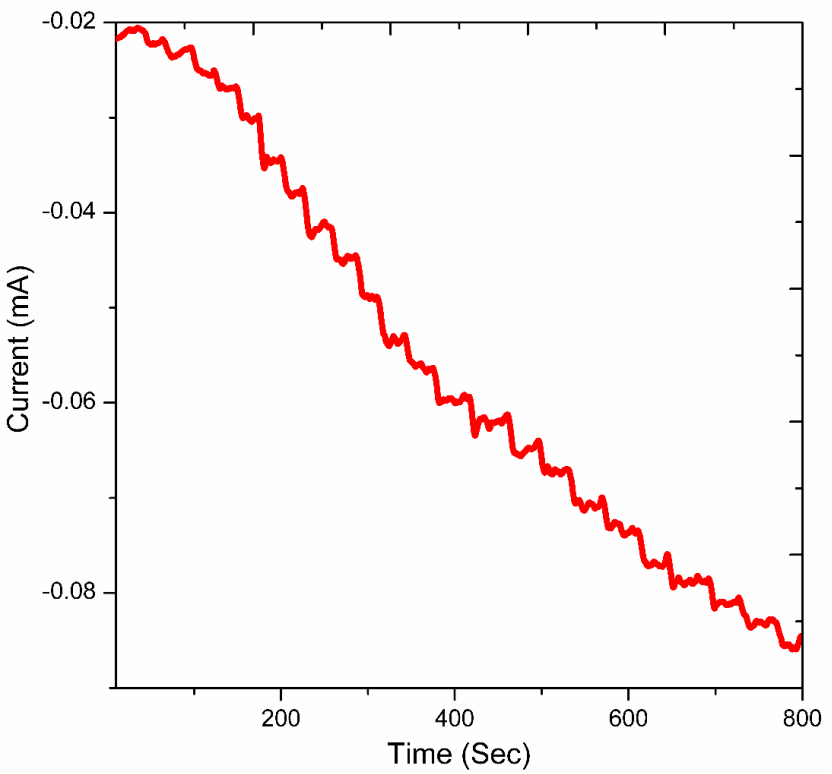

Figure. 3.13: Amperometric response of the electrode towards the solar graphene towards change in concentration.

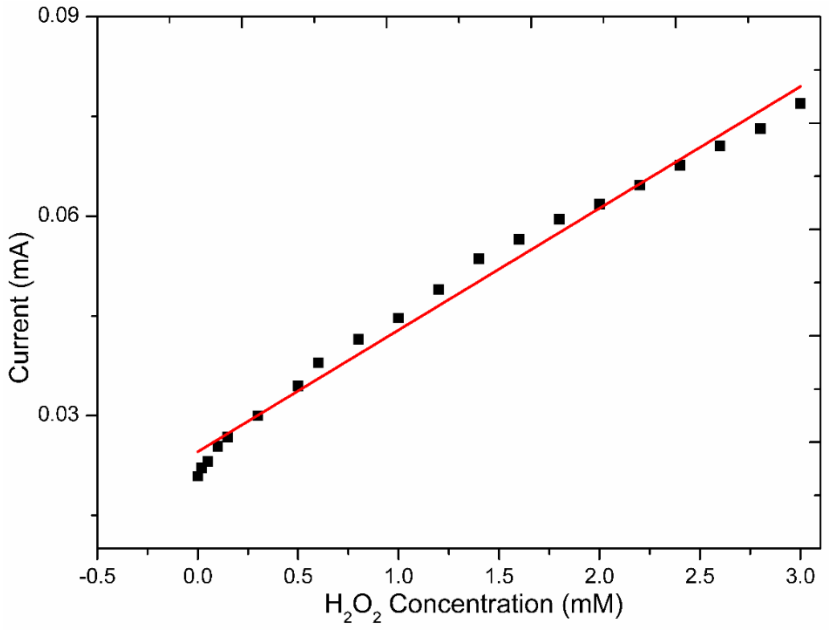

Figure. 3.14: Calibration curve for the H_2O_2 sensor

3.4 Summary

- Solar graphene is successfully synthesized via solar exfoliation of graphene oxide. The complete reduction of graphene oxide to graphene is confirmed from XRD and UV-Vis spectrum. Raman Spectrum indicated high purity and defect less nature of solar graphene. The samples produced have layered morphology as seen from SEM analysis. The layered structures possess surface nanopores as observed from TEM images.
- The CV studies showed greater specific capacitance for solar graphene, which can be attributed to the nanopores present on the surface and hence the interaction of available functional groups with the electrolyte. The charge-discharge curves show symmetric behaviour which in turn reflects the good capacitive behaviour, electro-chemical stability and reversibility.The Impedance analysis shows lower internal resistance for solar graphene.
- A higher sensitivity for the electrochemical detection of H_2O_2 using solar reduced graphene is reported. The solar graphene possess excellent electrocatalytic activity, low resistance and high electron transfer rate, high sensitivity and low response time making it one of the best graphene species available for the electrochemical detection. The preparation of solar reduced graphene is more cost effective as compared to the other existing methods and useful for applications in supercapacitors and sensors.

Chapter 4

Preparation and Characterization of Vanadium Oxide/Graphene Composites for Biosensors and Lithium Ion Batteries

This chapter deals with the preparation and characterization of Vanadium Oxide/ Graphene Oxide Composite. Melt quenching technique has been used for the preparation of the amorphous vanadium oxide. Hydrothermal method was used for the preparation of the composite. The prepared composites are characterized using XRD, Raman, TGA, FTIR, SEM and TEM. Applications in Lithium-ion battery and electrochemical sensing of dopamine is reported.

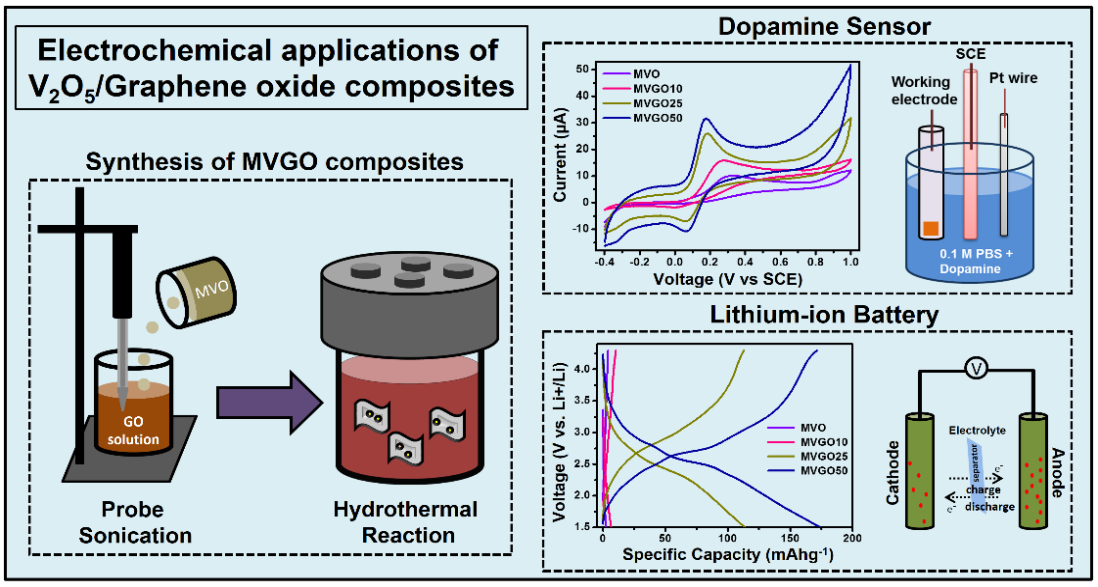

4.1 Preparation of Vanadium Oxide and Vanadium Oxide/Graphene Composite

4.1.1 Introduction

Vanadium pentoxide (V_2O_5) is an easily synthesizable transition metal oxide, occurring abundantly in nature, with a unique layered structure, having mixed oxidation states (V^{2+}, V^{3+}, $V^{4+}$and V^{5+}) and possessing high energy density (Yang et al. 2011). V_2O_5 is a promising cathode material in lithium-ion batteries (Tang et al. 2013). Composites of V_2O_5 hinder enhanced device performance owing to its poor electrical conductivity and bulk material properties (Van et al. 2006). However, nanoscale V_2O_5 provide more electrochemically active sites and enhance the concentration polarization of electrode material with large surface area and short diffusion paths (Shen et al. 2016, Li et al. 2010). Therefore, improving the electrical conductivity of V_2O_5 for using it as a cathode material in lithium ion batteris (LIB's) is another challenging topic of interest. In this regard, generally the enhanced electrochemical performance have been reported on nanocomposites of V_2O_5 with various carbon nanostructures especially graphene and graphene oxide (GO) owing to their nontoxicity, high electrical conductivity, chemical inertness and mechanical stability (Yoo et al. 2008). Different methodologies have been reported in literature for the synthesis of V_2O_5-reduced graphene oxide nanocomposites for example solvothermal approach (Chen et al. 2014), one-pot hydrothermal approach (Lee et al. 2015), xerogel annealing (Ban et al. 2009) and so on. In comparison to crystalline V_2O_5, amorphous V_2O_5 are reported to exhibit better electrochemical performance owing to the fast Faradaic reactions arising from their two dimensional layered percolated diffusion network (Uchakar et al. 2014). Although there are many reports on the usage of less crystalline bilayered $V_2O_5{\cdot}nH_2O$ synthesized through sol-gel synthesis approach (Moretti et al. 2016), reports on the usage of less crystalline V_2O_5 synthesized through the melt quenching process for electrochemical device applications are rare.

In this chapter, the synthesis of layered V_2O_5 using a sol prepared by annealing crystalline V_2O_5 powder (referred hereafter as VO) at 950 ^oC and quenching in

deionized water is reported. The as-synthesized melt quenched V_2O_5 sol is later employed for synthesizing V_2O_5/graphene oxide composites at different compositions. The electrochemical performance of the synthesized composites is compared for applications in sensing of dopamine as well for lithium-ion battery applications.

4.1.2 Experimental details

4.1.2.1 Preparation of melt quenched V_2O_5

In a typical melt quenching process, 3 g of V_2O_5 (*Loba chemicals, India*) taken in a silica crucible was heated to 950 ºC in a muffle furnace and was maintained at the same temperature for 30 min. Molten V_2O_5 solution collected from the furnace was poured into a beaker containing DI water and was probe sonicated for 60 min. Supernatant was separated from the sonicated solution to separate V_2O_5 nanoparticles from the bulk chunks settled at the bottom of the beaker. Samples obtained after drying the V_2O_5 supernatant solution were named as MVO while the precursor used for its preparation was denoted as VO.

4.1.2.2 Preparation of the melt quenched V_2O_5/graphene oxide (MVGO) composites

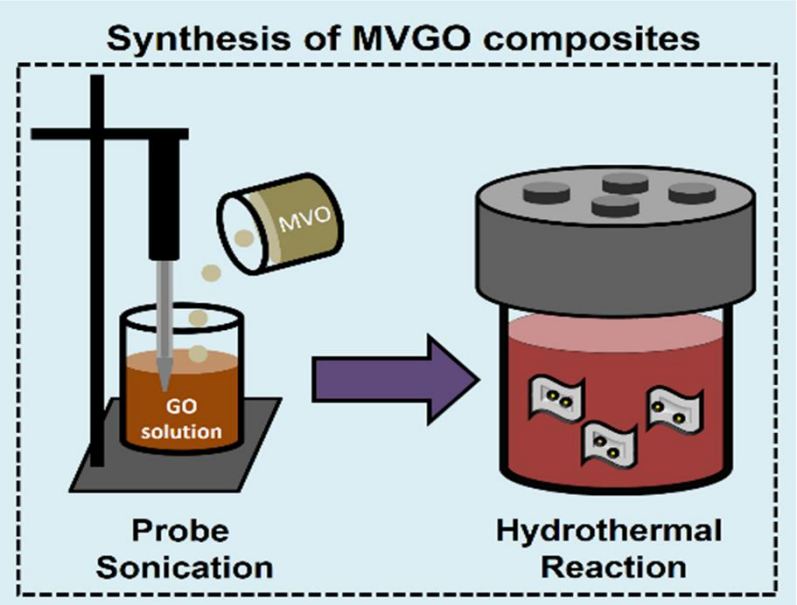

Figure 4.1. Schematic representation of the experimental procedure.

Graphene oxide was pre-synthesized using the modified Hummer's method as reported in the chapter 3. MVGO composites were prepared through a simple hydrothermal approach. Typically, a fresh solution was first prepared by ultrasonically dispersing 12 mg of as-synthesized GO in 12 ml DI water. Later, this solution was poured into a beaker containing 9 ml of supernatant solution (containing ~12 mg/ml of MVO) placed in an ultrasonic bath. The final composite precursor solution obtained after through mixing was transferred to a Teflon-lined stainless steel autoclave of 100 ml capacity and reacted hydrothermally by heating the sealed autoclave at 150 ^{o}C for 12 h. Fig. 4.1 schematically represent the experimental procedure. After the reaction the autoclave was allowed to cool down naturally and the precipitates were collected by washing with excess DI water and ethanol, followed by drying overnight at 60 ^{o}C. Final dried sample was named as MVGO10. Similarly, MVGO25 and MVGO50 were prepared following the same procedure by increasing the weight percentage of GO to 25% and 50 %, respectively.

4.1.2.3 Preparation of the electrodes and electrochemical measurement

Typically, a glassy carbon electrode (GCE) was finely cleaned by polishing its surface using alumina powder (0.05 µm), followed by electropolishing in 0.5 M H_2SO_4 and sonicating in DI water and ethanol for 5 s each. A slurry was prepared by sonicating 1 mg of as-synthesized VGO composites in 1 ml of DI water, after which 4 µl was carefully drop casted over the polished GCE surface (3 mm diameter). The modified GCE was dried and used as the working electrode for sensing dopamine on an electrochemical work station (*Biologic SP-150, Autolab*) with three-electrode configuration in 0.1 M phosphate buffer saline (PBS) electrolyte solution (pH 7.2), employing platinum wire and Ag/AgCl as the counter and reference electrode, respectively. All three electrodes were kept at an equal distance from each other for avoiding any abnormality during measurements. Amperometric sensing was performed by injecting dopamine into the system using a micropipette at regular intervals of time and the change in current was recorded.

4.1.2.4 Preparation of coin cells for battery measurements

The cathode was fabricated by first preparing slurry by mixing the as-synthesized active materials (VO, MVO, MVGO10, MVGO25 and MVGO50) with carbon black and polyvinylidene fluoride (PVDF) binder in the weight ratio of 80:10:10 with a few drops of N-Methyl-2-pyrrolidone (NMP) in an agate mortar. This slurry was then spread on a battery grade aluminum foil by doctor blade technique and dried in vacuum at 120 ºC. The coin cells (CR 2032) were assembled in an argon-filled glove box (*Mbraun, Germany*) using glass fiber membrane as separator, Li-metal as the anode, and 1 M $LiPF_6$ in ethylene carbonate/dimethyl carbonate (EC/DMC in 1:1 volume ratio) as the electrolyte. Electrochemical tests were performed by galvanostatically charging/discharging the assembled cells under room temperature in the potential range of 1.5 – 4.3 V (versus Li/Li^+) using a multichannel battery tester (*Neware, China*).

4.2 Characterization of the vanadium pentoxide/graphene oxide composites

The XRD patterns of the as-synthesized MVO and MVGO samples compared with pristine VO are presented in Fig. 4.2. The peaks of VO are consistent with the JCPDS file (Card No 01-072-0598). However, in comparison to VO, the absence of the prominent peaks in the XRD pattern of MVO suggests the formation of an amorphous like phase as reported elsewhere (Moreti et al. 2016, Wangoh et al. 2016) . The possible reason for the amorphous like XRD pattern could be attributed to the insertion of water molecules during the melt quenching process. The small peak appearing at $2\theta = 6^o$ for MVO can be attributed to the (001) plane (as indicated by ♣ the symbol). The small blue shift in the peak position of the (001) plane for MVO in comparison to those reported for $V_2O_5 \cdot nH_2O$ by Wangoh et al. (2016), could be attributed to the different synthesis methodology adopted. The XRD pattern of MVO synthesized here is consistent with the amorphous V_2O_5 reported elsewhere (Chen et al. 2009). The presence of graphene oxide in MVGO composites is confirmed from the XRD peaks appearing at $2\theta = 11.5^o$. The partial reduction of GO to graphene during hydrothermal

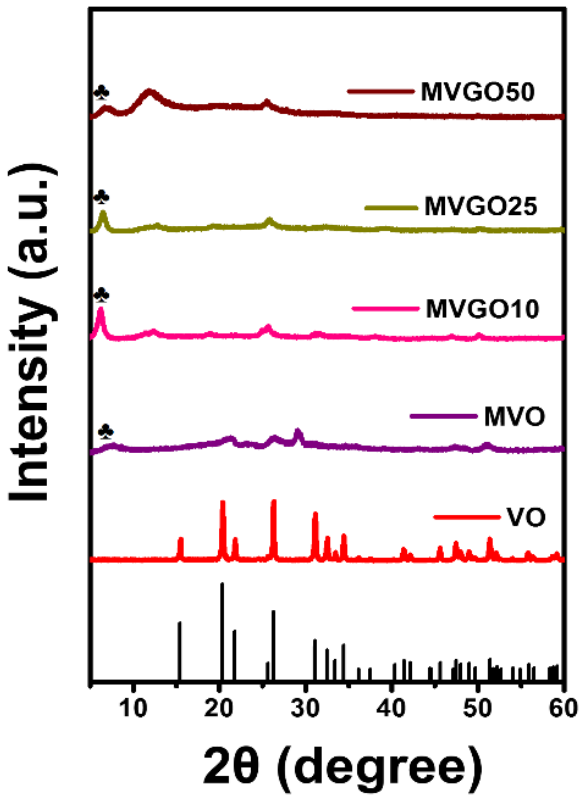

Figure 4.2: X-ray diffraction patterns of pristine VO, MVO, MVGO10, MVGO25 and MVGO50. The peak indexed with ♣ symbol correspond to the (001) plane of MVO.

treatment is confirmed from the XRD peak in MVGO composites appearing at 2θ = 26°, which is well documented in the literature (Viswanathamurthi et al. 2003). Surprisingly, the XRD peak of the (001) plane of MVO appearing at 2θ = 5° is higher in MVGO10 and MVGO25, which could be attributed to the growth processes happening under hydrothermal conditions. However, due to excess GO content the XRD peak intensity in MVGO50 decreases.

FTIR spectra of as-synthesized MVO and MVGO50 are compared with pristine VO, as shown in Fig. 4.3 The peak appearing at 1012, 1004 and 996 cm^{-1} in VO, MVO and MVGO50, respectively, can be assigned to the stretching vibration absorption peak of V=O. On the other hand, the peaks at 519, 510 and 521 cm^{-1} in VO, MVO and MVGO, respectively can be attributed to the asymmetric stretching vibrations of V-O-V, while the peaks at 719, 724 and 754 cm^{-1} can be assigned to the symmetric stretching vibration of V-O-V in VO, MVO and MVGO, respectively (Viswanathamurthi et al. 2003). The

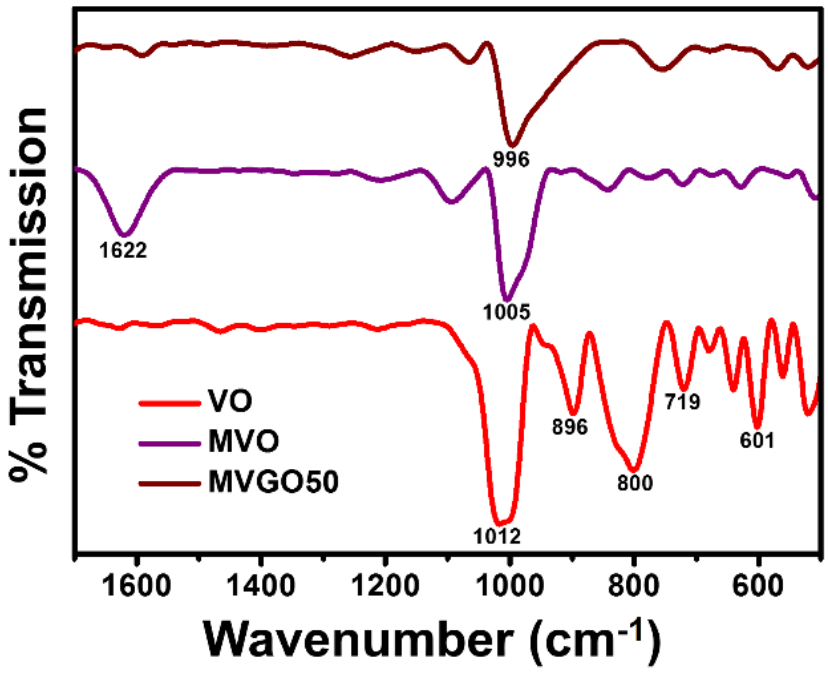

Figure 4.3: FTIR spectra of pristine VO, as-synthesized MVO and MVGO50.

intense peak at 1622 cm^{-1} in MVO indicates the presence of hydroxyl ions that get adsorbed on the surface of the vanadium oxide during the melt quenching process resulted in the disordered structure as observed from XRD (Jayalakshmi et al. 2013).

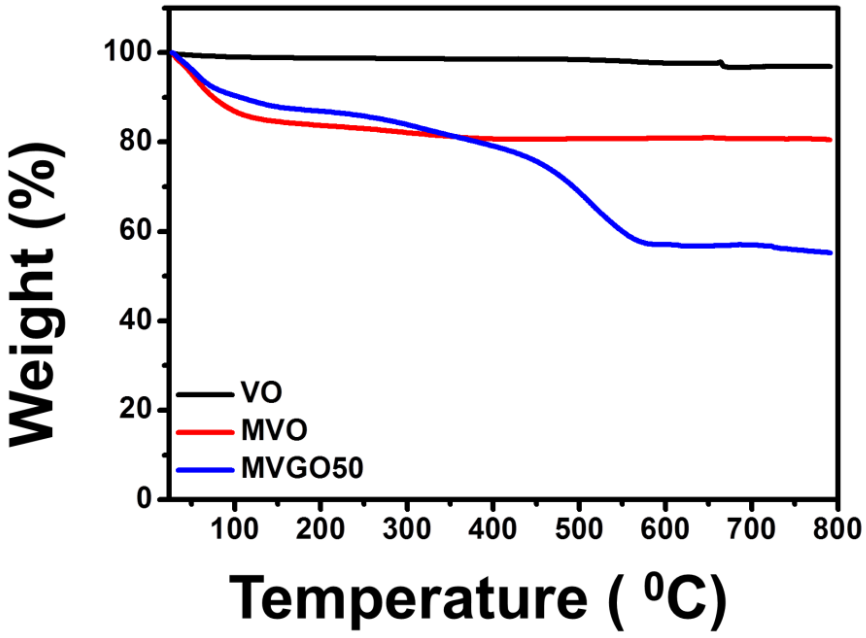

Figure 4.4:Thermo gravimetric analysis (TGA) curves of VO, MVO and MVGO50

The thermal characterization using thermo gravimetric analysis (TGA) is shown in Fig. 4.4. The crystalline vanadium oxide shows very small change in the weight up to 800 ºC. On the other hand, the MVO shows a gradual change in the weight. A steep weight loss around 100 ºC is due to the removal of the absorbed water molecules. The continued weight loss up to 400 ºC, indicates the gradual removal of the water contained in the MVO. The weight loss was around 20% up to 800 ºC. In the case of MVGO50 composite, the initial weight loss was less as compared to the vanadium oxide, indicating less crystal water in the sample. A steep weight loss around 500 ºC, indicates the removal of carbon from the composite. (TGA) also confirms the presence of hydroxyl ions in MVO as there is a sudden weight loss while MVO was heated at 100 ºC. Further, the presence of hydroxyl ions is far lesser in the composites as indicated by the less intense peak appearing at 1590 cm^{-1} in MVGO50.

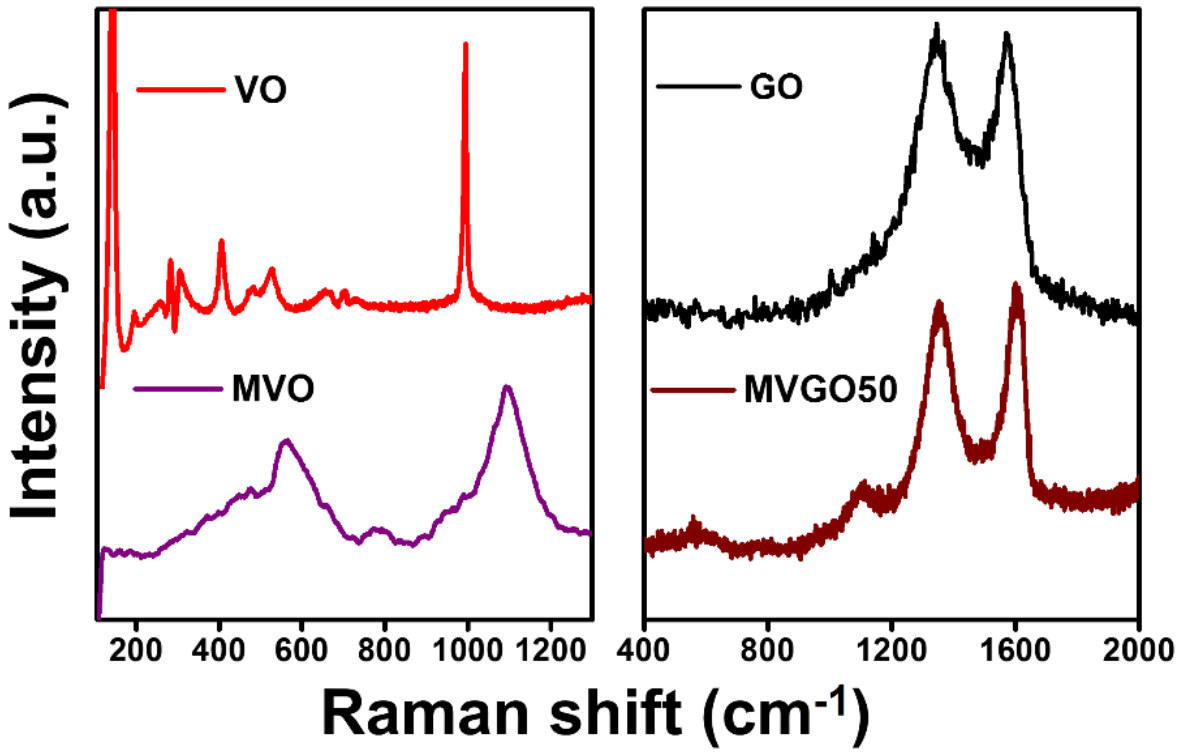

Figure 4.5: Raman spectra of VO, MVO, GO and MVGO50

Fig. 4.5 shows the Raman spectra of the as-synthesized MVO compared with pristine VO and pristine GO compared with MVGO50. The well resolved spectrum of VO exhibits several peaks among which, the peak centred at 993 cm^{-1} is assigned to the vibrational stretching mode related to vanadium oxygen bond V=O. Also the sharp peak at 137 cm^{-1} is owing to skeletal bent vibration of V-O-V bond (Fang 2008). Angle bending modes gives rise to peaks in the region 200-500 cm^{-1} (Perera et al. 2013). In MVGO50 two peaks at 1353 and 1599 cm^{-1} are observed, which correspond to the D (disordered) band and G (graphite) band of carbon respectively (Chen et al. 2014). In order to effectively transfer the electrons between MVO and graphene in the MVGO composites, it is important to have larger conducting domains (i.e. higher sp^2 carbon atoms). The D band and G bands of graphene oxide are associated with sp^3 and sp^2 carbons, respectively and it is well known that the D band intensity decreases (due to increase in the numbers of sp^2 carbon atoms) a little in comparison to G band while graphene oxide undergoes reduction (Perumbilavil et al. 2017) . As seen from the MVGO spectrum, the intensity of G band is slightly higher than that of the D band indicating that the graphene lattice consists of more sp^2 carbons due to the reduction of graphene oxide during hydrothermal treatment (Perera et al. 2013).

Surface morphology of MVO and MVGO50 were comprehensively characterized by TEM as shown in Fig. 4.6 (a) - (c), are TEM images of MVO obtained at different magnifications. It is evident from the micrographs that as-prepared MVO sheets are loosely stacked, irregular and rough with wrinkles made of one or few layers. TEM analysis indicates that the layered MVO sheets are prone to aggregation. On the other hand, Fig. 4.6 (d) – (f) are TEM images corresponding to MVGO50 obtained by hydrothermally reacting GO with MVO. The micrographs in Fig. 4 (d) clearly exhibit a layered structure of graphene sheets embedded with spherical MVO nanoparticles. The change in the morphology of MVO from 2D sheet like structure to 3D nanospheres can be attributed to the hydrothermal conditions and their vulnerability towards aggregation. However, interestingly the amorphous phase of MVO was found to be intact as evidenced from high-resolution TEM (HRTEM) analysis and MVO on the whole was found to evenly combine with graphene nanosheets. Further, the lattice spacing value of 0.37 nm obtained through HRTEM analysis (see Fig. 4.6 (f)) on

MVGO50 can be indexed to the (002) peak of graphene – reconfirms the reduction of graphene oxide under hydrothermal condition as evident through XRD studies (Chen et al. 2014).

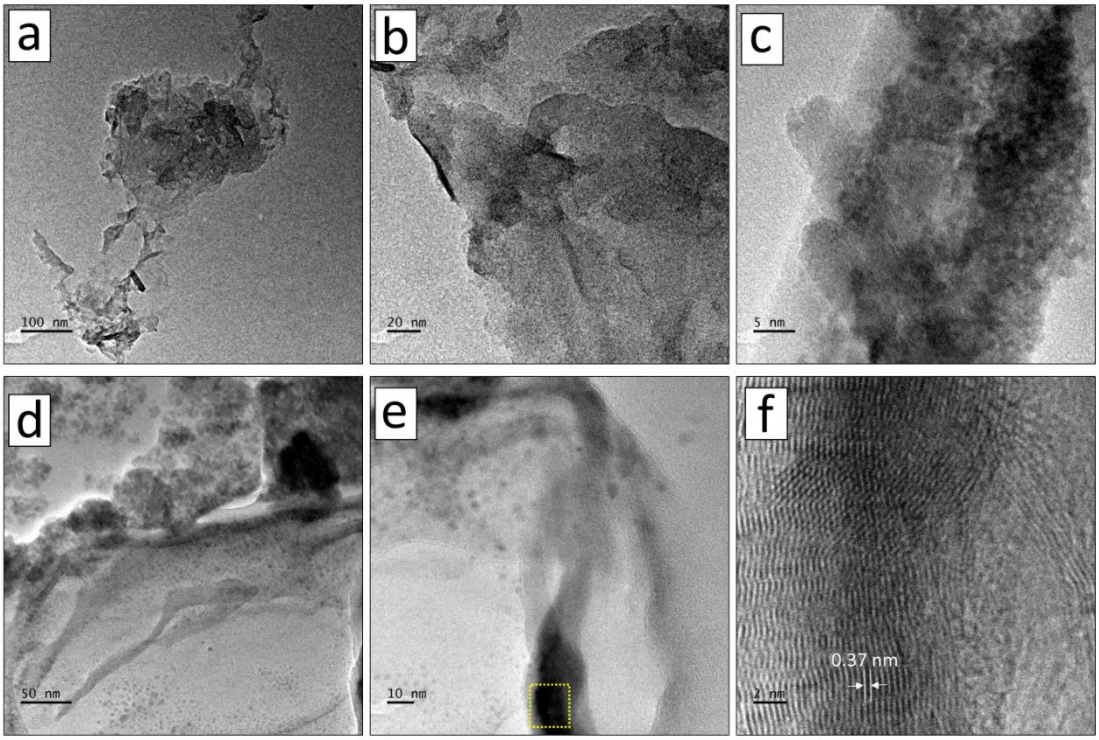

Figure 4.6 : (a, b, c) Transmission electron micrographs of MVO at different magnifications indicating the layered sheet like structure and (d, e) TEM images of MVGO50 obtained at two different magnifications. (f) High resolution TEM image obtained from the area marked in (e).

The chemical composition of the as-synthesized samples are analyzed through energy dispersive X-ray spectroscopy (EDS). EDS results of the MVGO50 presented in Fig. 4.7 indicates the presence of higher carbon content in comparison to MVGO10 and MVGO25, confirms the higher weight percentage of graphene oxide loading. On the other hand, EDS results also is an evidence that the samples are pure and are void of impurities.

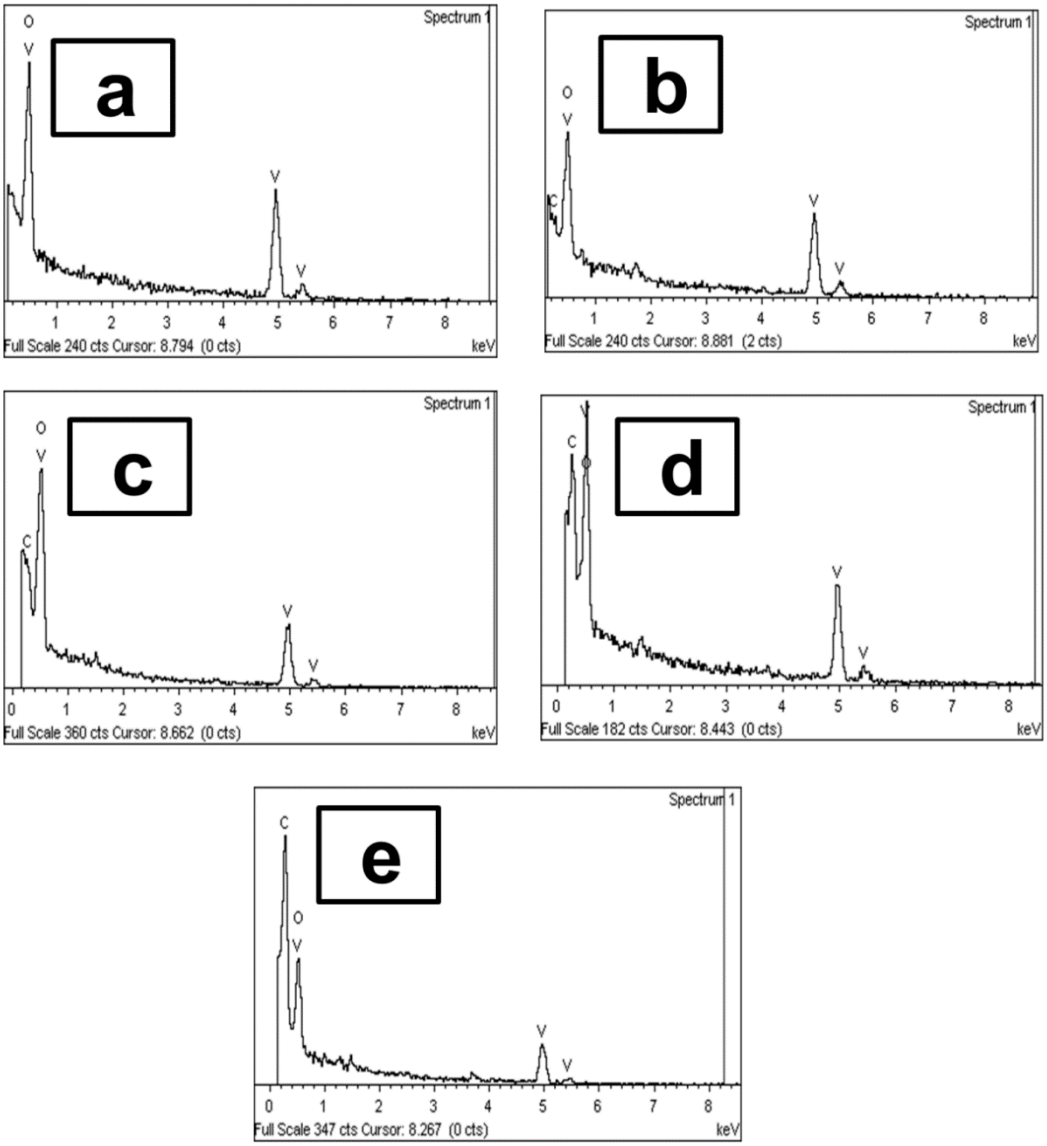

Figure 4.7 : Energy dispersive X-ray spectra corresponding to (a) crystalline VO, (b) MVO, (c) MVGO10, (d) MVGO25 and (e) MVGO50.

4.3 Applications of the vanadium pentoxide/graphene oxide composites.

4.3.1 Electrochemical dopamine sensing

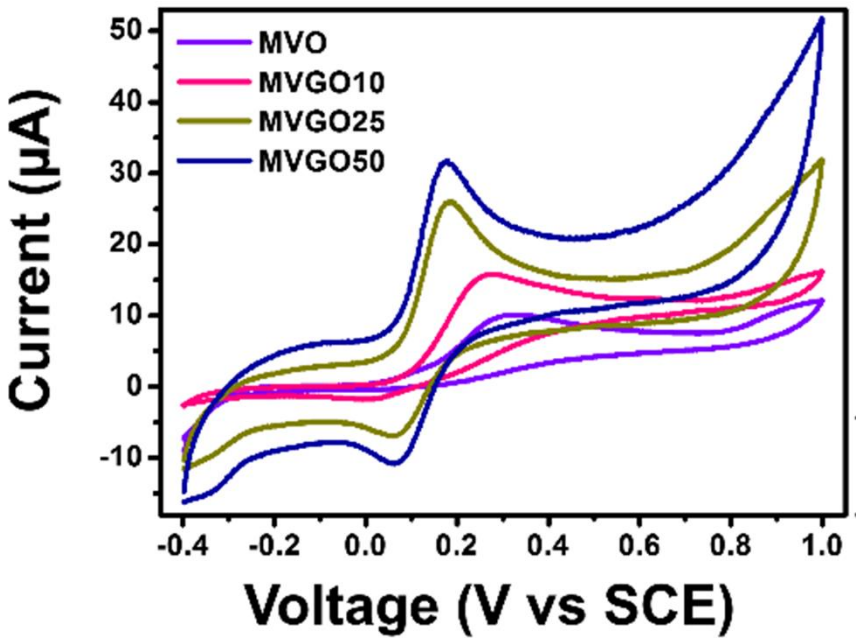

Figure 4.8: CV curves of MVO and MVGO composites at scan rate of 100 mV/s in 0.1 M PBS solution

Chemically modified electrodes were employed for sensing dopamine. Fig. 4.8 shows the response of the composite electrodes, towards 50 mM concentration of the dopamine, at a scan rate of 100 mV/s. Even at higher values of scan rate the redox peaks are more significant, indicating that the electrode material has a good rate capability (Yang et al. 2013). The higher peak intensity from the cyclic-voltammetric (CV) curves obtained with the composite signifies successive oxidation of electroactive dopamine into dopamine-quinone (DAQ) at the electrode surface. Fig. 4.9 (a) shows the dopamine oxidation at the electrode surface. Also, Fig. 4.9 (b) shows the dopamine oxidation and reduction happening at the electrode surface. The irreversible DAQ formation at the electrode surface is a serious problem, since the quinone formed has to be continuously converted back to dopamine for its detection. Further, oxidation of dopamine to DAQ

hinders the sensitivity and selectivity capabilities of the bare electrodes towards dopamine detection (Wieckohskie et al. 1984). Therefore, the higher the anodic/cathodic peak intensity ratio, the better is the reversible sensing reaction. It is evident from the Fig. 4.8 that among MVO, MVGO10, MVGO25 and MVGO50, the

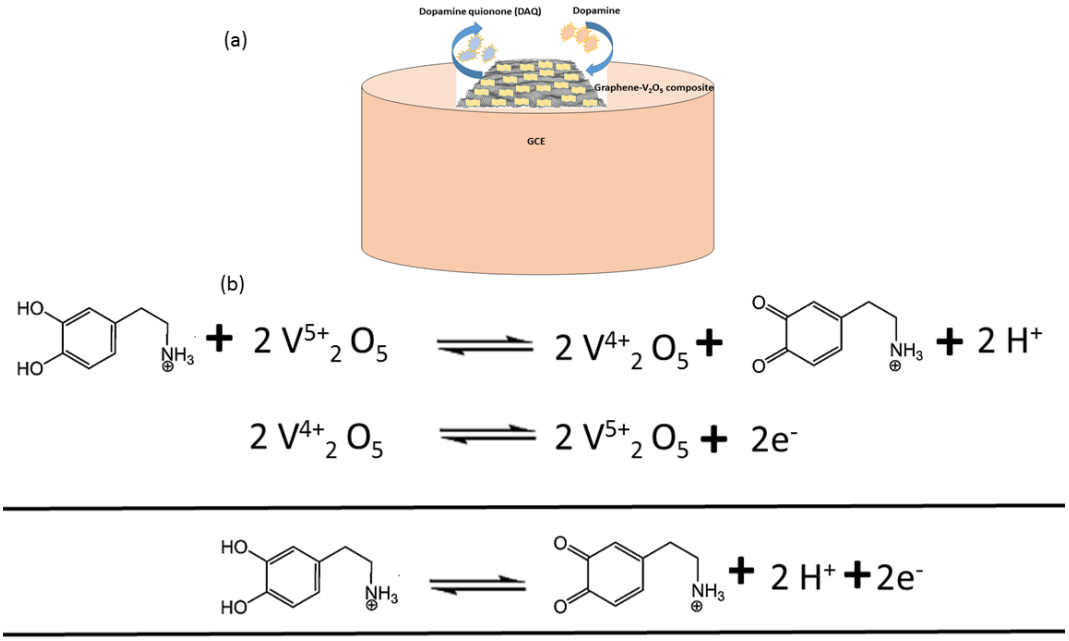

Figure 4.9: (a) Schematic representation of the dopamine oxidation at the electrode surface (b) shows the dopamine oxidation and reduction at the electrode surface.

composite with higher GO content (i.e. MVGO50) shows better response. The adequate presence of oxygen containing functional groups in MVGO50 assists in effective adsorption and pre-concentration of redox species by the rapid transfer of electrons between the biomolecules and electrode substrate, which resulted in excellent dopamine sensing performance. The distinctive peak in the graph appearing at 0.18 V for MVGO50 in comparison to the MVO at 0.3 V at a scan rate of 100 MV/s, indicates that the sensor can be operated at a relatively low voltage while there is a synergy between MVO and GO owing to the larger electroactive sites in graphene (Suresh et al. 2014). Incorporation of graphene in MVO is found to play a dual role: while it increases the surface area for enhanced dopamine adsorption, it also enables easy faster transfer of electrons owing to its higher electrical conductivity.

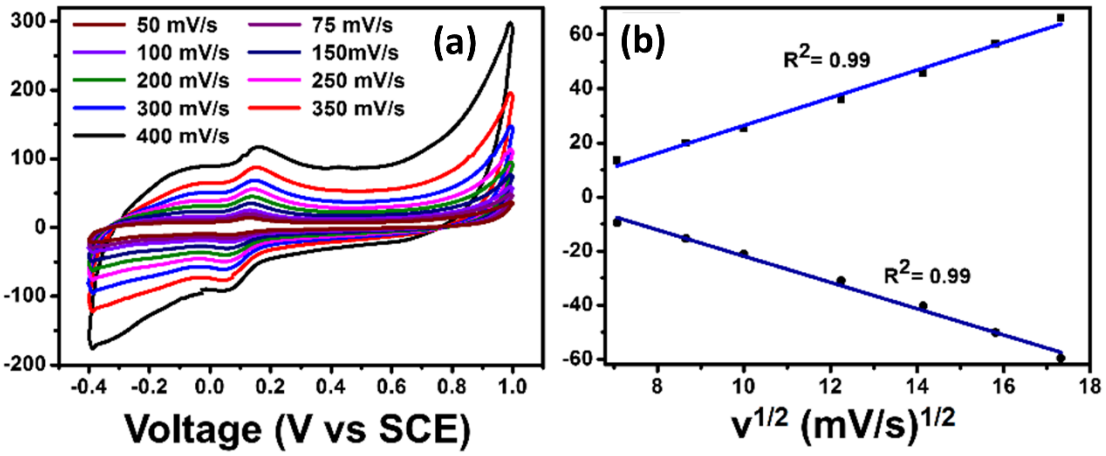

Figure 4.10: (a) CV curves of MVGO50 at various scan rates in 0.1 M PBS solution containing 10 µM dopamine and (b) linear plots of anodic and cathodic peak current against the square root of scan rate, where R-squared (R^2) value determines the best fit.

On the other hand, dopamine sensing performance using MVGO50 modified GCE (MVGO50/GCE) was investigated using CV at various scan rates as shown in Fig. 4.10 (a). A pair of quasi-reversible anodic and cathodic peaks caused by the redox process in dopamine was observed at the MVGO50/GCE and the corresponding dopamine sensing mechanisms are well discussed in literature (Pandikumar et al. 2015). With an increase in scan rates (50-400 mV/s) the anodic and cathodic peak currents and increased simultaneously. Since anodic peak current (I_{pa}) is found to be more pronounced than cathodic peak current (I_{pc}), electrooxidation of dopamine is significant. Fig. 4.10 (b) represents the linear plots of anodic and cathodic peak current against the square root of the scan rate, indicating the diffusion controlled redox process for which the regression relations can be written as follows (Suresh et al. 2014):

$$I_{pa}\ (mA) = 0.00512\ v^{1/2} + (-0.02477)\ (mA)\ [R^2 = 0.9904]$$

$$I_{pc}\ (mA) = -0.00486\ v^{1/2} + (0.02675)\ (mA)\ [R^2 = 0.9913]$$

Chronoamperometry (CA) was used for detection of dopamine owing to its higher current sensitivity compared to CV. Fig. 4.11(a) shows, the variation of current with increase in dopamine concentration. After the addition of dopamine (0 to 75 µM) into

the electrochemical cell, an obvious increase in current was observed as seen from the corresponding calibration plot in Fig. 4.11(b), wherein two linear portions are observed corresponding to the lower and higher concentrations regions. The data is fitted with a polynomial as, *Current (I, nA) = Intercept (I, nA) + B_1 × Concentration (µM) + B_2*×

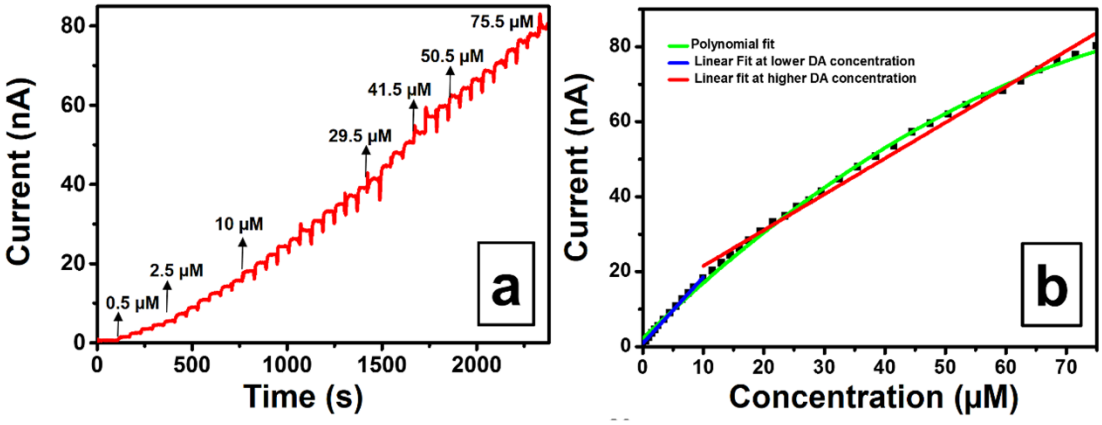

Figure 4.11 : (a) Chronoamperometric response of MVGO50 electrode during the successive addition of dopamine (0 to 75 µM) to 50 ml of 0.1 M PBS at an applied voltage of 0.18 V (b) plot indicating the variation in current (nA) with respect to change in the concentration of dopamine

Concentration (µM)^2, where B_1 = 1.55261 nA, B_2 = -0.00708 nA and intercept = 2.18243 nA . The R^2 (regression fit) value = 0.99 ensures the best fit. The unknown concentration can be directly deduced by substituting the known current values in the fitted polynomial. Further, to study the sensing capability of MVGO50 electrode a linear fit was determined for the data collected at lower (0 to 10 µM) as well as higher concentrations (10 to 75 µM) of dopamine. The fit at the lower concentrations follows the equation, *(I, nA)* = 0.89007 *(I, nA)* + 1.76772 nA/ µM × *concentration (µM)* with (R^2 = 0.99). Similarly, at higher dopamine concentrations, the fitted data follow the equation, *(I, nA)* = 11.92433 *(I, nA)* + 0.95644 nA/ µM × *concentration (µM)*, (R^2= 0.99137). The lower detection limit of dopamine using MVGO50 electrode as the sensor from the fitted data was found to be 0.07 µM with a high sensitivity limit of 25.02 µA mM^{-1} cm^{-2}.

Biomolecules like dopamine exist along with other biological species such as uric acid and ascorbic acid, owing to which selective sensing capability of electrochemical

sensors is of utmost importance (Ban et al. 2009). Here, we have studied the selective sensing capability of MVGO50 composite electrode as sensor by adding uric acid along with dopamine, after which CV measurements are recorded for evaluating the sensor performance. Two distinctive peaks are observed corresponding to the oxidation of dopamine and uric acid as shown in Fig. 4.12 (a), confirming that MVGO50 is capable

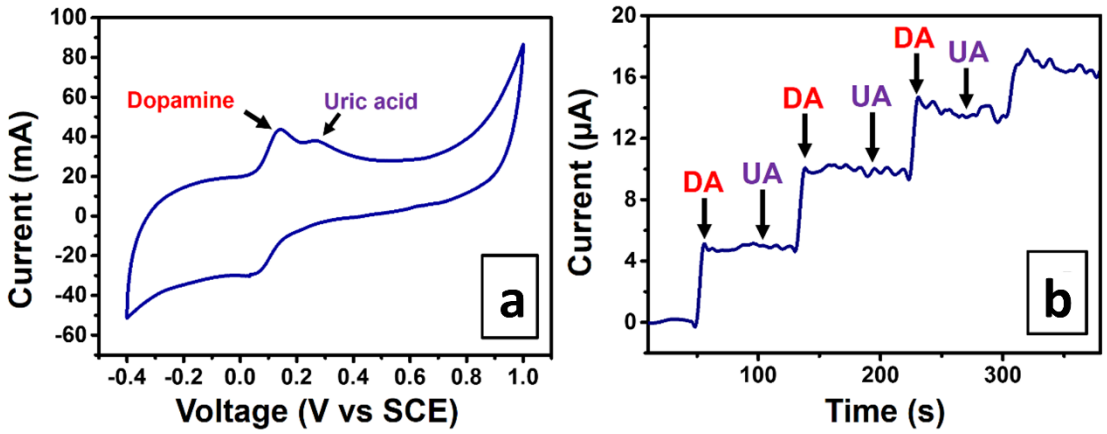

Figure 4.12 : (a) CV response of MVGO50 electrode in the presence of 50 mM of dopamine as well as uric acid at 50 mV/s and (b) chronoamperometric response of the MVGO50 electrode with the successive addition of 10 μM of dopamine in presence of 10 mM uric acid at 0.18 V.

of selectively detecting dopamine without being affected by the interference of uric acid (Suresh et al. 2014). The amperometric data as seen in Fig. 4.12 (b) showed a stepwise increase in current only with the addition of dopamine and remained insensitive to uric acid addition, indicating the selective sensing capability of MVGO50. Further, it should be noted that the sensor showed excellent selective sensitivity since, the concentration of dopamine added during amperometric studies was three orders of magnitude lower than that of uric acid. Therefore, at a given potential, MVGO50 composite is useful in selective detection of dopamine. Table.4.1 shows the coparison between the present work with earlier reports.

Table. 4.1. Comaprison of the dopamine sensor with earlier reports

Paper	Detection Limit	Linear range	Sensitivity	ref
Lithium doped vanadium oxide nanoribbons	1.0 × 10−7 M	2.0 × 10−6 to 1.0 × 10−4 M	-----	(Zhuo et al. 2011)
V2O5@polyailine nanohybrid	3.9 × 10−5 M	6.6 µ M to 1.1 × 10−4	-----	(Suresh et al. 2014)
Ni-doped V2O5	----	6.6–96.4 µM	132 nA M^{-1}	(Suresh et al. 2014)
This work	0.68 µM	0 to 10µ M and 10 to 70 µ M	25.02 µA mM^{-1} cm^{-2}	Present work

4.3.2 Applications of vanadium pentoxide/graphene oxide composites in lithium ion battery electrode

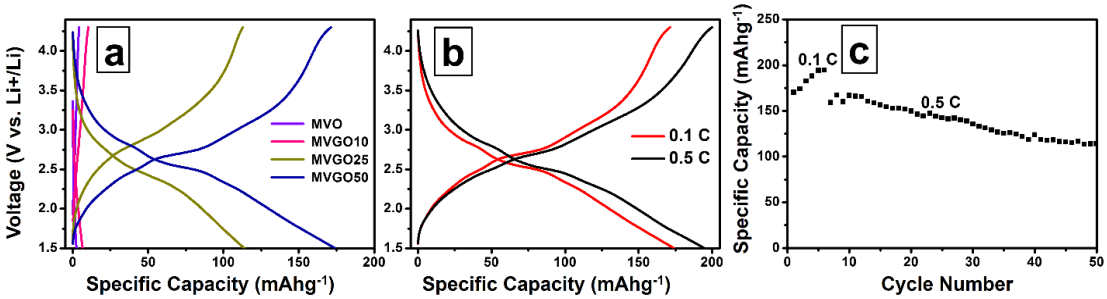

Figure 4.13 : The first cycle charge-discharge profiles at a current density of 0.1 C using MVO and MVGO composites as electrodes. (b) Charge-discharge profile and (c) comparison of cyclic behavior of MVGO50 electrode at two different current densities (0.1 C and 0.5 C).

The charge-discharge profiles for MVO and MVGO composites are illustrated in Fig. 4.13 (a). As observed from the results, MVO exhibited a poor charge-discharge capacity with a value of 2.2 mAg^{-1}. The poor rate capability of melt quenched vanadium oxides reported by Menictas et al. (2009) was attributed to a relatively high charge-transfer resistance. Similarly, Liu et al. reported poor rate capability of melt quenched vanadium oxides due to the irreversibility of the phase during deep discharging and owing to their poor electrical conductivity (Wieckohski 2014). Upon addition of GO, the material was found to exhibit improved electrochemical performance. Herein, as mentioned in the experimental section the MVGO50 composites were prepared by the embedment of MVO on GO under hydrothermal conditions where, GO is partially reduced to graphene as observed from XRD and Raman analysis. In comparison to electrodes prepared using composites with lower weight percentage of graphene oxide (i.e. MVGO10 and MVGO25), MVGO50 electrode delivers first discharge capacity around 175 $mAhg^{-1}$ and maintains high capacity in the range of 200 $mAhg^{-1}$ for the first 10 cycles (between 1.5 V and 4.3 V at 0.1 C rate). Obviously, the poor discharge capacity in case of MVGO10 and MVGO25 in comparison to MVGO50 can be attributed to the higher percentage of MVO and their poor electrical conductivity. On the other hand, the enhanced performance of MVGO50 electrodes can be attributed to the presence of the higher percentage of partially reduced graphene oxide (more sp^2 carbon atoms) leading to better electrical conductivity.

As evident from the TEM image of MVGO50, the nano-sized pores are believed to be favourable for the diffusion of electrolytes and Li ions to the active material. Fig. 4.13 (b) shows the comparison of cyclic behaviour of the MVGO50 at different current rates of 0.1 C and 0.5 C. The rate performance of the MVGO50 composite as a cathode in lithium ion delivery has been improved greatly. This is because of larger surface to volume ratio that shortens the distance for electron transport and reduces charge transfer resistance at the electrode/electrolyte interface (Jia et al. 2016). Therefore, the superior performance of the MVGO50 nanocomposite as electrodes can be attributed to uniform embedment of MVO over GO during hydrothermal conditions. Furthermore, the hybrid structure could also prevent structural degradation of the electrode upon cycling (Li et al. 2014). Fig. 4.13 (c) shows the variation of capacity while MVGO50 electrode was cycled. The capacity is found to increase in the initial cycles and a small dip is observed

owing to the fact that the liquid electrolyte may not be fully absorbed in the electrode film at the beginning of cycling. As the time progressed, the electrolyte is absorbed properly on the surface and available area increased to the maximum possible. Thereafter, the capacity of MVGO50 was found to decrease slowly up to 50^{th} cycle and then remains stable. Therefore, MVO composites with graphene with less water content are capable of exhibiting better capacity retention owing to their higher electrical conductivity.

4.4 Summary

- Vanadium oxide and graphene oxide composites have been prepared by melt quenching of vanadium oxide, followed by the hydrothermal treatment of the precursors.
- Chronoamperometry studies conducted on the MVGO50 composite electrodes, for the detection of dopamine over a wide range of concentration, exhibited a highest sensitivity of 25.02 μA mM^{-1} cm^{-2} with the lowest detection limit of 0.07 μM.
- Chronoamperometry studies revealed the excellent selective dopamine sensing capability of MVGO50 composites even in the presence of a highly concentrated solution of uric acid as the interfering species.
- MVGO50 composite was found to be a good candidate for lithium-ion battery applications as they exhibited an enhanced rate capacity of 200 $mAhg^{-1}$ at a current of 0.1 C rate through galvanostatic charge-discharge cycling studies.
- The excellent electrochemical sensing and energy storing capacity of the composites is attributed to the fast Faradaic reactions emanating from a percolated diffusion network, created by the synergistic embedment of vanadium oxide on graphene oxide.

Chapter 5

Preparation and Characterization of Reduced Graphene Oxide / ZnO Composites for Glucose Sensing and Supercapacitors

This chapter deals with the preparation and characterization of reduced graphene oxide and zinc oxide composites. A microwave assisted technique has been used for the preparation of the composite. The prepared composite was characterized for its structural properties using XRD, SEM, HRTEM and Raman spectroscopy. A supercapacitor electrode has been faricated and its performance was evaluated. Further, the electrochemical sensing properties are studied using chronoamperometry and found that the composite is useful in the hydrazine detection and non-enzymatic glucose sensing. A better sensitivity and lower detection limits are reported.

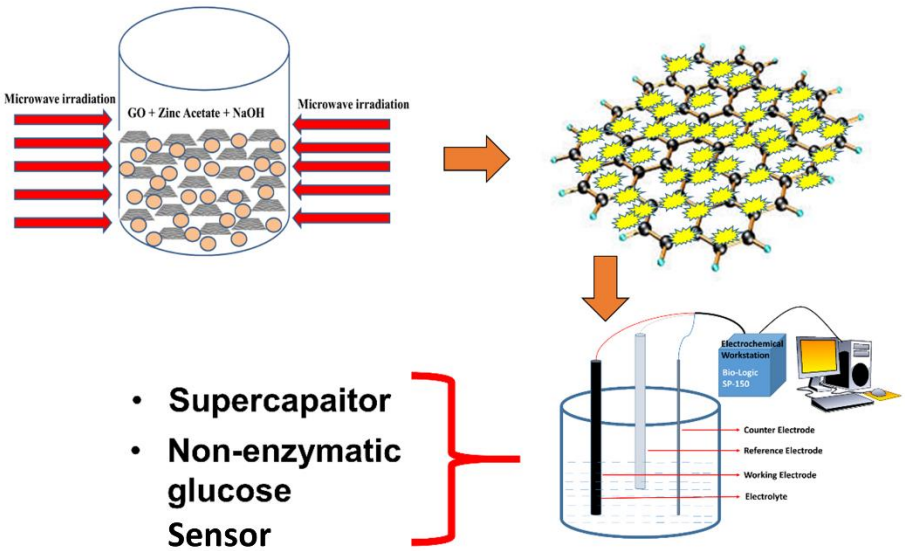

5.1 Preparation of reduced graphene oxide / zinc oxide composite

5.1.1 Introduction

Zinc Oxide (ZnO) is a material which is under the investigation of researchers across the world because of its exciting properties. ZnO, a wide band gap semiconductor finds promising electrical and optical properties. The properties of the ZnO can be tuned by the introduction of defects by doping. ZnO finds applications in transparent conducting oxide films, sensors, solar cells, electrochemical devices etc.

The challenging problem in working with ZnO is its relatively less stability. When the material is exposed to the atmospheric conditions or chemicals there is a chance that the material may undergo degradation affecting its properties. Making composites with other materials is one way to achieve better stability and better properties. In this chapter, zinc oxide/ Graphene oxide composite is prepared by a microwave assisted method. The prepared composites are studied using its structural characterization techniues. The applications in supercapacitors, non-enzymatic glucose sensing and hydrazine sensing are also studied.

5.1.2 Experimental details

5.1.2.1 Preparation of ZnO

Figure. 5.1 : Schematic representation of the experimental setup used for the preparation of ZnO and rGO/ZnO composite.

ZnO has been prepared with the aid of microwave irradiation. Zinc acetate (250 mg) was dispersed in 100 ml of DI water. 2g of NaOH was separately dispersed in 100 ml of DI water. The solutions were mixed together and treated with microwave irradiation (450 W) for 20 minutes. The product was washed several times with DI water and ethanol. The final product was separated and dried at 60 ^{o}C overnight to obtain the composite (Moghaddam et al. 2007, Zhang et al. 2007). Fig. 5.1 schematically represents the reaction setup for making the nanoparticles and the composites.

5.1.2.2 Preparation of GO/ZnO composite

The composite was prepared in situ along with the formation of ZnO. Initially, Zinc acetate (250 mg) and graphene oxide (100 mg) were dispersed in 100 ml of DI water using probe sonication and a solution (100 ml) of 2g NaOH was added to this. The solution was then subjected to microwave irradiation (450 W) for another 20 minutes. In the experiments a higher concentration of NaOH was used to enable in-situ reduction of GO while forming ZnO (Perera et al. 2012). The different weight percentage loading of ZnO was achieved by varying the zinc acetate precursor. The composites obtained were named as ZG1, ZG2 and ZG3 corresponding to the precursor concentrations of 250 mg, 500 mg and 1000 mg, respectively.

5.1.2.3 Preparation of the modified glassy carbon electrode (GCE)

Prior to the preparation of the electrodes, the glassy carbon electrode was cleaned by mechanical polishing using velvet cloth followed by electrochemical polishing. The electrode was mirror polished to remove noticeable scratches. 1 mg ZnO was dispersed in DI water along with 20 µL of Nafion® solution and was made up to 1 ml. Before coating the material onto the GCE surface, the solution was ultrasonically agitated for 15 minutes to obtain a proper dispersion. GCE was coated with 1 µL solution of active material. The modified electrode was dried at room temperature to obtain a uniform adhesive film over GCE. The same preparation steps were repeated for the preparation of the composite electrode. For the preparation of the supercapacitor electrode the same procedure was followed by adding conductive carbon black as a conducting agent. The ratios of the composite, nafion and conductive carbon black was kept at (80:10:10).

5.2 Characterization of reduced graphene oxide / zinc oxide composite

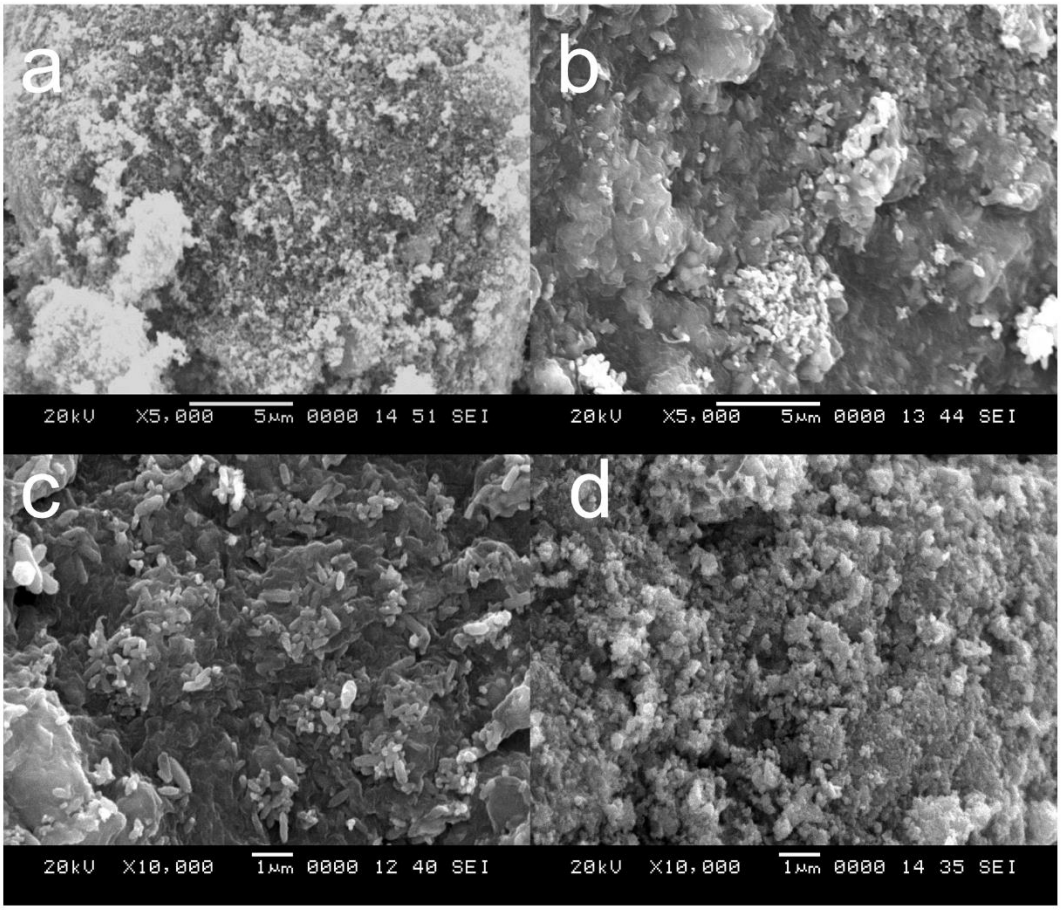

Figure. 5.2 : (a-d) SEM micrographs of ZnO, ZG1, ZG2 and ZG3 respectively

Fig. 5.2 (a-d) show the SEM images of the rGO-ZnO composites. The pristine ZnO electron micrograph shows nanosized particles which are agglomerated. ZG1, the sample containing highest GO content shows graphene sheets along with the ZnO nanoparticles embedded into it. It is evident from the SEM images that the ZnO particles are grown over the graphene sheets. With increase in the ZnO content in the composite from ZG1 to ZG3, the increase in the ZnO coverage over the graphene is witnessed.

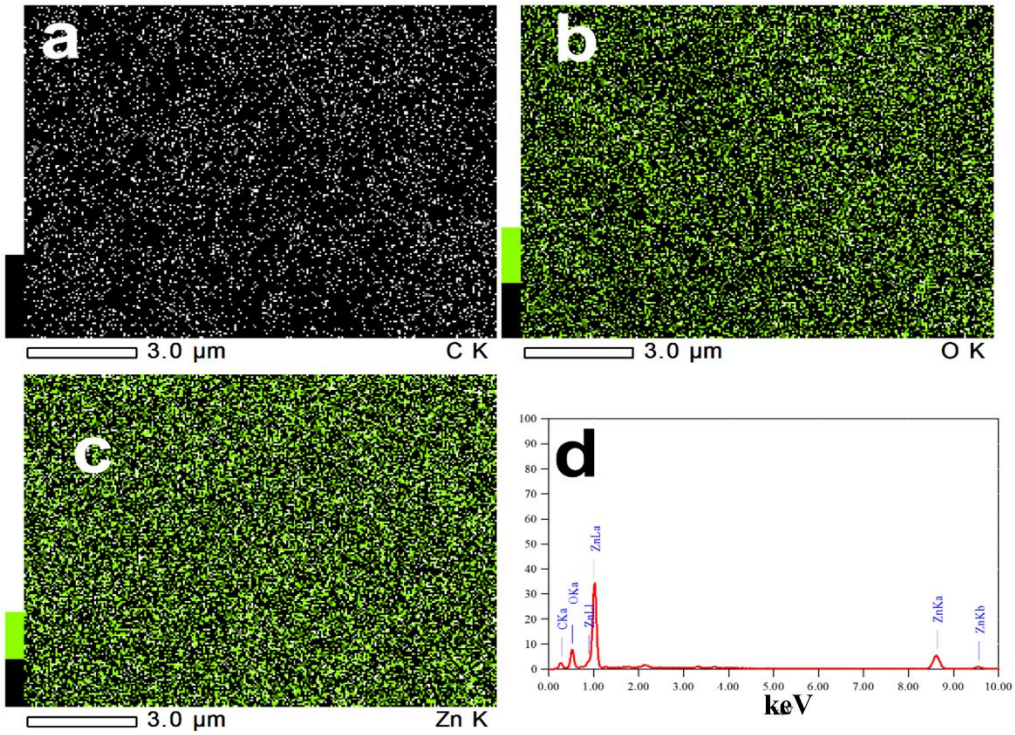

Figure. 5.3 : Elemental mapping of the ZG3 sample and (h) EDS analysis of ZG3.

The distribution of the carbon, zinc and oxygen was estimated using EDS mapping as shown in Fig. 5.3 (a-c). As expected the mapping shows that the zinc and oxygen contents are high compared to the carbon content of the ZG3 sample. To confirm this EDS analysis is also done and given as Fig. 5.3 (d). EDS result shows that Zinc and Oxygen comprise around 80% of the total mass and carbon content is 20%.

Fig. 5.4 corresponds to the high resolution TEM images of the composite (ZG1) at different resolutions, which reveals that the ZnO nanocrystals are anchored onto graphene sheets. The nanocrystals are 10-20 nm in size, which reasonably agrees with the crystallite size calculated from XRD results. The inset in the (Fig. 5.4 (b)) shows a magnified image, which clearly reveals the lattice arrangement in ZnO nanocrystal, with interplanar distance 0.28 nm. It is in agreement with the earlier report (Li et al. 2013). The heterogeneous nucleation of ZnO nanocrystals on graphene can be explained as follows. Initially, the Zn^{2+} ions get anchored onto graphene, allowing the

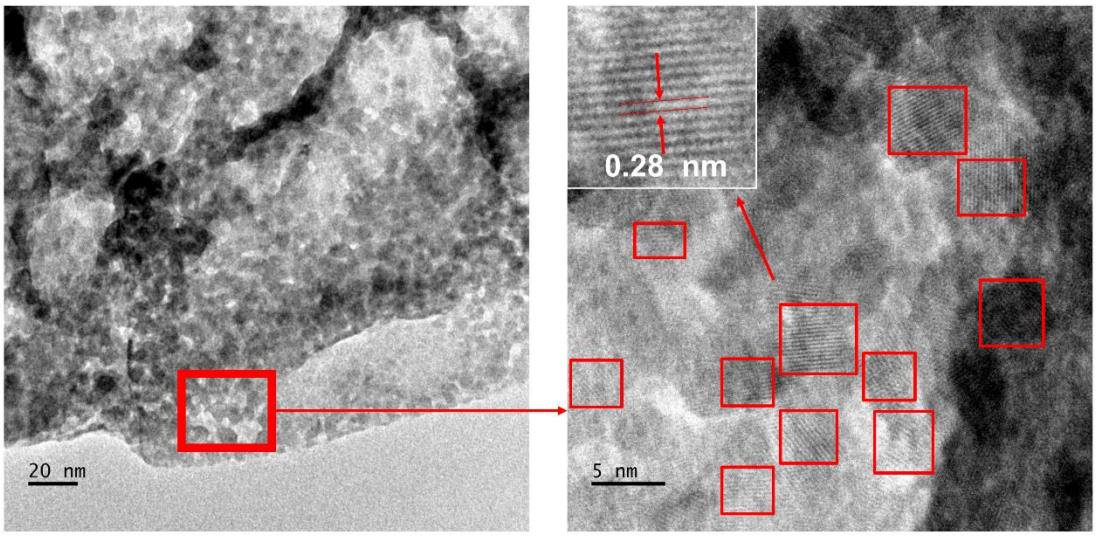

Figure. 5.4 : HRTEM image of the composite showing ZnO nanoparticles grown over the rGO sheets at different magnifications. The inset shows the lattice fringes of ZnO.

nucleation of Zn^{2+} with oxygen-containing groups, which initiates the reaction to form ZnO nanoseeds. In many cases the nucleation of ZnO to Zinc blende structure is favoured due to the hexagonal carbon arrangement of graphene (Liu et al. 2013). However, present microwave assisted growth favoured wurtzite structure, as evident from the X-ray diffraction pattern. The stacking structure and edges of graphene sheets provide the nucleation sites, since the nucleation rate depends on the breaking of C-C bonds of graphene. The pits or pores on the graphene sheets also provide additional nucleation sites (Li et al. 2013). Therefore seeding of large ZnO 2D nuclei is evident from TEM images, which later grow into 3D nanocrystals.

Figure. 5.5 shows the XRD patterns of the zinc oxide and the GO/ZnO composites. The crystalline peaks of ZnO nanocrystals are in agreement with the typical wurtzite structure (JCPDS file number 01-080-0075) (Farhat et al. 2015). The corresponding peaks were labeled with respective planes. Using XRD, the crystallite size of the nanoparticle was estimated using Debye - Scherrer formula, $D = k\lambda/\beta cos\theta$ where D is the crystallite size (nm), λ is the wavelength of incident X-ray (nm), β is the full width half maximum, and θ is the diffraction angle. The obtained values are tabulated

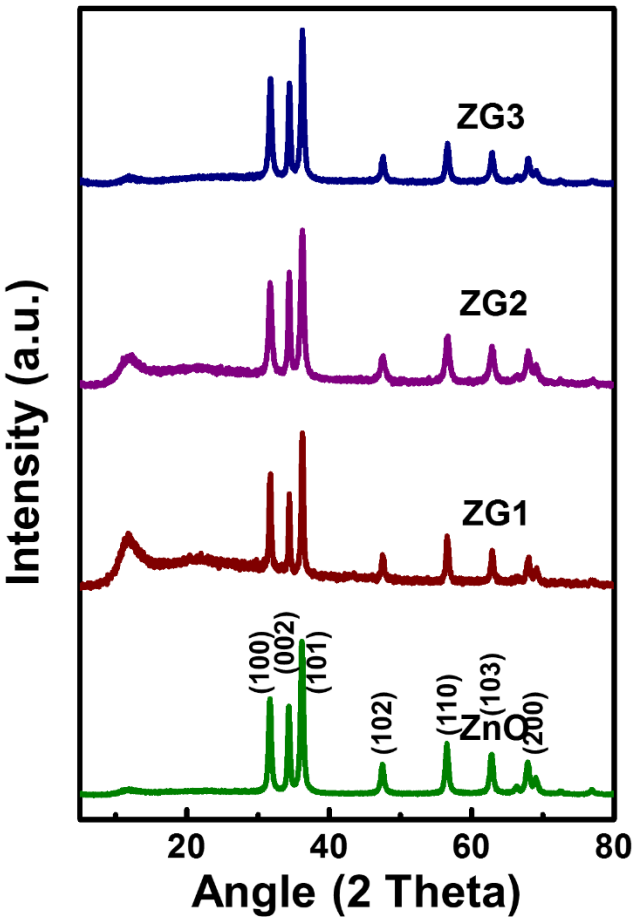

Figure. 5.5 : XRD patterns of the samples with different weight percentage loading of ZnO along with graphene oxide.

in Table. 5.1. The crystallite sizes estimated using XRD match well with the sizes calculated from TEM images.

Table 5.1. Crystallite sizes calculated from XRD data using Debye - Scherrer formula.

Sample	ZnO	ZG1	ZG2	ZG3
Crystallite Size (nm)	16.82	22.75	14.38	17.4

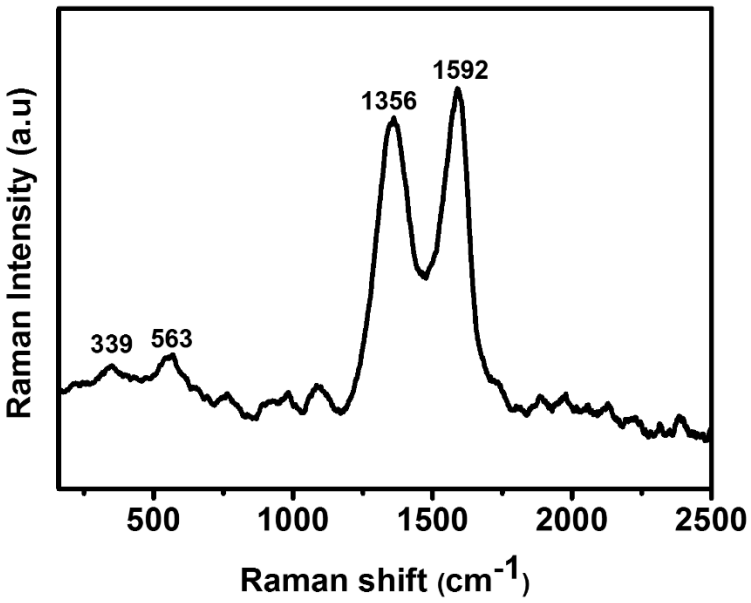

Figure. 5.6 : Raman spectrum of the reduced graphene/ Zinc oxide nanocomposite (ZG3).

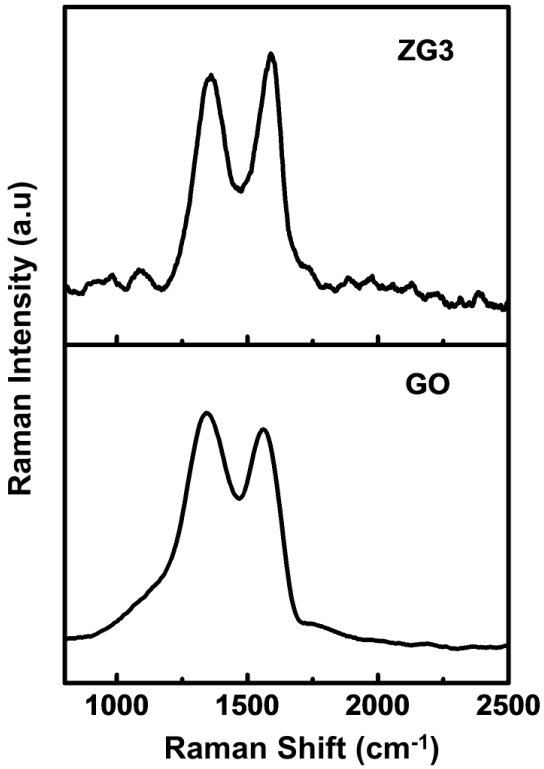

Figure. 5.7: Comparison of Raman spectra of ZG3 sample and the graphene oxide.

Fig. 5. 6 shows the Raman spectrum of the composite, ZG3. The peak at 1356 cm^{-1}, is the D band of graphene, corresponding to the breathing mode of *K* point phonons. The D band intensity is correlated with the defects in the graphene. The peak at 1592 cm^{-1} is the G band, which is attributed to the first order scattering mode of the E_{1g} phonons. The ratio of intensities of D band to G band is important as far GO is concerned. I_D/I_G for the sample ZG3 is found to be 0.90, which indicates lower defect concentration. To see the difference, the Raman spectra for GO was also recorded (Fig. 5.7) and the I_D/I_G ratio was found to be 1.003. The decrease in the ratio implies the restoration of sp^2 graphitic peaks through the deoxygenation process (Akhavan, 2014). This indicates that during the microwave irradiation under alkaline condition the GO in the reaction mixture is reduced to reduced graphene oxide. The reduction can restore the electronic conductivity of the sample which is very important in electrochemical applications. The peaks at 339 and 569 cm^{-1} correspond to ZnO, where the second order Raman process gives rise to the peak at 339 cm^{-1} and the peak at 569 cm^{-1} arises from the A_1(LO) and E_1 (LO) modes (Abdolhosseinzadeh et al. 2016).

5.3 Applications of reduced graphene oxide / zinc oxide composite

5.3.1 rGO-ZnO composite as an electrode in supercapacitor applications

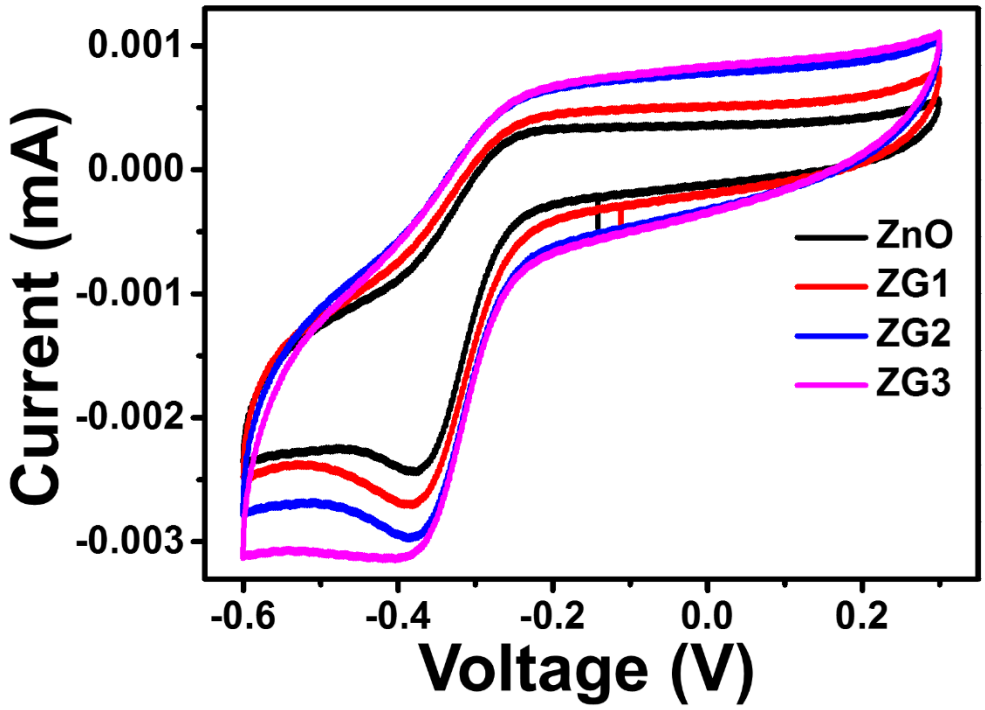

Figure. 5.8: CV curves of the nanocomposites showing the increase in supercapacitor performance

Fig. 5.8 shows the CV curves for the bare ZnO and the composites using three electrode system in 1M KOH electrolyte in the potential range -0.6 V to 0.3 V. The CV curve was recorded at a scan rate of 5 mV/s, which shows a broad redox peak at -0.37 V indicating the pseudocapacitive nature of the ZnO. The K^+ ions in the KOH electrolyte play an important role in the pseudocapacitive behavior. The ZnO particles interact with the K^+ ions to form ZnOK. ($ZnO + K^+ + e^- \Leftrightarrow ZnOK$) This process significantly enhances the supercapacitor performance (Zhang et al. 2015, Zhang et al 2009).

The specific capacitance (C_s) of the sample at different scan rates was calculated using the equation (Xiang et al. 2013),

$$C_s = \frac{\int I(v)dv}{m \times v \times \Delta V}$$

Where, I is the current, m is the mass in gram, v is the scanning rate and ΔV is the potential difference. The specific capacitance of pristine ZnO was found to be 453 F g^{-1}. The composite electrodes ZG1, ZG2 and ZG3 reveal a specific capacitance of 534 F g^{-1}, 588 F g^{-1} and 635 F g^{-1} respectively at 5 mV/s. Much of the contribution towards specific capacitance is attributed by pseudocapacitance reaction. The nano size crystals enhance the electrolyte-electrolyte interaction, thus electrochemical double layer capacitance also contributes to the enhanced specific capacitance. The incorporation of rGO resulted in the increase in surface area, as well as in better conductivity, enhancing electron transport. It may be noted that, the observed capacitance is far higher compared to the earlier reports as seen from Table. 5.2

Table 5.2. Comparison of ZnO capacitance values with reported values.

Paper	Capacitance (F g^{-1})	Reference
ZnO supported on porous electrode	300	(Ray et al. 2015)
ZnO/ activated carbon composite	160	(Selvakumar et al. 2010)
Graphene/ZnO composite	146	(Lu et al. 2011)
ZnO/Carbon nanotube composite	48	(Aravinda et al. 2013)
ZnO/reduced GO through chemical synthesis	308	(Chen et al. 2011)

Graphene-ZnO hybrid	156	(Li et al. 2013)
Activated carbon/ZnO composite	117.4	(Li et al. 2014)
Single crystal ZnO/ Metal oxide composite	405	(He et al. 2011]
reduced graphene/ZnO composite	635	Present work

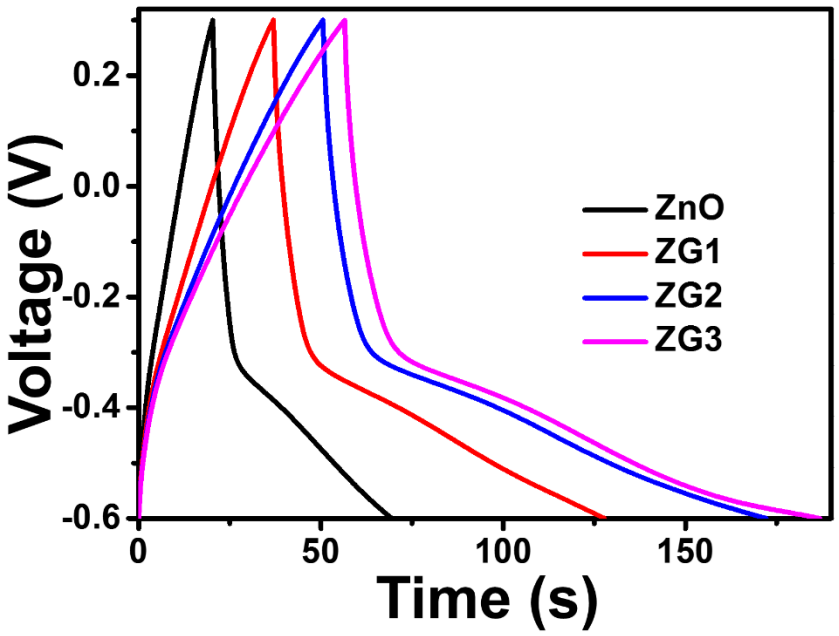

Figure. 5.9: Galvanostatic charge – discharge (GCD) curve for the samples at 1 mA g^{-1}.

Fig. 5.9 represents the galvanostatic charge-discharge curves of the samples recorded at 1 mA g^{-1}. It shows an IR drop followed by an electrochemical double layer capacitance and a plateau region which corresponds to the pseudocapacitance which is a typical ZnO charge-discharge characteristic (Zhang et al. 2015). The addition of graphene oxide resulted in the reduction of IR drop indicating the low internal resistance of the sample, leading to the enhancement of the performance of the material. TEM images showed that the ZnO particles are grown over the reduced graphene oxide sheets, which enables charge transport through a lesser ohmic path causing lesser ohmic drop (Fan et al. 2011). In the Fig. 5.9, the gradual discharge, which is contributed by the electrochemical double layer part shows an improvement in the case of composite

compared to pristine ZnO. This can be attributed to the increased surface area contributed by the reduced graphene oxide (Singh et al. 2016). GO surface can adsorb more ions as compared to the pristine ZnO crystal surface. The plateau region of the curve is due to the pseudocapacitive part which is again improved as a result of the addition of graphene oxide.

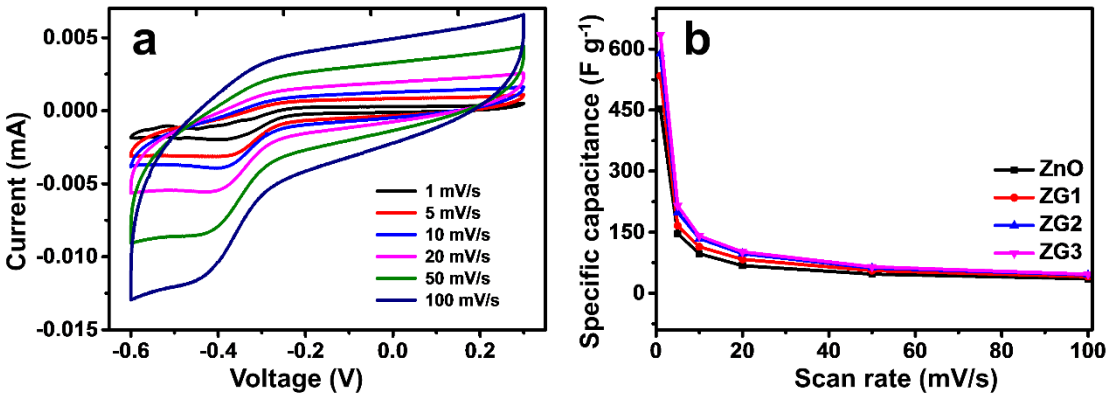

Figure. 5.10: (a) CV curves for the sample ZG3 at different scanning rates in 1M KOH solution and (b) shows the variation of specific capacitance along with the scanning rate.

Fig. 5.10 (a) represents the CV of the sample ZG3 at different scanning rates from 1 mV/s to 100 mV/s. The area under the curve increases with respect to scan rate. The capacitance of the samples was calculated at different scan rates and is represented in Figure 5.10 (b). It is evident that the capacitance increases with the decrease in the scanning rate. This is correlated with the adsorption and desorption of ions at available sites. At higher scan rates the ions do not get enough time to get into the available sites. However, at lower scan rates the ions diffuse and get adsorbed at available sites, increasing the specific capacity of the material (Zhao et al. 2012).

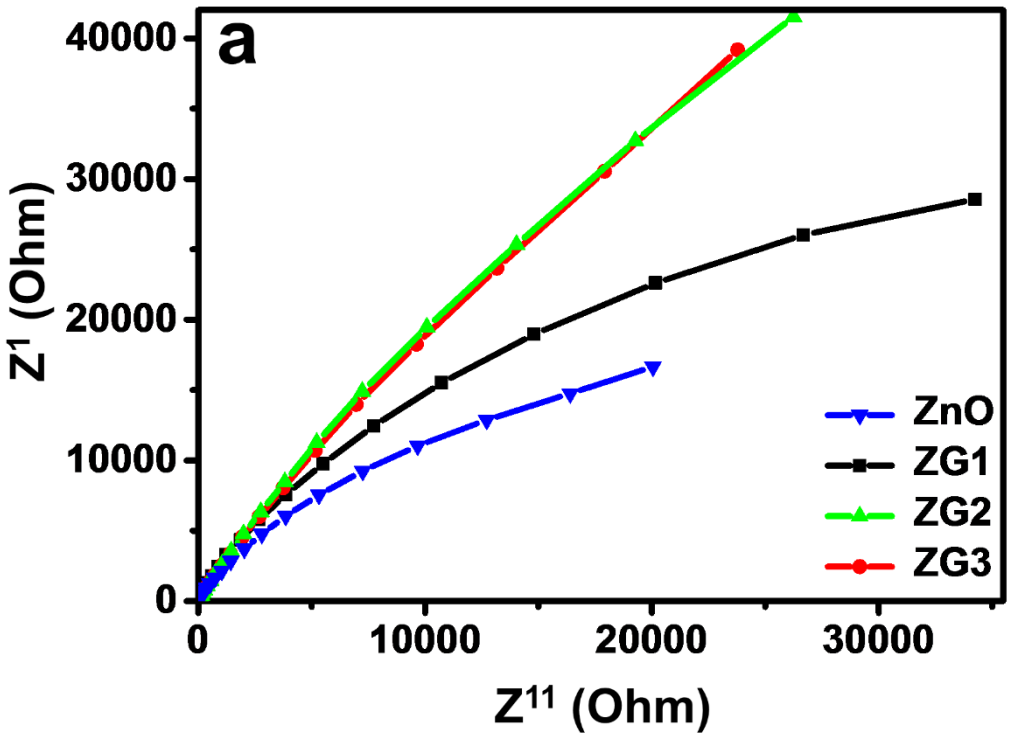

Figure. 5.11: Electrochemical impedance spectra (EIS) for the composite samples

Fig. 5.11 shows the electrochemical impedance spectra (EIS) of the sample, where the low- frequency behaviour is important for a supercapacitor. The straight line, known as Warburg resistance is due to the frequency dependent ion transport/diffusion of electrolyte in the electrode. It is evident that on moving from ZnO to ZG3 the slope of the straight line region becomes maximum, implying improved capacitive performance of the sample. It also shows the better charge transfer performance of the sample.

Fig. 5.12 shows the capacitance retention performance of the composite supercapacitor. The pristine ZnO retains around 78% of the initial capacitance after 1000 cycles. Whereas, all the composites retained almost 100% of the capacity even after 1000 cycles, which reveals that graphene not only increases the capacitance but also increases the cyclic life of the electrode. It was found that ZG1, which is having the highest amount of GO content performed better in the cyclic testing. Therefore, rGO sheets not only increase the conductivity but acts as a cushion to reduce any mechanical stress.

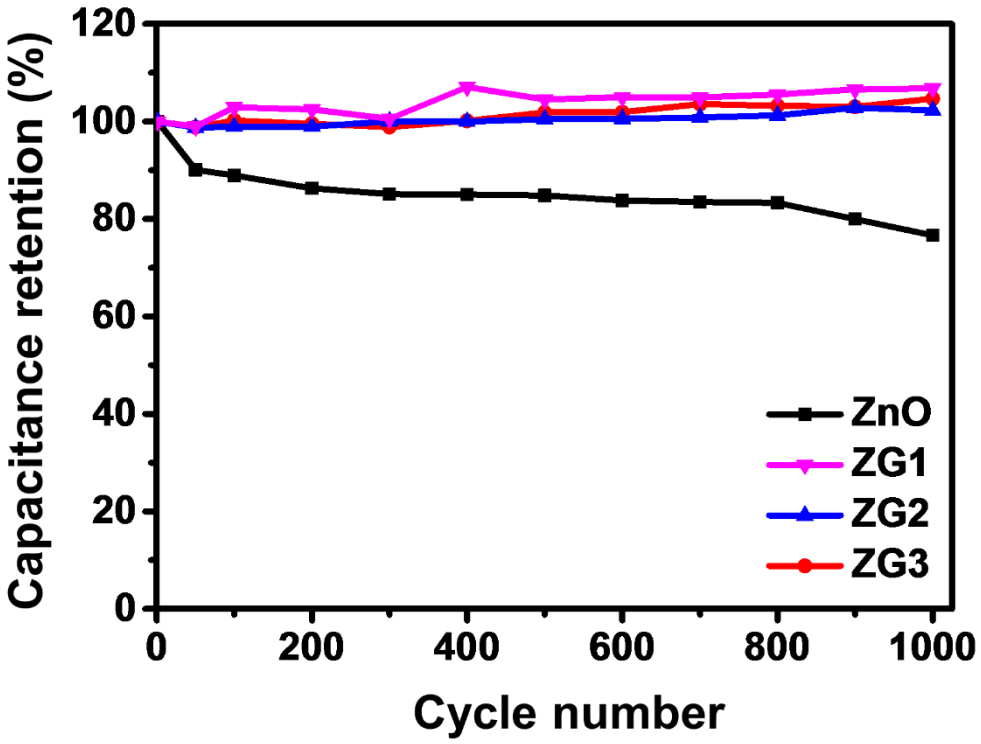

Figure. 5.12: cyclic stability of the sample.

5.3.2 Application of rGO-ZnO composite in non-enzymatic glucose sensing.

Glucose sensing experiments were done using a three electrode system. 1M sodium hydroxide was used as the electrolyte throughout the experiment. Saturated calomel electrode and platinum electrode were used as the reference and counter electrode respectively. The modified GCE was used as the working electrode. During the experiments, the glucose concentration in the electrolyte was varied by injecting the glucose from a stock solution using a micropipette.

Fig. 5.13 shows the cyclic voltammetry (CV) curves of the modified GCE sensor with ZnO and GO in 1M NaOH electrolyte containing 5 µM glucose. The electrode was cycled between -0.8 V and 0.8 V at a scan rate of 50 mV/s. The peak around -0.43 V indicates the electrocatalytic reaction at the electrode surface. Also, it can be understood

that the GO shows a little sensitivity towards the glucose compared to the ZnO nanoparticles.

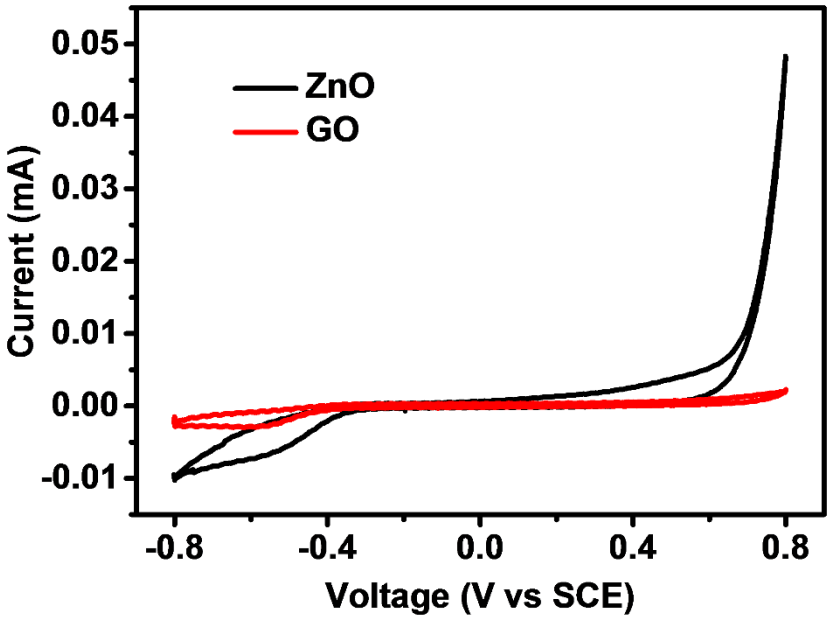

Figure. 5.13: The comparison between the CV curves of GO and ZnO in the presence of glucose.

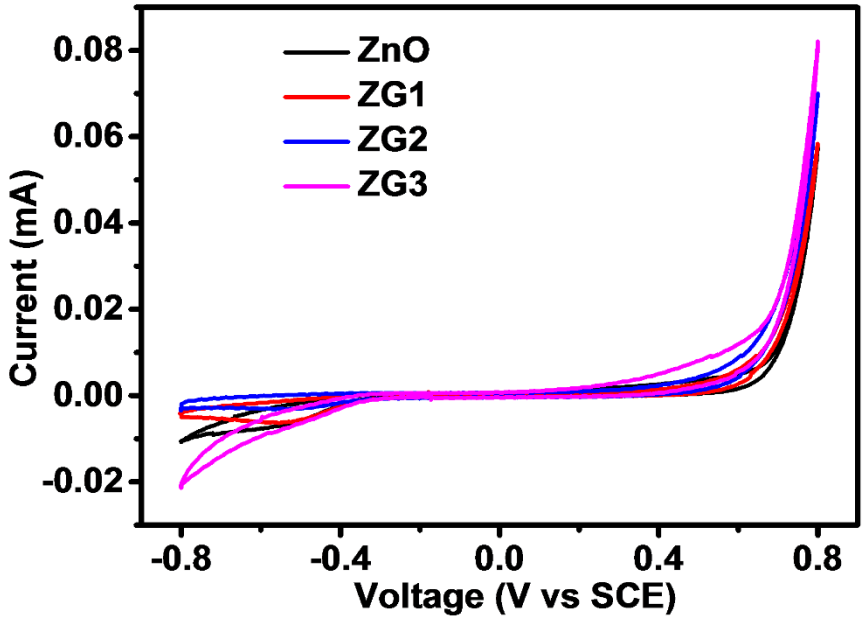

Figure. 5.14: The CV curves for the composites in 1 M NaOH solution containing 5 µM glucose

Fig. 5.14 shows the CV curves for the composites. It may be noted that the edge peak current varies significantly in the case of modified electrodes compared to pristine ZnO/GCE and rGO/GCE. Among all modified GCE sensors, ZG3 composite modified electrode exhibits the highest current towards glucose sensing. ZG3 composite is selected for subsequent experiment and analysis.

This can be understood on the basis of the proposed electrochemical reaction where surface confined Zn^{2+}/Zn^{1+} plays the major role (Baby et al. 2011),

$$ZnO\,(OH) + Glucose \longrightarrow Zn(OH)_2 + Glutonic\ Acid$$

$$Zn(OH)_2 + OH^- \longrightarrow ZnO\,(OH) + H_2O + e^-$$

During the electrocatalytic reaction in the presence of alkaline solution, the ZnO reacts with glucose to form glutonic acid. Therefore, ZnO plays an active role in the reduction of glucose. A change in current during the process is recorded as a function of glucose concentration in order to obtain the calibration curve. In the case of ZnO/rGO composites, the ZnO nanoparticles are crystallised over the surface of graphene. These ZnO nanoparticles over the reduced graphene oxide sheets are directly involved in the electrocatalytic reaction. Whereas, the graphene sheets increase the surface area of the material which enhances the adsorption of ions helping in electrocatalytic reaction. Graphene also enhances the sensitivity of electrodes due to increase in the electronic conductivity. On the other hand, the growth of ZnO nanocrystals embedded in graphene matrix creates more interfaces at the boundary. The increased surface area and interfaces will trap more glucose, enhancing its adsorption to the ZnO nanocrystal surface, while increased conductivity helps electron transport to the electrode.

5.3.2.1 Chronoamperometric non-enzymatic glucose detection

The chronoamperometric technique is used for the glucose detection and response characteristics of the sensors. The experiments were carried out at an applied potential of 0.8 V. On addition of glucose, the change in concentration is evident from a step-like increase in the current. Fig. 5.15 shows the change in current with respect to the

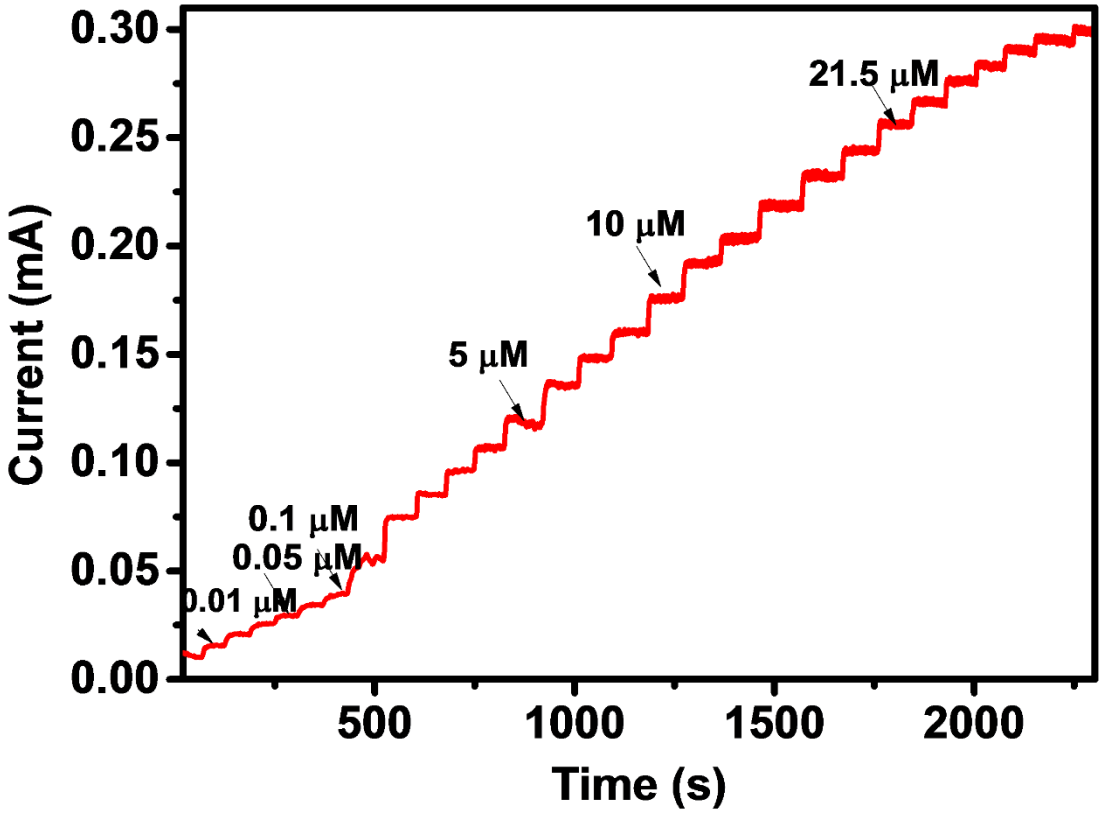

Figure. 5.15: The chronoamperometric response of the electrode with the increase in the glucose concentration.

change in glucose concentration. Each increment in the glucose concentration appears as a step in the curve. The faster response of the electrode is also evident from the graph. The glucose concentration was varied from 10 nM to 33.5 µM as shown in the Fig. 5.16, the current versus concentration graph is fitted with a polynomial using the equation, *Current (I mA) = Intercept (I, mA) + B1 × Concentration (µM) + B2× Concentration (µM)* ^{2}, where *B1* = 0.16756 mA, *B2* = -0.02716 mA and intercept = 0.03166 mA with $R^2 = 0.988$.

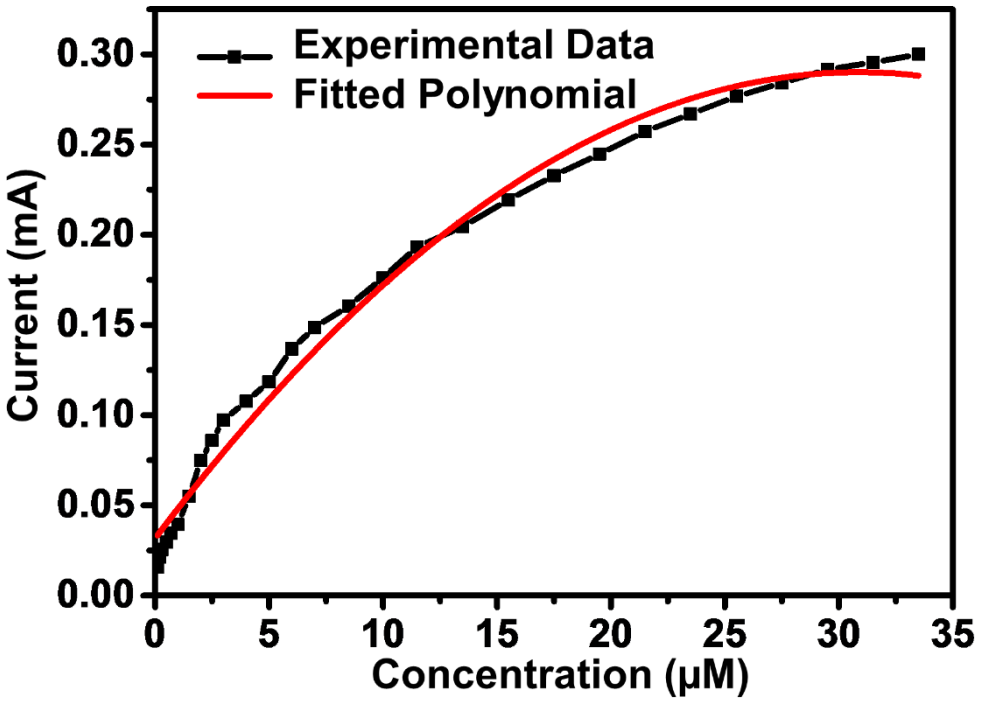

Figure. 5.16: The calibration curve for the modified electrode and fitted data.

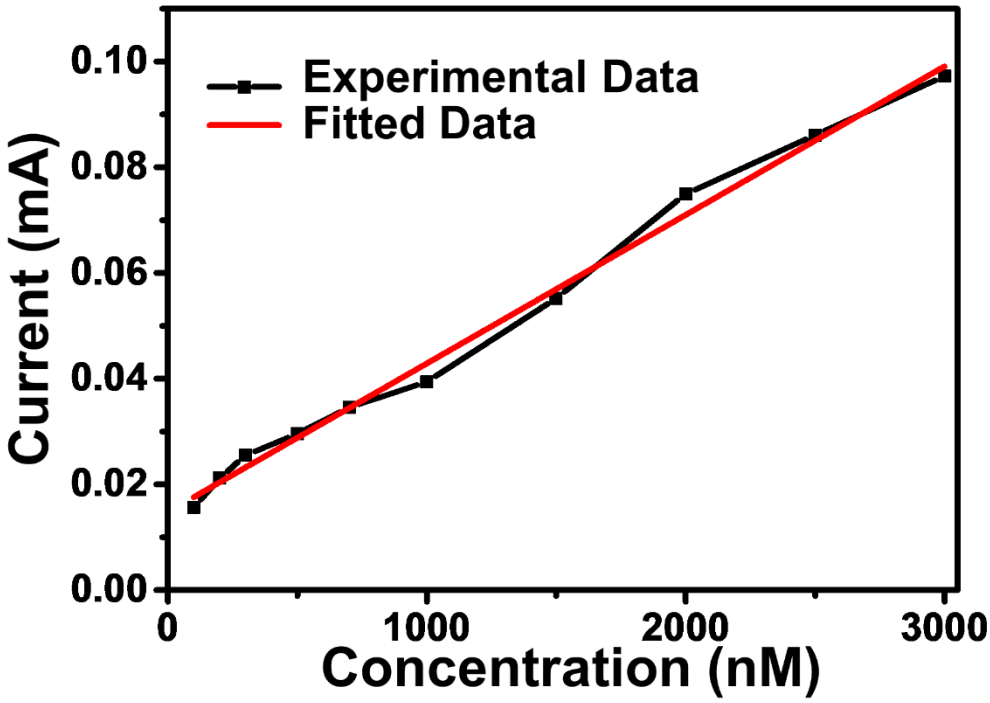

Figure. 5.17: Response of the electrode at lower glucose concentration regime (1-3 μM).

Fig. 5.17 reveals the sensor response at lower concentrations in the nanomolar concentration region. The sensor shows a linear response from 100 nM to 3000 nM concentration, following the regression equation, *(I, nA)* = 0.01477 *(I, mA)* + 2.81114 $\times 10^{-5}$ mA/ nM × *concentration (nM)* with R^2 = 0.993. The Table. 5.3 shows the comparison of the results with the earlier reports. It may be noted that the present rGO-ZnO sensor exhibits far superior performance with broad linear range (0 to 3000 nM) and high sensitivity (39.78 mA cm^{-2} mM^{-1}) and lower detection limit 0.2 nM at the signal to noise ratio 3.

Table 5.3 : A comparison of performance of glucose sensors with earlier reports.

Paper	Enzymatic/ Non-enzymatic	Detection Limit	Range	Sensitivity	Reference
ZnO nanotubes	Enzymatic	1 µM	50 µM to 12 mM	21.7 mA/mM cm^2	(Kong et al. 2009)
ZnO nanowires	Enzymatic	----	1 µM to 0.76 mM	26.3 mA cm^{-2} mM^{-1}	(Zhang et al. 2007)
ZnO nanorods	Enzymatic	0.22 µM.	0.6 to 1.4 mM	10.911 mA/mM·cm2	(Marie et al. 2015)
ZnO/CNT	Non-enzymatic	500 nM	------	37.25 µA cm^{-2} mM^{-1}	(Baby et al. 2011)
ZnO/rGO	Non-enzymatic	0.2 nM	0 to 33.5 µM	39.78 mA cm^{-2} mM^{-1}	Present work

5.3.3 Hydrazine sensing properties of the composite.

Hydrazine sensing experiments were done in phosphate buffer solution (PBS) having pH 8. A three electrode configuration was used for the sensing experiment. The hydrazine concentration was varied by adding required volumes of the hydrazine solutions from a freshly prepared stock solution.

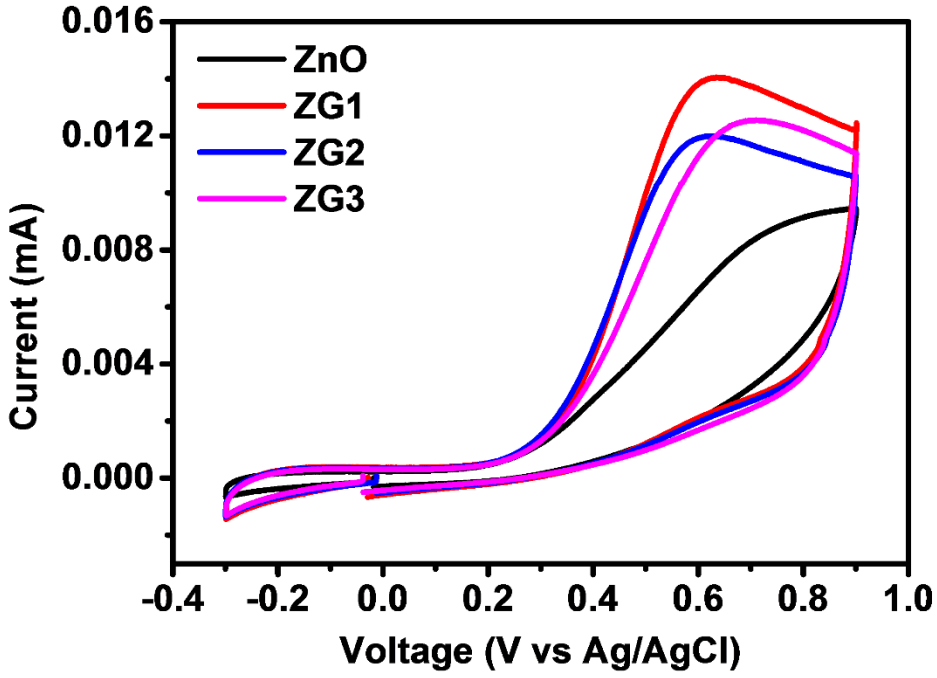

Figure. 5.18: CV curves of the ZnO and the composites in PBS buffer solution (pH 8) containing 10 µM hydrazine.

Fig. 5.18 represents the cyclic voltammograms in the PBS solution contains hydrazine. The ZnO shows a peak which is around 0.75 V. The inherent low conductivity hinders the performance of the bare ZnO. The presence of reduced graphene oxide along with the ZnO can help in dealing with the conductivity issues. As seen from the TEM images the ZnO nanoparticles are grown over the graphene sheets, which really acts as a bridge between the ZnO and the GCE. The reduced graphene oxide can also take part in the reduction of hydrazine. As a result the synergistic enhancement can be observed from the composites. The composite ZG1 having higher content of GO and ZnO shows the

highest response and is chosen as the material for the further studies. The oxidation process of the hydrazine at the ZnO-reduced graphene oxide surface can be written as,

$$N_2H_4 + 5/2\ OH^{-1} \longrightarrow 1/2\ N_3^{-1} + 1/2\ NH_3 + 5/2\ H_2O + 2e^-$$

During the anodic reaction hydrazine is oxidized into ammonia and water. There was no cathodic peaks observed which implies that the reaction is irreversible in nature (Liu et al. 2010).

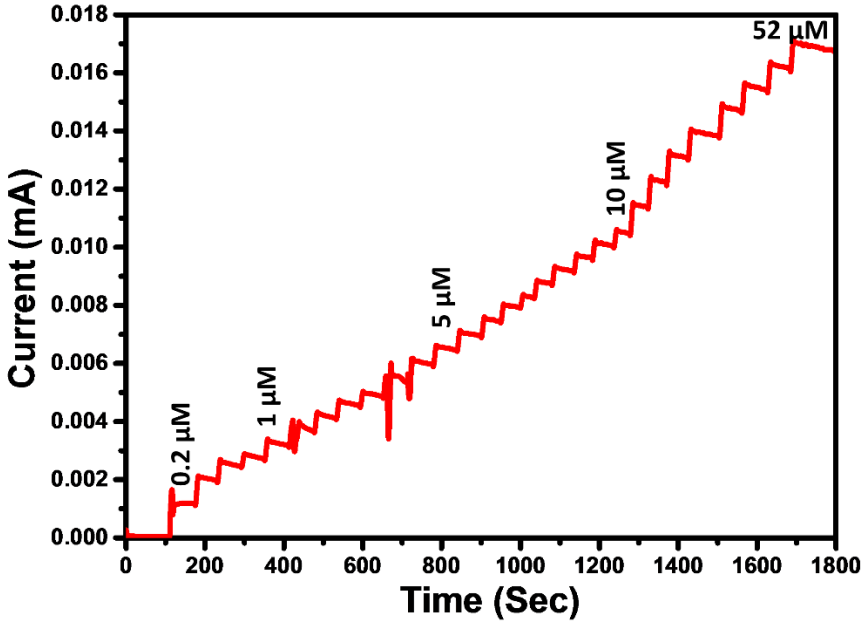

Figure. 5.19: Chronoamperometric response of the composite (ZG1) towards the increase in the hydrazine concentration.

Fig. 5. 19 shows the chronoamperometric response of the composite (ZG1) at the fixed potential. The sensor shows an increase in current with respect to the increase in the hydrazine concentration. During the experiment the hydrazine concentration was varied by injecting required volume of the solutions at constant stirring to ensure the homogeneity of the solution. The concentration was varied between 0.2 µM to 52 µM. The sensor response was found to be quick (< 2 Sec) pointing to the better performance of the electrode.

To calibrate the electrode calibration curve was drawn for the sample. It was found that the electrode shows two linear portions at low concentration (0.2 µM to 10 µM) and higher concentration (10 µM to 52 µM) regimes. At lower concentrations (Fig. 5.20 (a)), the calibration curve was following the regression equation *I(mA) = 0.00238 + 6.5023×10^{-4}×C(µM)[R2=0.93]*and at higher concentrations(Fig. 5.20 (b)) it was following *I (mA) = 0.00634+ 2.069×10-4 ×C (µM) [R2 =0.998]*. The sensitivity at lower concentration was calculated from the slope and found to be 9.6 mA mM^{-1} cm^{-2}, which is better than the reported results for ZnO and ZnO composites with carbon. The lower detection limit was determined to be 0.09 µM

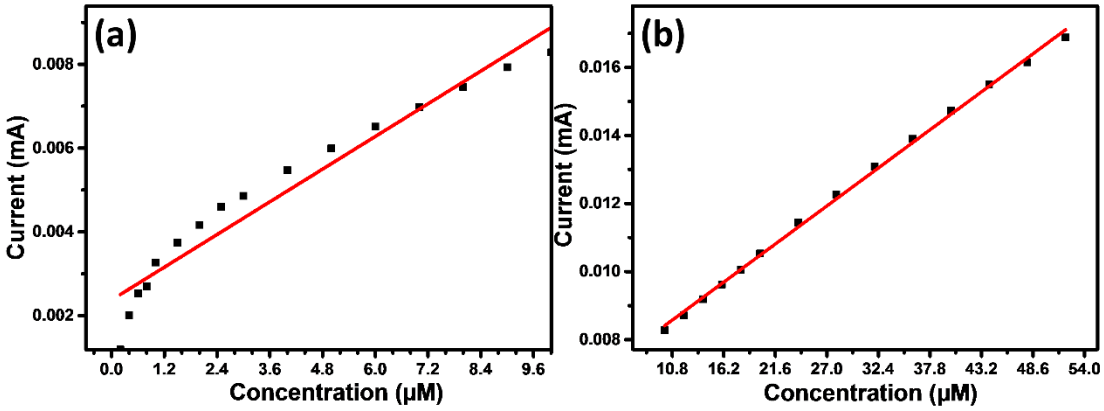

Figure. 5.20: (a) calibration curves for hydrazine at lower concentrations (0.2 µM to 10 µM) and (b) calibration curves for hydrazine at higher concentrations (10 µM to 52 µM).

5.4 Summary

- In summary, zinc oxide and graphene oxide nanocomposites were successfully prepared using a microwave assisted synthesis method. The graphene oxide content was varied and composites of different weight ratios were prepared. TEM studies showed that the ZnO nanoparticles are grown over the graphene oxide sheets. Raman studies showed that during the microwave reaction graphene oxide partially converted to reduced graphene oxide which restore its graphene properties.
- The rGO/ZnO nanocomposite supercapacitor electrodes were found to possess very high capacitance reaching as high as 635 F g^{-1} with long cyclic life tested up to 1000 cycles.
- The non-enzymatic glucose nanocomposite sensor tested using chronoamperometry and the composite VG3 having the highest ZnO content exhibits a high sensitivity of 39.78 mA cm^{-2} mM^{-1} and lower detection limit of 0.2 nM, making it better than earlier reports.
- A hydrazine sensor was tested using the composite. Tests revealed that the composite VG1 having an optimum graphene oxide and ZnO content shows the highest sensitivity. Also, it shows that sensitivity towards different materials can be tuned by controlling the weight ratios and properties. The tested hydrazine sensor shows a high sensitivity of 9.6 mA mM^{-1} cm^{-2} and a lower detection limit of 0.09 μM.

Chapter 6

Summary, conclusions and future directions

The conclusions of the thesis and scope for future directions are presented in this chapter.

6.1 Summary

Preparation, characterization and applications of graphene oxide and solar exfoliated graphene

- Solar graphene is successfully synthesized via solar exfoliation of graphite oxide.
- The complete reduction of graphite oxide to graphene is confirmed from XRD and UV-Vis spectrum.
- Raman Spectrum indicated high purity and defect less nature of solar graphene.
- The samples produced have layered morphology as seen from SEM analysis.
- The layered structures possess surface nanopores as observed from TEM images.
- The CV studies showed greater specific capacitance for solar graphene, which can be attributed to the nanopores present on the surface and hence the interaction of available functional groups with the electrolyte.
- The charge-discharge curves show symmetric behaviour which in turn reflects good capacitive behaviour, electro-chemical stability and reversibility.
- The Impedance analysis shows lower internal resistance for solar graphene.

- A higher sensitivity for the electrochemical detection of H_2O_2 using solar reduced graphene is reported [64.79 μA mM^{-1} cm^{-2}].
- The solar graphene possess excellent electrocatalytic activity, low resistance and high electron transfer rate, high sensitivity and lower response time making it one of the best graphene species available for the electrochemical detection.
- Further, the preparation of solar reduced graphene is more cost effective as compared to the other existing methods and useful for applications in supercapacitors and sensors.

Preparation and characterization of vanadium oxide/graphene composites for biosensing and lithium ion batteries

- Composites of vanadium oxide and graphene oxide have been prepared by melt quenching of vanadium oxide followed by the hydrothermal treatment of the precursors.
- Chronoamperometry studies conducted on the MVGO50 composite electrodes for the detection of dopamine over a wide range of concentration, exhibited a highest sensitivity of 25.02 μA mM^{-1} cm^{-2} with the lowest detection limit of 0.07 μM.
- Chronoamperometry studies also revealed, the excellent selective dopamine sensing capability of MVGO50 composites, even in the presence of a highly concentrated solution of uric acid as the interfering species.
- MVGO50 composites were also found to be good candidate for lithium-ion battery applications, as they exhibited an enhanced rate capacity of 200 $mAhg^{-1}$ at a current of 0.1 C rate, through galvanostatic charge-discharge cycling studies.
- The excellent electrochemical sensing and energy storing capacity of the composites are attributed to the fast Faradaic reactions emanating from a percolated diffusion network, created by the synergistic embedment of vanadium oxide on graphene oxide.

Preparation and characterization and of reduced Graphene oxide / ZnO composites for glucose sensing and supercapacitors

- Zinc oxide and graphene oxide nanocomposites were successfully prepared using a microwave assisted synthesis method. The graphene oxide content was varied and composites of different weight ratios were reported.
- TEM studies show that the ZnO nanoparticles are grown over the graphene oxide sheets.
- Raman studies show that during the microwave reaction graphene oxide is partially converted to reduced graphene oxide which restore its graphene properties.
- The rGO/ZnO nanocomposite supercapacitor electrodes were found to possess very high capacitance, reaching as high as 635 F g^{-1},with long cyclic life, tested up to 1000 cycles.
- The non-enzymatic glucose nanocomposite sensor tested using chronoamperometry and the composite VG3 having the highest ZnO content, exhibits a high sensitivity of 39.78 mA cm^{-2} mM^{-1} and lower detection limit of 0.2 nM, making it better than earlier reports.
- A hydrazine sensor was tested using the composite. Studies reveal that the composite VG1 having optimum graphene oxide and ZnO content shows the highest sensitivity. Also, it shows that sensitivity towards different materials can be tuned by controlling the weight ratios.
- The tested hydrazine sensor shows a high sensitivity of 9.6 mA mM^{-1} cm^{-2} and a lower detection limit of 0.09 μM.

6.2 Conclusions

The studies conducted show that graphene can be prepared in an energetically favourable way and is a potentaial candidate for electrochemical energy storage and biosensing applications. The specific capacitance of solar geaphene electrode was found to be 223 Fg^{-1} and the H_2O_2 sensitivity was 64.79 μA mM^{-1} cm^{-2} which was higher than the reported values [15.16 μA mM^{-1} cm^{-2}] . Graphene can also act as a potential additive to metal oxides, to improve the electrochemical properties. The synergestic interaction between the graphene sheets and the metal oxides improves material properties such as electrical conductivity, porosity etc. Graphene-vanadium oxide composites shows high capacity [200 $mAhg^{-1}$] as lithium ion battery electrode and high sensitivity [25.02 μA mM^{-1} cm^{-2}] towards dopamine, a neurotransmitter. Graphene-Zinc oxide composites also, exhibited high capacitance [635 F g^{-1}] as a supercapacitor electrode and better sensitivity towards glucose [39.78 mA cm^{-2} mM^{-1}] and hydrazine [9.6 mA mM^{-1} cm^{-2}]. Therefore, graphene and its composites are efficient electrode materials for supercapacitor and LIB's to enhance the capacity and cycle life. Also, they can be used a sensor material for trace detection of important biomolecules and additives. These results can also be extended to other materials also to obtain better engineering materials.

6.3 Future directions

The future work in this field may be focussed on,

- Improving the supercapacitor performance of graphene by making composites with other materials, like conducting polymers and making prototypes for the industrial applications.
- Improving the non-enzymatic glucose sensing of ZnO/graphene oxide composite and making prototype, for the testing of blood glucose levels of the body fluids.
- Improving the lithium-ion battery performance and making prototype cells.

References:

Abdolhosseinzadeh, S. and Asgharzadeh, H. (2016). "UV-assisted synthesis of reduced graphene oxide – ZnO nanorod composites immobilized on Zn foil with enhanced photocatalytic performance." *Res. Chem. Intermed.*, *42* (5), 4479–4496.

Adams, D.D., Knight, J.G. and Ebringer, A. (2012). "The Autoimmune Model of Schizophrenia." *Int. Sch. Res. Netw. Psychiatry*, *2012* 1–8.

Akhavan, O. (2014). "Bacteriorhodopsin as a superior substitute for hydrazine in chemical reduction of single-layer graphene oxide sheets." *Carbon N. Y.*, *81* 158–166.

Alwarappan, S., Erdem, A., Liu, C. and Li, C.-Z. (2009). "Probing the Electrochemical Properties of Graphene Nanosheets for Biosensing Applications." *J. Phys. Chem. C*, *113* (20), 8853–8857.

An, H., Li, Y., Long, P., Gao, Y., Qin, C., Cao, C. and Feng, Y. (2016). "Hydrothermal preparation of fl uorinated graphene hydrogel for high-performance supercapacitors." *J. Power*, *312* 146–155.

Aravinda, L.S., Nagaraja, K.K., Nagaraja, H.S., Bhat, K.U. and Ramachandra, B. (2013). "Electrochimica Acta ZnO / carbon nanotube nanocomposite for high energy density supercapacitors." *Electrochim. Acta*, *95* 119–124.

Atabaki, M.M. and Kovacevic, R. (2013). "Graphene Composites as Anode Materials in Lithium-Ion Batteries." *Electron. Mater. Lett.*, *9* (2), 133–153.

Avouris, P. and Dimitrakopoulos, C. (2012). "Graphene : Synthesis and Applications." *Mater. Today*, *15* (3), 86–97.

Baby, T.T. and Ramaprabhu, S. (2011). "Non-Enzymatic Amperometric Glucose Biosensor from Zinc Oxide Nanoparticles Decorated Multi-Walled Carbon Nanotubes." *J. Nanosci. Nanotechnol.*, *11* 4684–4691.

Baby, T.T., Ramaprabhu, S. (2011) "Non-Enzymatic Amperometric Glucose Biosensor from Zinc Oxide Nanoparticles Decorated Multi-Walled Carbon Nanotubes." *Journal of Nanoscience and Nanotechnology*, 11 4684-4691

Ban, C., Chernova, N.A. and Whittingham, M.S. (2009). "Electrochemistry Communications Electrospun nano-vanadium pentoxide cathode." *Electrochem. Commun.*, *11* (3), 522–525.

Becerril, H. a, Mao, J., Liu, Z., Stoltenberg, R.M., Bao, Z. and Chen, Y. (2008). "Evaluation of solution-processed reduced graphene oxide films as transparent conductors." *ACS Nano*, *2* (3), 463–70.

Biswas, S. and Drzal, L.T. (2010). "Multilayered Nano-Architecture of Variable Sized Graphene Nanosheets for Enhanced Supercapacitor Electrode Performance." *ACS Appl. Mater. Interfaces*, *2* (8), 2293–2300.

Bose, S., Kim, N.H., Kuila, T., Lau, K. and Lee, J.H. (2011). "Electrochemical performance of a graphene-polypyrrole nanocomposite as a supercapacitor electrode." *Nanotechnology*, *22* (29), 295202.

C. Menictas, M. Skyllas-Kazacos, T.M. Lim, Advances in Batteries for Medium and Large-Scale Energy Storage: Types and Applications, Elsevier, 2014.

Cao, A., Hu, J., Liang, H. and Wan, L. (2005). "Self-Assembled Vanadium Pentoxide (V 2 O 5) Hollow Microspheres from Nanorods and Their Application in Lithium-Ion Batteries**." 4391–4395.

Cao, G. and Wang, Y. (2011). "Nanostructures and Nanomaterials: Synthesis, Properties and Applications", World Scientific publishing, Imperial College Press, London.

Chabot, V., Higgins, D., Yu, A., Xiao, X., Chen, Z. and Zhang, J. (2014). "A review of graphene and graphene oxide sponge: material synthesis and applications to energy and the environment." *Energy Environ. Sci.*, *7* (5), 1564.

Chang, C., Lee, Y. and Chen-yang, Y.W. (2013). "Improvement of Crystalline Vanadium Oxide Anode for Lithium Ion Battery by Amorphous Vanadium Oxide". In 223rd ECS Meeting, p 2113.

Cheah, Y.L., Gupta, N., Pramana, S.S., Aravindan, V., Wee, G. and Srinivasan, M. (2011). "Morphology , structure and electrochemical properties of single phase

electrospun vanadium pentoxide nanofibers for lithium ion batteries." *J. Power Sources*, *196* (15), 6465–6472.

Chen, D., Yi, R., Chen, S., Xu, T., Gordin, M.L., Lv, D. and Wang, D. (2014). "Solvothermal synthesis of V2O5/graphene nanocomposites for high performance lithium ion batteries." *Mater. Sci. Eng. B*, *185* 7–12.

Chen, L., Lai, Q. and Hao, Y. (2009). "Investigations on capacitive properties of the AC / V 2 O 5 hybrid supercapacitor in various aqueous electrolytes." *J. Alloys Compd.*, *467* (1–2), 465–471.

Chen, Y. and Ma, Y. (2010). "High performance supercapacitors based on reduced graphene oxide in aqueous and ionic liquid electrolytes." *Carbon* , *49* (2), 573–580.

Chen, Y., Hu, Z., Chang, Y., Wang, H., Zhang, Z. and Yang, Y. (2011). "Zinc Oxide / Reduced Graphene Oxide Composites and Electrochemical Capacitance Enhanced by Homogeneous Incorporation of Reduced Graphene Oxide Sheets in Zinc Oxide Matrix." *The Journal of Phys. Chem. C* 2563–2571.

Chiku, M., Takeda, H., Matsumura, S., Higuchi, E. and Inoue, H. (2015). "Amorphous Vanadium Oxide/Carbon Composite Positive Electrode for Rechargeable Aluminum Battery." *Appl. Mater. Interfaces*, 1–5.v

Conway, B.E., "Electrochemical Supercapacitors: Scientific Fundamentals and Technological Applications. Electrochemical Supercapacitors" Scientific Fundamentals and Technological Applications. 1999, New York: Plenum Publishers.

Cullity. B.D, Stock, S. , "Elements of X-ray diffraction" (2014) *Pearson Education India*.

Davis, M., Gu, C., Black, B., Korzeniewski, C. and Hope-weeks, L. (2012). "Tailoring cobalt doped zinc oxide nanocrystals with high capacitance activity : factors affecting structure and surface morphology ." *RSC Adv.*, *2* 2061–2066.

Dreyer, D.R., Ruoff, R.S. and Bielawski, C.W. (2010). "Minireviews Genealogy of Graphene From Conception to Realization : An Historial Account of Graphene and Some Perspectives for Its Future." 9336–9345.

Du, Q., Zheng, M., Zhang, L., Wang, Y., Chen, J., Xue, L., Dai, W., Ji, G. and Cao, J. (2010). "Electrochimica Acta Preparation of functionalized graphene sheets by a low-temperature thermal exfoliation approach and their electrochemical supercapacitive behaviors." *Electrochim. Acta, 55* (12), 3897–3903.

El-Kady, M.F., Strong, V., Dubin, S. and Kaner, R.B. (2012). "Laser scribing of high-performance and flexible graphene-based electrochemical capacitors." *Science*, *335* (6074), 1326–30.

Eswaraiah, V., Aravind S.S.J and Ramaprabhu S."Top down method for synthesis of highly conducting graphene by exfoliation of graphite oxide using focused solar radiation †."*J. Mater. Chem.*, 2011, 21, 6800–6803

Fan, Z., Yan, J., Wei, T., Zhi, L., Ning, G. and Li, T. (2011). "Asymmetric Supercapacitors Based on Graphene / MnO 2 and Activated Carbon Nanofi ber Electrodes with High Power and Energy Density." *Adv. Funct. Mater.*, *21* 2366–2375.

Fang, B., Zhang, C., Zhang, W. and Wang, G. (2009). "A novel hydrazine electrochemical sensor based on a carbon nanotube-wired ZnO nanoflower-modified electrode." *Electrochim. Acta*, *55* (1), 178–182.

Fang, W.-C. (2008). "Synthesis and Electrochemical Characterization of Vanadium Oxide/Carbon Nanotube Composites for Supercapacitors." *J. Phys. Chem. C*, *112* (30), 11552–11555.

Farhat, O.F., Halim, M.M., Abdullah, M.J., Ali, M.K.M. and Allam, N.K. (2015). "Morphological and structural characterization of single-crystal ZnO nanorod arrays on flexible and non-flexible substrates." *Beilsterin J. Nanotechnol.*, *6* 720–725.

Fernandez, M.J., Guardia, L., Paredes, J.I., Solı, P. and Tasco, J.M.D. (2010). "Vitamin C Is an Ideal Substitute for Hydrazine in the Reduction of Graphene Oxide Suspensions ´ n." 6426–6432.

Gass, M.H., Bangert, U., Bleloch, A.L., Wang, P., Nair, R.R. and Geim, A.K. (2008). "Free-standing graphene at atomic resolution." *Nature Nanotechnology*. *3*(11), 676-681.

Geim, A.K., Novoselov, K.S., Morozov, S. V and Jiang, D. (2004). "Electric Field Effect in Atomically Thin Carbon Films." *Science.*, *306* : 666–669.'

Grande, L., Chundi, V.T., Wei, D., Bower, C., Andrew, P. and Ryhänen, T. (2012). "Graphene for energy harvesting/storage devices and printed electronics." *Particuology*, *10* (1), 1–8.

Guo, Y., Chang, B., Wen, T., Zhao, C., Yin, H. and Zhou, Y. (2016). "One-pot synthesis of graphene/zinc oxide by microwave irradiation with enhanced supercapacitor performance." *RSC Adv.*, *6* 19394–19403.

Haldorai, Y., Voit, W. and Shim, J. (2014). "Electrochimica Acta Nano ZnO @ reduced graphene oxide composite for high performance supercapacitor : Green synthesis in supercritical fluid." *Electrochim. Acta*, *120* 65–72.

Hantel, M.M., Kaspar, T., Nesper, R., Wokaun, a. and Kötz, R. (2011). "Partially reduced graphite oxide for supercapacitor electrodes: Effect of graphene layer spacing and huge specific capacitance." *Electrochem. Commun.*, *13* (1), 90–92.

Hernandez, Y., Nicolosi, V., Lotya, M., Blighe, F.M., Sun, Z., De, S., McGovern, I.T., Holland, B., Byrne, M., Gun'Ko, Y.K., Boland, J.J., Niraj, P., Duesberg, G., Krishnamurthy, S., Goodhue, R., Hutchison, J., Scardaci, V., Coleman, J.N. (2008). "High-yield production of graphene by liquid-phase exfoliation of graphite." *Nat. Nanotechnol.*, *3* (9), 563–8.

Heyrovský J, K˚ uta J (1966) Principles of polarography. Academic Press, New York

Hummer W.J and Offman R.E "Preparation of Graphitic Oxide." Journal of Am. Chem. Soc. (1957). *208* (1937), 1937.

Hummers W.S., R.E. Offeman, Preparation of Graphitic Oxide, J. Am. Chem. Soc. 80 (1958) 1339–1339

Jeyalakshmi, K., Purushothaman, K.K. and Muralidharan, G. (2013). "Thickness dependent supercapacitor behaviour of sol-gel spin coated nanostructured vanadium pentoxide thin films." *Philos. Mag.*, *93* (13), 1490–1499.

Jia, G., Deng, Z., Liu, X., Jiang, H. and Li, C. (2016). "Building radially oriented architecture by tailorable V 2 O 5 nanoribbons toward enhanced lithium storage." *Chem. Eng. J.*, *304* 194–200.

Jianfeng Shen, Yizhe Hu, Min Shi, Xin Lu, Chen Qin, Chen Li, and Mingxin Ye Fast and Facile Preparation of Graphene Oxide and Reduced Graphene Oxide Nanoplatelets*Chemistry of Materials* 2009 *21* (15), 3514-3520 DOI: 10.1021/cm901247t

Jung, H., Cheah, C.V., Jeong, N., Lee, J., Jung, H., Cheah, C.V., Jeong, N. and Lee, J. (2014). "Direct printing and reduction of graphite oxide for flexible supercapacitors Direct printing and reduction of graphite oxide for flexible supercapacitors." *Appl. Phys. Lett.*, *53902* (105), 3–8.

Kaniyoor, A. and Ramaprabhu, S. (2012). "A Raman spectroscopic investigation of graphite oxide derived graphene." *AIP Adv.*, *2* (3), 032183.

Kim, B., Hyo, C., Seung, K., Rahy, A. and Yang, D.J. (2012). "Electrochimica Acta Electrospun vanadium pentoxide / carbon nanofiber composites for supercapacitor electrodes." *Electrochim. Acta*, *83* 335–340.

Kong, T., Chen, Y., Ye, Y., Zhang, K., Wang, Z. and Wang, X. (2009). "Sensors and Actuators B : Chemical An amperometric glucose biosensor based on the immobilization of glucose oxidase on the ZnO nanotubes." *Sensors Actuators B. Chem.*, *138* (96), 344–350.

L.E., Lv, W., Tang, D., He, Y., You, C., Shi, Z. and Chen, X. (2009). "Low-Temperature Exfoliated Graphenes: Vacuum-Promoted Exfoliation and Electrochemical Energy Storage." *ACS Nano*, *3* (11), 3730–3736.

Landau, L. D. (1937) "Theory of phase transformations. I" *Zh. Eksp. Teor. Fiz. Phys. Z. Sowjetunion* 7 19; 11-26 (1937)

Lee, H.Y. and Goodenough, J.B. (1999). "Ideal Supercapacitor Behavior of Amorphous V2O5·nH2O in Potassium Chloride (KCl) Aqueous Solution." *J. Solid State Chem.*, *148* (1), 81–84.

Lee, M., Balasingam, S.K., Jeong, H.Y., Hong, W.G., Lee, H., Kim, B.H. and Jun, Y. (2015). "One-step hydrothermal synthesis of enhanced electrochemical energy storage." *Sci. Rep.*, *5* 1–8.

Li, G., Pang, S., Jiang, L., Guo, Z. and Zhang, Z. (2010). "Environmentally Friendly Chemical Route to Vanadium Oxide Single-Crystalline Nanobelts." *J. Phys. Chem. B*, *110* (19), 9383–9386.

Li, Y. and Liu, X. (2014). "Activated carbon / ZnO composites prepared using hydrochars as intermediate and their electrochemical performance in supercapacitor." *Mater. Chem. Phys.*, *148* (1–2), 380–386.

Li, Y., Zijll, M. van, Chiang, S. and Pan, N. (2011). "KOH modified graphene nanosheets for supercapacitor electrodes." *J. Power Sources*, *196* (14), 6003–6006.

Li, Z., Zhang, H., Liu, Q., Liu, Y., Stanciu, L. and Xie, J. (2014). "Hierarchical Nanocomposites of Vanadium Oxide Thin Film Anchored on Graphene as High-Performance Cathodes in Li-Ion Batteries." *ACS Appl. Mater. Interfaces.*, *6* (21), 18894–18900.

Li, Z., Zhou, Z., Yun, G., Shi, K., Lv, X. and Yang, B. (2013). "High-performance solid-state supercapacitors based on graphene-ZnO hybrid nanocomposites." *Nanoscale Res. Lett.*, *8* 1–9.

Lin, Z., Liu, Y., Yao, Y., Hildreth, O.J., Li, Z., Moon, K. and Wong, C. (2011). "Superior Capacitance of Functionalized Graphene." 7120–7125.

Liu, D., Fu, C., Zhang, N., Zhou, H. and Kuang, Y. (2016). "Electrochimica Acta Three-Dimensional Porous Nitrogen doped Graphene Hydrogel for High Energy Density supercapacitors." *Electrochim. Acta*, *213* 291–297.

Liu, H. and Yang, W. (2011). "Ultralong single crystalline V2O5 nanowire/graphene composite fabricated by a facile green approach and its lithium storage behavior." *Energy Environ. Sci.*, *4* (10), 4000.

Liu, J., Li, Y. and Huang, X. (2010). "C @ ZnO nanorod array-based hydrazine electrochemical sensor with improved sensitivity and stability." *Dalt. Trans.*, *39* 8693–8697.

Liu, J., Li, Y., Jiang, J. and Huang, X. (2010). "C@ZnO nanorod array-based hydrazine electrochemical sensor with improved sensitivity and stability." *Dalt. Trans.*, *39* (37), 8693.

Liu, J., Lu, R., Xu, G., Wu, J., Thapa, P. and Moore, D. (2013). "Development of a Seedless Floating Growth Process in Solution for Synthesis of Crystalline ZnO Micro / Nanowire Arrays on Graphene : Towards High-Performance Nanohybrid Ultraviolet Photodetectors." *Adv. Funct. Mater.*, *23* 1–8.

Liu, Q., Li, Z., Liu, Y., Zhang, H., Ren, Y., Sun, C., Lu, W., Zhou, Y., Stanciu, L., Stach, E.A. and Xie, J. (2015). "Graphene-modified nanostructured vanadium pentoxide hybrids with extraordinary electrochemical performance for Li-ion batteries." *Nat. Commun.*, *6* 1–10.

Livage. J. (1991). "Vanadium Pentoxide." (8), Journal of Material chem. 578–593.

Lu, T., Pan, L., Li, H., Zhu, G., Lv, T., Liu, X., Sun, Z., Chen, T. and Chua, D.H.C. (2011). "Microwave-assisted synthesis of graphene – ZnO nanocomposite for electrochemical supercapacitors." *J. Alloys Compd.*, *509* (18), 5488–5492.

M.D. Stoller, R.S. Ruoff, Best practice methods for determining an electrode material's performance for ultracapacitors, Energy Environ. Sci. 3 (2010) 1294. doi:10.1039/c0ee00074d.

Mai, L.-Q., Minhas-Khan, A., Tian, X., Hercule, K.M., Zhao, Y.-L., Lin, X. and Xu, X. (2013). "Synergistic interaction between redox-active electrolyte and binder-free functionalized carbon for ultrahigh supercapacitor performance." *Nat. Commun.*, *4* (May), 2923.

Marcano, D.C., Kosynkin, D. V, Berlin, J.M., Sinitskii, A., Sun, Z., Slesarev, A., Alemany, L.B., Lu, W. and Tour, J.M. "Improved Synthesis of Graphene Oxide." ACS Nano 4. 8 4806–4814

Marie, M., Mandal, S. and Manasreh, O. (2015). "An Electrochemical Glucose Sensor Based on Zinc Oxide Nanorods." *Sensors*, *15* (8), 18714–18723.

Marie, M., Mandal, S. and Manasreh, O. (2015). "An Electrochemical Glucose Sensor Based on Zinc Oxide Nanorods." *Sensors*, *15* (8), 18714–18723.

Meneghelli, B.J. (2004). A review of hydrazine sensors the state of artthe. In 40th AIAA/ASME/SAE/ASEE Joint Propulsion Conference and Exhibit; 11-14 Jul. 2004; Fort Lauderdale, FL; United States, p.

Miao, X., Tongay, S., Petterson, M.K., Berke, K., Rinzler, A.G., Appleton, B.R. and Hebard, A.F. "High Efficiency Graphene Solar Cells by Chemical Doping." Arxiv 1–14.

Moghaddam, F.M. and Saeidian, H. (2007). "Controlled microwave-assisted synthesis of ZnO nanopowder and its catalytic activity for O -acylation of alcohol and phenol." *139* 265–269.

Moretti, A. and Passerini, S. (2016). "Bilayered Nanostructured V 2 O 5 · n H 2 O for Metal Batteries." *Adv. Energy Mater.*, 1600868–1600868.

Nicholson RS, Shain I (1964) Anal Chem 36: 706

Novoselov, K.S., Fal, V.I., Colombo, L., Gellert, P.R., Schwab, M.G. and Kim, K. (2012). "REVIEW A roadmap for graphene." *Nature*, *490* , 192–200.

Novoselov, K.S., Geim, A.K., Morozov, S. V and Jiang, D. (2004). "Electric Field Effect in Atomically Thin Carbon Films." Science *306* (October), 666–669.

Obraztsov, A.N. (2007). "Chemical vapor deposition of thin graphite films of nanometer thickness." *45* (2007), 2017–2021.

Obraztsov, A.N., Zolotukhin, A.A., Ustinov, A.O., Volkov, A.P., Svirko, Y. and Jefimovs, K. (2003). "DC discharge plasma studies for nanostructured carbon CVD." *12* 917–920.

Pan, A., Zhang, J., Nie, Z., Cao, G., Arey, B.W. and Li, G. (2010). "Facile synthesized nanorod structured vanadium pentoxide for high-rate lithium batteries †." *Journal od Materials Chemistry*. 9193–9199.

Pandikumar, A., Soon How, G.T., See, T.P., Omar, F.S., Jayabal, S., Kamali, K.Z., Yusoff, N., Jamil, A., Ramaraj, R., John, S.A., Lim, H.N. and Huang, N.M. (2014).

"Graphene and its nanocomposite material based electrochemical sensor platform for dopamine." *RSC Adv.*, *4* (108), 63296–63323.

Park, S., An, J., Potts, J.R., Velamakanni, A., Murali, S. and Ruoff, R.S. (2011). "Hydrazine-reduction of graphite- and graphene oxide." *Carbon N. Y.*, *49* (9), 3019–3023.

Pearton, S.J., Norton, D.P. and Ip, K. (2005). "Recent progress in processing and properties of ZnO." *Prog. Mater. Sci.*, *50* (3), 293–340.

Perera, S.D., Liyanage, A.D., Nijem, N., Ferraris, J.P., Chabal, Y.J. and Balkus, K.J. (2013). "Vanadium oxide nanowire – Graphene binder free nanocomposite paper electrodes for supercapacitors: A facile green approach." *J. Power Sources*, *230* 130–137.

Perera, S.D., Mariano, R.G., Nijem, N., Chabal, Y., Ferraris, J.P. and Balkus, K.J. (2012). "Alkaline deoxygenated graphene oxide for supercapacitor applications: An effective green alternative for chemically reduced graphene." *J. Power Sources*, *215* 1–10.

Perera, S.D., Mariano, R.G., Nijem, N., Chabal, Y., Ferraris, J.P. and Balkus, K.J. (2012). "Alkaline deoxygenated graphene oxide for supercapacitor applications: An effective green alternative for chemically reduced graphene." *J. Power Sources*, *215* 1–10.

Perumbilavil, S., Sridharan, K., Koushik, D., Sankar, P., Pillai, V.P.M. and Philip, R. (2017). "Ultrafast and short pulse optical nonlinearity in isolated, sparingly sulfonated water soluble graphene." *Carbon N. Y.*, *111* 283–290.

Qian, Y., Vu, A., Smyrl, W. and Stein, A. (2012). "Facile Preparation and Electrochemical Properties of V 2 O 5 -Graphene Composite Films as Free-Standing Cathodes for Rechargeable Lithium Batteries." *J. Electrochem. Soc.*, *159* (8), 1135–1140.

Qian, Y., Vu, A., Smyrl, W. and Stein, A. (2012). "Facile Preparation and Electrochemical Properties of V 2 O 5 -Graphene Composite Films as Free-Standing

Cathodes for Rechargeable Lithium Batteries." *J. Electrochem. Soc.*, *159* (8), 1135–1140.

Qin, Y., Fan, G., Liu, K. and Hu, M. (2014). "Sensors and Actuators B : Chemical Vanadium pentoxide hierarchical structure networks for high performance ethanol gas sensor with dual working temperature characteristic." *Sensors Actuators B. Chem.*, *190* 141–148.

Quinten, M. (2010). *Optical Properties of Nanoparticle Systems: Mie and beyond*, John Wiley & Sons, Germany.

R. Ko, M. Carlen, Principles and applications of electrochemical capacitors, 45 (2000) 2483–2498.

Ray, R.S., Sarma, B. and Misra, M. (2015). "Random shaped ZnO supported on a porous substrate as supercapacitor." *Mater. Lett.*, *155* 102–105.

Ray, R.S., Sarma, B. and Misra, M. (2015). "Random shaped ZnO supported on a porous substrate as supercapacitor." *Mater. Lett.*, *155* 102–105.

Sahu, V., Grover, S., Tulachan, B., Sharma, M., Srivastava, G., Roy, M., Saxena, M., Sethy, N., Bhargava, K., Philip, D., Kim, H., Singh, G., Kumar, S., Das, M. and Kishore, R. (2015). "Electrochimica Acta Heavily nitrogen doped , graphene supercapacitor from silk cocoon." *Electrochim. Acta*, *160* 244–253.

Saranya, M., Ramachandran, R. and Wang, F. (2016). "Journal of Science : Advanced Materials and Devices Graphene-zinc oxide (G-ZnO) nanocomposite for electrochemical supercapacitor applications." *J. Sci. Adv. Mater. Devices*, *1* (4), 454–460.

Selvakumar, M., Krishna Bhat, D., Manish Aggarwal, a., Prahladh Iyer, S. and Sravani, G. (2010). "Nano ZnO-activated carbon composite electrodes for supercapacitors." *Phys. B Condens. Matter*, *405* (9), 2286–2289.

Shen P.K. Shen, C.-Y. Wang, S.P. Jiang, X. Sun, J. Zhang (2016), Electrochemical Energy: Advanced Materials and Technologies, CRC Press

Shin, B.H., Kim, K.K., Benayad, A., Yoon, S., Park, K., Jung, I., Jin, M.H., Jeong, H., Kim, J.M., Choi, J. and Lee, Y.H. (2009). "Efficient Reduction of Graphite Oxide by Sodium Borohydride and Its Effect on Electrical Conductance." *Adv. Funct. Mater.* 20091987–1992.

Singh, K.P., Bhattacharjya, D., Razmjooei, F. and Yu, J. (2016). "Effect of pristine graphene incorporation on charge storage mechanism of three-dimensional graphene oxide : superior energy and power density retention." *Nat. Publ. Gr.*, *6* (April), 1–10.

Singh, V., Joung, D., Zhai, L., Das, S. (2011). "Progress in Materials Science Graphene based materials : Past , present and future". *Progress in Materials Science, 56(8), 1178–1271. doi:10.1016/j.pmatsci.2011.03.003*

Somani, P.R., Somani, S.P. and Umeno, M. (2006). "Planer nano-graphenes from camphor by CVD." *Chemical Physics Letters 430* 56–59.

Stoller, M.D., Park, S., Zhu, Y., An, J. and Ruoff, R.S. (2008). "Graphene-Based Ultracapacitors." *Nano Lett.*, *8* (10), 3498–3502.

Suresh, R., Giribabu, K., Manigandan, R., Kumar, S.P., Munusamy, S., Muthamizh, S., Stephen, A. and Narayanan, V. (2014). "Sensors and Actuators B : Chemical New electrochemical sensor based on Ni-doped V 2 O 5 nanoplates modified glassy carbon electrode for selective determination of dopamine at nanomolar level." *Sensors Actuators B. Chem.*, *202* 440–447.

Suresh, R., Giribabu, K., Manigandan, R., Kumar, S.P., Munusamy, S., Muthamizh, S. and Narayanan, V. (2014). "Characterization and dopamine sensing property of V 2 O 5 @ polyailine nanohybrid." *Synth. Met.*, *196* 151–157.

Talledo, A., Granqvist, C.G. and Pentoxide, L.V. (1996). "Electrochromic vanadium pentoxide based films: structural , electrochemical and optical properties,." J. Appl. Phys 77 4655-4666

Tang, Y., Rui, X., Zhang, Y., Lim, M. and Dong, Z. (2013). "high-performance lithium-ion batteries enabled by a." *J. Mater. Chem. A*, *2* (1), 82–88.

Taylor, P., Choi, W., Lahiri, I., Seelaboyina, R., Kang, Y.S., Choi, W., Lahiri, I. and Seelaboyina, R. (2010). "Critical Reviews in Solid State and Materials Sciences

Synthesis of Graphene and Its Applications : A Review Synthesis of Graphene and Its Applications : A Review." (May 2012), 37–41.

Uchaker, E., Zheng, Y.Z., Li, S., Candelaria, S.L., Hu, S. and Cao, G.Z. (2014). "Better than crystalline: amorphous vanadium oxide for sodium-ion batteries." *J. Mater. Chem. A*, *2* (43), 18208–18214.

Uchaker, E., Zheng, Y.Z., Li, S., Candelaria, S.L., Hu, S. and Cao, G.Z. (2014). "Better than crystalline: amorphous vanadium oxide for sodium-ion batteries." *J. Mater. Chem. A*, *2* (43), 18208–18214.

Umar, A., Muzibur, M., Kim, S.H., Rusling, J.F., Schubert, U.S., Umar, A., Rahman, M.M., Kim, S.H. and Hahn, Y. (2008). "Zinc oxide nanonail based chemical sensor for hydrazine detection." *Chem. Commun. (Camb).*, *7345* (2), 1–4.

Umar, A., Rahman, M.M. and Hahn, Y. (2009). "Talanta Ultra-sensitive hydrazine chemical sensor based on high-aspect-ratio ZnO nanowires." *Talanta*, *77* 1376–1380.

Van, K. Le, Groult, H., Mantoux, A., Perrigaud, L., Lantelme, F., Lindstr, R., Badour-hadjean, R., Zanna, S. and Lincot, D. (2006). "Amorphous vanadium oxide films synthesised by ALCVD for lithium rechargeable batteries." *Journal of Power Sources*, *160* (1), 592–601.

Van, K. Le, Groult, H., Mantoux, A., Perrigaud, L., Lantelme, F., Lindstr, R., Badour-hadjean, R., Zanna, S. and Lincot, D. (2006). "Amorphous vanadium oxide films synthesised by ALCVD for lithium rechargeable batteries." *Journal of Power Sources*, *160* (1), 592–601.

Viswanathamurthi, P., Bhattarai, N., Kim, H.Y. and Rae, D. (2003). "Vanadium pentoxide nanofibers by electrospinning." *Scr. Mater.*, *49* (6), 577–581.

Vivekchand, S.R.C., Rout, C.S., Subrahmanyam, K.S., Govindaraj, A. and Rao, C.N.R. (2008). "Graphene-based electrochemical supercapacitors." *J. Chem. Sci.*, *120* (1), 9–13.

Wang, B.X., You, H., Liu, F., Li, M., Wan, L., Li, S., Li, Q., Xu, Y., Tian, R. and Yu, Z. (2009). "Large-Scale Synthesis of Few-Layered Graphene using CVD ." *Chemical Vapor Deposition, 15*(1-3), 53-56.

Wang, J.J., Zhu, M.Y., Outlaw, R.A., Zhao, X., Manos, D.M., Wang, J.J., Zhu, M.Y., Outlaw, R.A., Zhao, X., Manos, D.M. and Holloway, B.C. (2012). "Free-standing subnanometer graphite sheets." *Applied physics letters, 85*(7), 1265-1267.

Wang, X., Jiao, L., Sheng, K., Li, C., Dai, L. and Shi, G. (2013). "Solution-processable graphene nanomeshes with controlled pore structures." *Sci. Rep., 3* 1996.

Wang, X., Zhi, L. and Mu, K. (2008). "Transparent, Conductive Graphene Electrodes for Dye-Sensitized Solar Cells." NanoLett., Vol. 8, No. 1, 2008.

Wang, Y., Shi, Z., Huang, Y., Ma, Y., Wang, C., Chen, M. and Chen, Y. (2009). "Supercapacitor Devices Based on Graphene Materials." *J. Phys. Chem. C, 113* (30), 13103–13107.

Wangoh, L.W., Huang, Y., Jezorek, R.L., Kehoe, A.B., Watson, G.W., Quackenbush, N.F., Chernova, N.A., Whittingham, M.S., Piper, L.F.J., Whittingham, M.S. and Piper, L.F.J. (2016). "Correlating lithium hydroxyl accumulation with capacity retention in V 2 O 5 aerogel cathodes." *ACS Appl. Mater. Interfaces, 8* (18), 11532–11538.

Wen, Z., Wang, X., Mao, S., Bo, Z., Kim, H., Cui, S., Lu, G., Feng, X. and Chen, J. (2012). "Crumpled nitrogen-doped graphene nanosheets with ultrahigh pore volume for high-performance supercapacitor." *Adv. Mater., 24* (41), 5610–6.

Wieckohski, (1984). "Electrochemical processes at well-defined surfaces." *J. Electroanal. Chem. Interfacial Electrochem., 168* (1–2), 43--66.

Wieckohski, (1984). "Electrochemical processes at well-defined surfaces." *J. Electroanal. Chem. Interfacial Electrochem., 168* (1–2), 43--66.

Woo, S., Kim, Y.-R., Chung, T.D., Piao, Y. and Kim, H. (2012). "Synthesis of a graphene–carbon nanotube composite and its electrochemical sensing of hydrogen peroxide." *Electrochim. Acta, 59* 509–514.

Wu, Q., Sun, Y., Bai, H. and Shi, G. (2011). "High-performance supercapacitor electrodes based on graphene hydrogels modified with 2-aminoanthraquinone moieties w." *Phys. Chem. Chem. Phys.*, *13* 11193–11198.

Wu, Z.-S., Wang, D.-W., Ren, W., Zhao, J., Zhou, G., Li, F. and Cheng, H.-M. (2010). "Anchoring Hydrous RuO2 on Graphene Sheets for High-Performance Electrochemical Capacitors." *Adv. Funct. Mater.*, *20* (20), 3595–3602.

Xiang, C., Li, M., Zhi, M., Manivannan, A. and Wu, N. (2013). "A reduced graphene oxide/Co3O4 composite for supercapacitor electrode." *J. Power Sources*, *226* 65–70.

Xiao, X., Han, B., Chen, G., Wang, L. and Wang, Y. (2017). "Preparation and electrochemical performances of carbon sphere @ ZnO core-shell nanocomposites for supercapacitor applications." *Sci. Rep.*, (December 2016), 1–13.

Xu, J., Tan, Z., Zeng, W., Chen, G., Wu, S., Zhao, Y. and Ni, K. (2016). "A Hierarchical Carbon Derived from Sponge-Templated Activation of Graphene Oxide for High-Performance Supercapacitor Electrodes." *Adv. Mater.*, *28* (26), 1–7.

Xu, Y., Lin, Z., Huang, X., Wang, Y., Huang, Y. and Duan, X. (2013). "Functionalized Graphene Hydrogel-Based High- Performance Supercapacitors." *Adv. Mater.*, *25* (40), 1–6.

Yan, J., Liu, J., Fan, Z., Wei, T. and Zhang, L. (2012). "High-performance supercapacitor electrodes based on highly corrugated graphene sheets." *Carbon N. Y.*, *50* (6), 2179–2188.

Yang, J., Lan, T., Liu, J., Song, Y. and Wei, M. (2013). "Supercapacitor electrode of hollow spherical V2O5 with a high pseudocapacitance in aqueous solution." *Electrochim. Acta*, *105* 489–495.

Yang, S., Sun, Y., Chen, L., Hernandez, Y., Feng, X. and Müllen, K. (2012). "Porous iron oxide ribbons grown on graphene for high-performance lithium storage." *Sci. Rep.*, *2* (Ii), 427.

Yang, Y., Kim, D., Yang, M. and Schmuki, P. (2011). "ChemComm Vertically aligned mixed V 2 O 5 – TiO_2 nanotube arrays for supercapacitor applications ." *Chem. Commun. (Camb).*, *47* (27), 7746–7748.

Yoo, E., Kim, J., Hosono, E., Zhou, H., Kudo, T. and Honma, I. (2008). "Large Reversible Li Storage of Graphene Nanosheet Families for Use in Rechargeable Lithium Ion Batteries 2008." *Nano Lett.*, *8* (8), 13–18.

Yu, Xuegong., Yanga, L., Lva, Q., Xub, M., Chenb, H., Yang, D., (2015). "Enhanced efficiency of graphene-silicon solar cells by electric field doping" Nanoscale., **7**, 7072-7077

Yuan, W., Zhou, Y., Li, Y., Li, C., Peng, H., Zhang, J., Liu, Z., Dai, L. and Shi, G. (2013). "The edge- and basal-plane-specific electrochemistry of a single-layer graphene sheet." *Sci. Rep.*, *3* (Cvd), 2248.

Yun-Bo He, Gao-Ren Li, Zi-Long Wang, C.-Y.S. and Y.-X.T. (2011). "Energy & Environmental Science Single-crystal ZnO nanorod / amorphous and nanoporous metal oxide shell composites : Controllable electrochemical synthesis and enhanced." *Energy Environ. Sci.*, *4* 1288–1292.

Yuxi Xu, Sheng, K. and Chun Li, and G.S. (2010). "Self-Assembled Graphene Hydrogel." *ACS Nano*, *4* (7), 4324–4330.

Zang, J., Li, M., Cui, X., Wang, J., Sun, X., Dong, H. and Sun, Q. (2007). "Tailoring Zinc Oxide Nanowires for High Performance Amperometric Glucose Sensor." *Electroanalysis*, *19* (9), 1008–1014.

Zhang, L. and Shi, G. (2011). "Preparation of Highly Conductive Graphene Hydrogels for Fabricating Supercapacitors with High Rate Capability." *J. Phys. Chem. C*, *115* 17206–17212.

Zhang, Y. and Mu, J. (2007) "Controllable synthesis of flower- and rod-like ZnO nanostructures by simply tuning the ratio of sodium hydroxide to." *75606* IOP Nanotechnology

Zhang, Y., Li, H., Pan, L., Lu, T. and Sun, Z. (2009). "Capacitive behavior of graphene – ZnO composite film for supercapacitors." *J. Electroanal. Chem.*, *634* (1), 68–71.

Zhang, Y., Sun, X., Pan, L., Li, H., Sun, Z., Sun, C. and Tay, K. (2009). "Carbon nanotube – zinc oxide electrode and gel polymer electrolyte for electrochemical supercapacitors." *J. Alloys Compd.*, *480* 17–19.

Zhang, Y., Sun, X., Pan, L., Li, H., Sun, Z., Sun, C. and Tay, K. (2009). "Carbon nanotube – ZnO nanocomposite electrodes for supercapacitors." *Solid State Ionics*, *180* (32–35), 1525–1528.

Zhang, Z., Ren, L., Han, W., Meng, L. and Wei, X. (2015). "One-pot electrodeposition synthesis of ZnO / graphene composite and its use as binder-free electrode for supercapacitor." *Ceram. Int.*, *41* (3), 4374–4380.

Zhang, Z., Ren, L., Han, W., Meng, L. and Wei, X. (2015). "One-pot electrodeposition synthesis of ZnO / graphene composite and its use as binder-free electrode for supercapacitor." *Ceram. Int.*, *41* (3), 4374–4380.

Zhao, B., Liu, P., Jiang, Y., Pan, D., Tao, H., Song, J., Fang, T. and Xu, W. (2012). "Supercapacitor performances of thermally reduced graphene oxide." *J. Power Sources*, *198* 423–427.

Zhao, B., Liu, P., Jiang, Y., Pan, D., Tao, H., Song, J., Fang, T. and Xu, W. (2012). "Supercapacitor performances of thermally reduced graphene oxide." *J. Power Sources*, *198* 423–427.

Zhao, W., Wang, H., Qin, X., Wang, X., Zhao, Z., Miao, Z., Chen, L., Shan, M., Fang, Y. and Chen, Q. (2009). "A novel nonenzymatic hydrogen peroxide sensor based on multi-wall carbon nanotube/silver nanoparticle nanohybrids modified gold electrode." *Talanta*, *80* (2), 1029–33.

Zhu, J., Cao, L., Wu, Y., Gong, Y., Liu, Z., Hoster, H.E., Zhang, Y., Zhang, S., Yang, S., Yan, Q., Ajayan, P.M. and Vajtai, R. (2013). "Building 3D Structures of Vanadium Pentoxide Nanosheets and Application as Electrodes in Supercapacitors." 1–6.

Zhu, Y., Murali, S., Stoller, M.D., Velamakanni, A., Piner, R.D. and Ruoff, R.S. (2010). "Microwave assisted exfoliation and reduction of graphite oxide for ultracapacitors." *Carbon N. Y.*, *48* (7), 2118–2122.

Zhu, Y., Murali, S., Stoller, M.D., Velamakanni, A., Piner, R.D. and Ruoff, R.S. (2010). "Letter to the Editor Microwave assisted exfoliation and reduction of graphite oxide for ultracapacitors." *Carbon N. Y.*, *8* (7), 8–11.

Zhu, Y., Stoller, M.D., Cai, W., Velamakanni, A., Piner, R.D., Chen, D. and Ruoff, R.S. (2010). "Exfoliation of Graphite Oxide in Propylene Carbonate and Thermal Oxide Platelets." *ACS Nano*, *4* (2), 1227–1233.

Zhu, Y., Zhu, Y., Murali, S., Stoller, M.D., Ganesh, K.J., Cai, W., Ferreira, P.J., Pirkle, A., Wallace, R.M., Cychosz, K.A., Thommes, M., Su, D., Stach, E.A. and Ruoff, R.S. (2011). "Produced by Activation of Graphene." *Science*, *332* 1537–1541.

Zhuo, S., Shao, M., Zhou, Q. and Liao, F. (2011). "Preparation, characterization, and electrochemical properties of lithium vanadium oxide nanoribbons." *Electrochim. Acta*, *56* (18), 6453–6458.

Zilberberg, K., Trost, S., Schmidt, H. and Riedl, T. (2011). "Solution Processed Vanadium Pentoxide as Charge Extraction Layer for Organic Solar Cells." *Adv. Energy Mater*. 377–381.

List of Publications

International journals

1. **Sreejesh M**, N.M.Huang and H. S. Nagaraja. (2015). "Solar Exfoliated Graphene and its Application in Supercapacitors and Electrochemical H_2O_2 Sensing". *Electrochim. Acta*, 160, 94-99 (Impact factor : 4.803). doi:http://www.sciencedirect.com/science/article/pii/S0013468615002807.
2. **Sreejesh M**, Dhanush S, F. Rossignol and H.S.Nagaraja. (2017). "Microwave assisted synthesis of rGO/ZnO composites for non-enzymatic glucose sensing and supercapacitor applications". *Ceram. Int.*, 43, 4895¸S4903. (Impact factor: 2.758) doi:http://www.sciencedirect.com/science/article/pii/S0272884216324105.
3. **Sreejesh M**, Sulakshana Shenoy, Kishore Sridharan, D Kufian, AK Arof, H. S Nagaraja. (2017). "Melt quenched vanadium oxide embedded in graphene oxide sheets as composite electrodes for amperometric dopamine sensing and lithium ion battery applications". *Appl. Surf. Sci.*, 410, 336¸S343. (Impact factor: 3.150) doi:http://www.sciencedirect.com/science/article/pii/S0169433217306207.
4. Dhanush Shanbhag, K Bindu, AR Aarathy, Martha Ramesh, **Sreejesh M** HS Nagaraja. (2017). "Hydrothermally synthesized reduced graphene oxide and Sn doped manganese dioxide nanocomposites for supercapacitors and dopamine sensors"*Mat.Tod. Energy*., 4, 66-74. doi:http://www.sciencedirect.com/science/article/pii/S2468606917300011

Conference Procedings

1. **Sreejesh M**, Udaya Baht and H.S. Nagaraja. (2015), "Preparation and characterization of solar exfoliated graphene". *AIP: Conf. Proc*., 1,536-540. doi:http://aip.scitation.org/doi/abs/10.1063/1.4898
2. **Sreejesh M**, H.S. Nagaraja and Udaya Baht. (2015). "Hydrazine sensing properties" of microwave synthesized graphene/ZnO composites. *AIP: Conf. Proc*., 1728,020255.doi:http://aip.scitation.org/doi/abs/10.1063/1.4946306.

International and national conferences

1. **Sreejesh M**, and H.S.Nagaraja. “Electrochemical Studies of Flake Type Polyaniline Prepared by Chemical Oxidation” ICAPM 2013 , 11-13th October 2013, M.G. University Kottayam.
2. **Sreejesh**, H.S. Nagaraja and Udaya Bhat K. "Preparation and Characterization of Solar Exfoliated Graphene" Optics14, International Conference on Light. 19-21st of March 2014 NIT Calicut, Kerala, India.
3. **Sreejesh M**, H.S. Nagaraja and H.D. Shashikala. " Preparation and Characterization ofGraphene Oxide/Polyaniline Composite"- International Conference on Polymer Composites (ICPC-2014), NITK Surathkal, Karnataka , India.
4. **Sreejesh M**, H.S. Nagaraja and udaya Bhat K., “Preparation and Characterization of Graphene Oxide/PANI Composite for Supercapacitor Applications” - 8th Inda-Singapore Symposium on Condensed Matter Physics, 25th -27th February 2015, IIT Kanpur, India.
5. **Sreejesh M** and H.S Nagaraja “Microwave Reduced Graphene Oxide/ZnO Composite as the Sensing Platform for Dopamine” ICFMD, 2015 Johor Baru, Malaysia.
6. **Sreejesh M**,H.S. Nagaraja and Udaya Bhat K., “Hydrazie Sensing Properties of Microwave Synthesized Graphene/ZnO Composite” International Conference on Condensed Matter and Applied Physics (ICC-2015) 30-31st October, Bikaneer, India.
7. **Sreejesh M**,Karthik S Bhat, Bindu K and H. S. Nagaraja., “Single Step Hydrothermal Synthesis of Ag Nanoparticle Embedded Reduced Graphene Oxide Nanocomposite” Fourth International Conference on Frontiers in Nanoscience and Technology Cochin Nano- 016 20-23rd February 2015 , Cusat, Cochin, India.
8. **Sreejesh M**, Smrithika Subramani, Sulakshana Shenoy, Bindu K and Nagaraja H.S., “Synthesis and characterization of ZnO nanostructures” 27- 28th March 2015 CMPA ,MIT Manipal Karnataka, India.

9. **Sreejesh M** Aarathy A. R, Dhanush S, Ramesh M, Sreejesh M, Bindu K and Nagaraja H.S., "Dopamine sensing properties of MnO2 nanowires prepared by hydrothermal method",Think Nano-2016, IISc Bangalore (Best paper award).

CURICULUM VITAE

Sreejesh M

Ph.D student

Materials Research Laboratory, Department of Physics,

NITK Surathkal, Mangalore

India – 575 025

Email : sreejeshmnasc@gmail.com

Ph: +91-9035082010

Academic Records

1) M.Sc in Materials Science from Mangalore University (2009-2011)
2) B.Sc in Physics from Kannur Univeristy (2006-2009)